OPTICS OF NANOSTRUCTURES AND TOPOLOGICAL MATERIALS

A Dissertation

by

ZHONGQU LONG

Submitted to the Office of Graduate and Professional Studies of
Texas A&M University
in partial fulfillment of the requirements for the degree of

DOCTOR OF PHILOSOPHY

Chair of Committee,	Alexey Belyanin
Committee Members,	Alexei Sokolov
	Artem Abanov
	Christi Madsen
Head of Department,	Grigory Rogachev

May 2019

Major Subject: Physics

ABSTRACT

Nanostructured materials and topological materials have many unique and fascinating electronic and optical properties. In this dissertation, we explore the optics in those new materials from three aspects: 1. Optical properties of Weyl semimetals, a novel topological material recently observed in experiments, in a strong magnetic field. Our results show that the magneto-polaritons in Weyl semimetals have peculiar properties, such as hyperbolic dispersion, photonic stop bands, coupling-induced transparency, and broadband polarization conversion. 2. Superfluorescence in quasi one-dimensional structures, carbon nanotubes. We show that due to the enhanced density of states and confinement of electrons in nanotubes, superfluorescence could be achieved with high enough pumping. This result indicates potential application of carbon nanotubes as effective radiative emitter. 3. Purcell enhancement in subwavelength quasi two-dimensional materials. We use Heisenberg-Langevin approach which includes dissipation and fluctuation in both the fermionic ensemble and the electromagnetic field. We develop a general formalism and derive analytical expression for spontaneous emission and parametric down-conversion in such systems.

CONTRIBUTORS AND FUNDING SOURCES

Contributors

This work was supported by a dissertation committee consisting of Professor Alexey Belyanin [advisor], Professor Alexei Sokolov, and Professor Artem Abanov of the Department of Physics and Astronomy and Professor Christi Madsen of the Department of Electrical and Computer Engineering.

Work in Chapter 2 was collaborated with Dr. Yongrui Wang and Dr. Mikhail Tokman. They helped with the calculation of magneto-polariton modes and graphs. The student completed the model formulation, calculations of electronic transitions and dielectric tensor. Work in chapter 3 was completed by student independently. Work in Chapter 4 and 5 was collaborated with Dr. Mikhail Tokman, Dr. Yongrui Wang, and Sultan AlMutairi. They proposed and finished the framework of Heisenber-Langevin approach, the student did the analytical expression derivation and numerical calculation of the radiative transition power in such systems.

Funding Sources

Graduate study was supported by a fellowship from Department of Physics and Astronomy from Texas A&M University and Air Force Office of Scientific Research under Awards No. FA9550-17-1-0341, No. FA9550-14-1-0376, and No. FA9550-15-1-0153.

TABLE OF CONTENTS

Page

LIST OF FIGURES

FIGURE Page

1. INTRODUCTION

1.1 Optics of nanostructures and topological materials

Optics have always been an essential tool for human beings to understand the world, from daily activities way before the formation of civilization, to all aspects of scientific research nowadays. Thanks to the development of fundamental theories and novel materials, we are able to build more and more powerful optical engineering devices, to perceive and manipulate the world in a much deeper and finer way. We are even able to observe and control chemical reactions on the femtosecond time scale [1, 2], or perform quantum computing with the manipulation of single photon [3]. That is the reason that research of interaction between light and materials is both fascinating and significant.

Topological materials are one of the most fascinating novel materials. Topology is a mathematical term describing some spatial properties unchanging under the continuous variation of shapes or sizes. For Topological materials, their bulk states have different topological invariants. There are many unique electronic and optical properties arising from these topological invariants: such as quantum spin hall effect [4], topological magneto-electric effect [5], Kerr effect and Faraday rotation.

In chapter 2, we discuss the magetic optical properties of topological materials — Weyl semimetals [6]. Weyl fermions were brought up by Herman Weyl in 1929 [7]. A relativistic particle can be described by the Dirac Hamiltonian

$$H = p_x\alpha_x + p_y\alpha_y + p_z\alpha_z + m\beta. \tag{1.1}$$

Here α and β are Dirac matrices. When the particle is massless, this four components Dirac spinor could be reduced to a pair of two components spinors, namely Weyl fermions. The corresponding Hamiltonian is

$$H = \chi v_F \vec{p}\vec{\sigma}. \tag{1.2}$$

Here χ is the chirality index, $\vec{\sigma}$ is the Pauli matrix vector, v_F represents the isotropic electron dispersion, energy $E = \pm|v_F\vec{p}|$.

Weyl fermion has not been found as an elementary particle in high energy experiments. However, in some semiconductor materials, there are band touching points that could be described by the Weyl equation. Only recently, quasiparticles near these touching points with low excitation energy were studied extensively and proved to behave like Weyl Fermions [8]. Those materials are called Weyl semimetals (WSMs).

WSMs have unusual electronic and transport properties originating from the nontrivial topology of the Brillouin zone [9, 10, 11], such as topologically protected surface states (Fermi arcs), the non-conservation of the chiral charge in parallel electric and magnetic fields (the chiral anomaly), and the resulting anomalous magneto-resistance [12, 13, 14]. In this dissertation, we focus on the optical response of chiral Weyl fermions in a strong magnetic field, when the electron motion transverse to the field becomes quantized. We start with the Hamiltonian, band gaps and wavefunctions of WSMs. Then we derive its dielectric tensor from interband and intraband transitions. After that, we explore the dispersion and propagation of EM waves in WSMs. Results show that hybridization of magneto-plasmons with electromagnetic waves in WSMs leads to fascinating optical phenomena involving magnetopolaritons: hyperbolic dispersion, the absence of Landau damping for strongly localized excitations, photonic stop bands, coupling-induced transparency, efficient polarization conversion, and pulse compression, to name a few.

Nanostructured materials is another category of fascinating novel materials. Comparing to conventional materials, the distinctive feature of nanomaterials is that they have nanoscale structures. These materials could be found in nature (graphene, photonic crystals), or be artificially fabricated (carbon nanotubes, fullerenes, quantum wells, ceramic nanoparticles, semiconductor quantum dots). This feature affects the optical properties of these materials in two aspects: quantum confinement and quantization of the charged quasi-particle motion resulting in unique optical response [15, 16], and the subwavelength scale of waveguide or cavity modifying the interaction between resonating light and active medium [17, 18]. The research of optics in nanostructured ma-

terials is quite broad. In this dissertation, we are focused on the superfluorescence of single wall carbon nanotubes (SWCNT), which has unique optical response due to first aspect, and Purcell effect in two-dimensional materials, due to the second aspect.

In chapter 3, we show that superfluorescence could be generated with enough excitation in SWCNTs. SWCNTs are quasi one-dimensional structures of fullerene family. Their electronic and photonic properties are very sensitive to its diameters and chirality. They could be either metallic or semiconducting material with band gaps ranging from zero to several eV. Besides, semiconducting SWCNTs has enhanced density of states at band edges, which makes them very promising in applications of optoelectronic devices [19, 20, 21]. However, when SWCNTs are used as radiative emitter for lasing, it's not as efficient as people would expect. Time-resolved pump-probe spectroscopy [22, 23] shows that SWCNTs have multi-exponential behavior of the decay of photoluminescence: a fast non-radiative decay and a slow radiative decay. But this is only in conventional laser regime. In superfluorescence formalism, if the growth rate of field is larger than the dephasing rate, the radiative decay would be significantly enhanced. In this chapter, we calculate SWCNTs' optical response numerically with Semiconductor Bloch equations. Results show that with high enough excitation, the growth rate of the field in SWCNTs will exceed the dephasing rate, and thus make the radiative decay process as the dominant process in the decay of photoluminescence.

In chapter 4 and chapter 5, Purcell enhancement of spontaneous emission and parametric down-conversion in subwavelength quasi two-dimensional materials have been discussed [24, 25]. Purcell effect refers to the enhancement of radiative process due to the localization of emitters in a subwavelength cavity. In cavity quantum electrodynamics, Purcell effect has been explained as the result of enhanced density of final states for the transition process. According to Fermi's golden rule, the transition rate is proportional to the density of final states. However, when there is strong dissipation and fluctuation in the cavity, we need to use a more consistent quantum electrodynamics (QED) approach. In this dissertation, we use QED Heisenberg-Langevin equations to describe the radiative process including strong dissipation and fluctuations in both the electron ensemble in

active medium, and in the electromagnetic field in a subwavelength cavity. In chapter 4, we applied this formalism for spontaneous emission in a subwavelength quasi two-dimensional waveguide. In chapter 5, we applied the same formalism to both spontaneous and stimulated parametric down-conversion. We have derived a general framework and convenient analytic expressions for such radiative process in a subwavelength quasi 2D system.

1.2 References

[1] A. H. Zewail, Science 242, 1645-1653 (1988).

[2] L. R. Khundkar and A. H. Zewail, Ann. Rev. phys. Chem. 41, 15-40 (1990).

[3] J. D. Franson, B. C. Jacobs, and T. B. Pittman, Phys. Rev. A 70, 062302 (2004).

[4] B. A. Bernevig, T. L. Hughes, S.-C. Zhang, Science 314, 1757 (2006).

[5] X. L. Qi, T. L. Hughes, and S. C. Zhang, Phys. Rev. B 78, 195424 (2008)

[6] Z. Long, Y. Wang, M. Erukhimova, M. Tokman, and A. Belyanin, Phys. Rev. Lett. 120, 037403 (2018).

[7] H. Weyl, I. Z. Phys. 56, 330-352 (1929).

[8] X. Su-Yang, B. Ilya, A. Nasser, N. Madhab, B. Guang, and et. al., Science 349(6248), 613-617(2015).

[9] X. Wan, A. M. Turner, A. Vishwanath, S. Y. Savrasov, Phys. Rev. B 83, 205101 (2011).

[10] P. Hosur and X. Qi, Comp. Rend. Phys. 14, 857 (2013).

[11] O. Vafek and A. Vishwanath, Ann. Rev. Condens. Matter Phys. 5, 83 (2014).

[12] Jun Xiong, Satya K. Kushwaha, Tian Liang, Jason W. Krizan, Max Hirschberger, Wudi Wang, R. J. Cava, N. P. Ong, Science 350, 413 (2015).

[13] H. Xiaochun, Z. Lingxiao, L. Yujia, W. Peipei, C. Dong, Y. Zhanhai, L. Hui, X. Mianqi, W. Hongming, F. Zhong, D. Xi, C. Genfu, Phys. Rev. X 5, 031023 (2015).

[14] D. T. Son and B. Z. Spivak, Phys. Rev. B 88, 104412 (2013).

[15] U. Banin and O. Millo, Annu. Rev. Phys. Chem. 54, 465 (2003).

[16] L. E. Ramos, J. FurthmuÌĹller, and F. Bechstedt, Phys. Rev. B 72, 45351 (2005).

[17] M. O. Scully and M. S. Zubairy, Quantum Optics, Cambridge University Press, Cambridge (1997).

[18] P. Maunz, T. Puppe, I. Schuster, N. Syassen, P. W. H. Pinkse, and G. Rempe, Phys. Rev. Lett. 94, 033002 (2005).

[19] R. Martel, V. Derycke, C. Lavoie, J. Appenzeller, K.K. Chan, J.Tersoff, Ph. Avouris, Phys. Rev. Lett. 87, 256805 (2001).

[20] M. Itkis, F. Borondics, A. Yu, R. Haddon, Science 312, 413 (2006).

[21] E. Gaufres, N. Izard, X. Le Roux, D. Marris-Morini, S. Kazaoui, E. Cassan, L. Vivien, Appl. Phys. Lett. 96, 231105 (2010).

[22] G. D. Scholes, S. Tretiak, T. J. McDonald, W. K. Metzger, C. Engtrakul, G. Rumbles and M. J. Heben, J. Phys. Chem. C 111, 11139-11149 (2007).

[23] Z. Zhu, J. Crochet, M. S. Arnold, M. C. Hersam, H. Ulbricht, D. Resasco and T. Hertel, J. Phys. Chem. C, 111, 3831-3835 (2007).

[24] M. Tokman, Z. Long, S. AlMutairi, Y. Wang, M. Belkin, and A. Belyanin, Phys. rev. A 97, 043801 (2018).

[25] M. Tokman, Z. Long, S. AlMutairi, Y. Wang, V. Vdovin, M. Belkin, and A. Belyanin, APL Photonics 4, 034403 (2019)

[26] Q. Zhang, Y. Wang, W. Guo, Z. Long, J. D. Watson, M. J. Manfra, A. Belyanin, and J. Kono, Phys. Rev. Lett. 117, 207402 (2016).

2. MAGNETO-POLARITONS IN WEYL SEMIMETALS IN STRONG MAGNETIC FIELD *

2.1 Introduction

Weyl semimetals (WSMs) have unusual electronic and transport properties originating from the nontrivial topology of the Brillouin zone [1, 2, 3]. They have been studied experimentally, mostly with angle-resolved photoemission spectroscopy; e.g. [4, 5, 6]. The most intensely studied phenomena include topologically protected surface states known as Fermi arcs, the chiral anomaly, or the non-conservation of the chiral charge in parallel electric and magnetic fields, and the resulting anomalous magnetoresistance [7, 8, 9, 10]. Optics of WSMs received relatively less attention so far. Far-infrared optical spectroscopy studies of TaAs without the magnetic field have been recently reported [11]. The conductivity, magnetoplasmons, and polaritons in a magnetic field were calculated recently in quasiclassical approximation [12, 13, 14, 15, 16, 17, 18]. The strong-field optical conductivity was calculated in [19]. Here we concentrate on the wave propagation in WSMs in a strong magnetic field, when the electron motion transverse to the field becomes quantized. We show that hybridization of magnetoplasmons with electromagnetic (EM) waves in WSMs leads to fascinating optical phenomena involving magnetopolaritons: hyperbolic dispersion, the absence of Landau damping for strongly localized excitations, photonic stop bands, coupling-induced transparency, efficient polarization conversion, and pulse compression, to name a few. We show that optical spectroscopic techniques provide a straightforward and "clean" way of detecting topological properties of low-energy electron states and in particular the chiral anomaly. Moreover, WSMs show strong promise for future photonic chips enabling a wide array of broadband optoelectronic applications, such as polarizers, modulators, switches, and pulse shapers for mid-infrared through terahertz wavelengths.

2.2 Dielectric tensor for a WSM in a magnetic field

We consider the material which has only one pair of Weyl nodes for simplicity, with low-energy excitations around each node described by the Weyl Hamiltonian,

$$H = \chi \hbar v_F \boldsymbol{\sigma} \boldsymbol{k}. \tag{2.1}$$

Here $\chi = \pm 1$ is the chirality index, $\boldsymbol{\sigma}$ is a 3D vector of Pauli matrices, $\boldsymbol{k}$ is the 3D quasimomentum of electrons counted from the Weyl node, and we assumed an isotropic electron dispersion (scalar constant v_F). In a strong magnetic field oriented along z axis the 3D conical spectrum of quasiparticles near each node is split into Landau-level (LL) subbands W_n labeled by the quantum number n:

$$W_n = \mathrm{sgn}(n)\hbar v_F \sqrt{\frac{2|n|}{l_b^2} + k_z^2} \text{ for } n \neq 0, \tag{2.2}$$

$$W_0^{(\chi)} = -\chi \hbar v_F k_z \tag{2.3}$$

where $l_b = \sqrt{\frac{\hbar c}{eB}}$ is the magnetic length. The electron wavefunctions are given in [20]. We assume that the field is strong enough so that $W_1 - W_0$ at $k_z = 0$ is much larger than the LL broadening determined by disorder.

The salient feature of the electron spectrum is the presence of chiral electron states with 1D linear dispersion at $n = 0$ LL. The $n = 0$ electrons near each node are able to move only in one direction, depending on the sign of χ and neglecting internode scattering. The majority of peculiar optical properties of WSMs originates from the response of these electron states and its interplay with inter-LL transitions.

The dielectric tensor for chiral fermions in WSMs has a general structure typical for a magne-

tized electron-hole plasma:

$$\epsilon_{ij} = \begin{pmatrix} \epsilon_\perp & ig & 0 \\ -ig & \epsilon_\perp & 0 \\ 0 & 0 & \epsilon_{zz} \end{pmatrix} \tag{2.4}$$

where $i, j = x, y, z$. However, the expressions for its components and the resulting optical response are far from typical. Consider first the longitudinal component $\epsilon_{zz} = \epsilon_b + 4\pi i\sigma_{zz}/\omega$ where ϵ_b is the background dielectric constant of a crystal. The conductivity σ_{zz} can be found by calculating the linear response to the longitudinal field $E_z = \mathrm{Re}[\mathcal{E}e^{iq_z z - i\omega t}]$. It is convenient to define the optical field through the scalar potential $\phi = \mathrm{Re}[\Phi e^{iq_z z - i\omega t}]$ as $\mathcal{E} = -iq_z\Phi$. We will assume for simplicity that the Fermi energy for each chirality is between $n = -1$ and $n = 1$ and the temperature is low enough so that the states with $n \neq 0$ are either completely filled or empty. The general result for an arbitrary position of the Fermi level is given in [20]. Note also that for the longitudinal field $\boldsymbol{E} \| \boldsymbol{B}$ the transitions between the Landau levels are forbidden in the electric dipole approximation. The resulting linearized density matrix equation for the density matrix elements $\rho^{(\chi)}_{kk'}$ for each chirality is

$$\begin{aligned} &-i\omega\rho^{(\chi)}_{k_z,k'_z} + i\frac{W_0^{(\chi)}(k_z) - W_0^{(\chi)}(k'_z)}{\hbar}\rho^{(\chi)}_{k_z,k'_z} = -\frac{i}{\hbar}e\Phi \\ &\left\langle n=0, k_z | e^{iq_z z} | n=0, k'_z \right\rangle \left[f_0^{(\chi)}(k_z) - f_0^{(\chi)}(k'_z) \right], \end{aligned} \tag{2.5}$$

where $f_0^{(\chi)}(k_z)$ are populations at $n = 0$ unperturbed by the optical field and we neglected relaxation, which will be added later. The matrix element in Eq. (2.5) is calculated using the electron states in a magnetic field [20]; it is equal to the delta-function $\delta_{k_z - q_z, k'_z}$. The solution of Eq. (2.5) in the limit $k_z \gg q_z$ is

$$\rho^{(\chi)}_{k_z,k_z-q_z} = \frac{ie\mathcal{E}}{\omega - \chi q_z v_F}\frac{\partial f_0^{(\chi)}(k_z)}{\hbar\partial k_z}. \tag{2.6}$$

The complex amplitude of the Fourier component of the electric current $j_z = \mathrm{Re}\tilde{J}e^{iq_z z - i\omega t}$ is given

by

$$\tilde{J} = \sum_{k_z,\chi} (j_z)^{(\chi)}_{k_z-q_z,k_z}\, \rho^{(\chi)}_{k_z,k_z-q_z}, \tag{2.7}$$

where the matrix element of the spatial Fourier component of the current is

$$(j_z)^{(\chi)}_{k_z',k_z} = -e\left\langle n=0,k_z'|e^{-iq_z z}\chi v_F\sigma_z|n=0,k_z\right\rangle \tag{2.8}$$

and the sum can be replaced by integration. The resulting longitudinal component of the conductivity tensor is

$$\sigma_{zz} = \frac{ie^3Bv_F\omega}{2\pi^2\hbar^2 c}\frac{1}{\omega^2-q_z^2v_F^2}, \tag{2.9}$$

where the B-dependence appeared due to the density of states in a quantizing magnetic field. The longitudinal dielectric tensor component therefore takes the form

$$\epsilon_{zz} = \epsilon_b - \omega_p^2/(\omega^2-q_z^2v_F^2). \tag{2.10}$$

This result can be also obtained from the kinetic equation [20]. This expression has several peculiar features. First, since the electrons at $n=0$ can move only in one direction with the same velocity v_F, they cannot bunch in the velocity space and there is no Landau damping. Mathematically, the Landau damping emerges due to contribution from the pole in the integral over electron momenta in the linear conductivity. However, in our case there is no pole in the integral in Eq. (2.7) since the denominator in Eq. (2.6) does not depend on the electron momentum.

Second, the effective plasma frequency in Eq. (2.10) does not depend on the electron density: $\omega_p^2 = \dfrac{2\alpha}{\pi}\dfrac{eBv_F}{\hbar}$, where $\alpha = \dfrac{e^2}{\hbar c}$; see also [9, 12]. In the limit of a uniform electric field $q_z = 0$ Eq. (2.9) immediately gives the chiral anomaly. Indeed, if only $n=0$ electrons are involved, the chiral current $j_{\rm chir} = \partial[N^{(\chi=+1)} - N^{(\chi=-1)}]/\partial t$ is related to the charge current in a uniform but time-dependent field $\boldsymbol{E}\|\boldsymbol{B}$ as $\partial j_z/\partial t = -ev_F j_{\rm chir}$. This gives the chiral anomaly current $j_{\rm chir} = -e^2\boldsymbol{EB}/(2\pi^2\hbar^2 c)$, in agreement with previous results; see e.g. [2, 3] for review.

2.3 The dispersion equation and propagation

2.3.1 The dispersion equaiton

EM waves incident on a magnetized WSM propagate as eigenmodes that can be called magneto-polaritons. They are the solutions of Maxwell's equations for plane waves with the dielectric tensor from Eq. (2.4). For the photon wave vector $\boldsymbol{q}$ in the (xz)-plane making an angle θ with the magnetic field direction along z-axis, they can be written as

$$\begin{pmatrix} \epsilon_+ - \frac{1}{2}\mu^2\left(1+\cos^2\theta\right) & \frac{1}{2}\mu^2\sin^2\theta & \frac{1}{\sqrt{2}}\mu^2\sin\theta\cos\theta \\ \frac{1}{2}\mu^2\sin^2\theta & \epsilon_- - \frac{1}{2}\mu^2\left(1+\cos^2\theta\right) & \frac{1}{\sqrt{2}}\mu^2\sin\theta\cos\theta \\ \frac{1}{\sqrt{2}}\mu^2\sin\theta\cos\theta & \frac{1}{\sqrt{2}}\mu^2\sin\theta\cos\theta & \epsilon_{zz} - \mu^2\sin^2\theta \end{pmatrix} \begin{pmatrix} E_+ \\ E_- \\ E_z \end{pmatrix} = 0, \quad (2.11)$$

where $\mu^2 = \dfrac{c^2q^2}{\omega^2}$, $\epsilon_\pm = \epsilon_\perp \pm g$, and $E_\pm = \frac{1}{\sqrt{2}}(E_x \pm iE_y)$.

2.3.2 Longitudinal propagation

For the waves propagating strictly along the magnetic field, i.e. $\theta = 0$, the solution to Eqs. (2.11) consists of two eigenmodes with transverse polarization ("photons"),

$$\mu^2_{L,R} = \epsilon_\pm,\ \boldsymbol{E_{L,R}} = \frac{1}{\sqrt{2}}E_\pm(\boldsymbol{x_o} \pm i\boldsymbol{y_o}), \quad (2.12)$$

and the wave with the longitudinal polarization $\boldsymbol{E} = E_z\boldsymbol{z_o}$ and dispersion equation $\epsilon_{zz} = 0$ ("plasmon"). The plasmon dispersion is

$$\omega^2 = \frac{\omega_p^2}{\epsilon_b} + v_F^2q^2. \quad (2.13)$$

We emphasize again that, in contrast to "usual" plasmons, there is no cutoff in Eq. (2.13) due to Landau damping at large wave vectors $q > \omega/v_F$. Therefore, a much stronger plasmon localization

is allowed, with propagation only limited by absorption due to scattering on impurities etc.

2.3.3 Oblique propagation

For oblique propagation, even at very small angles θ, the plasmons and transverse waves are coupled to form hybrid plasmon-polaritons. To determine general trends and obtain analytic results, we neglect the spatial dispersion (q_z-dependence) of ϵ_{zz} in Eq. (2.10), which is possible as long as $\mu^2 \sin^2\theta \ll c^2/v_F^2$. This is not so restrictive since $c/v_F > 100$. We also neglect any spatial dispersion in $\epsilon_\pm$ in the dipole approximation.

It is instructive first to consider the case when the Fermi level is exactly at the Weyl point for both chiralities. In this case, due to electron-hole symmetry the off-diagonal terms in Eq. (2.4) vanish and the dielectric tensor looks like the one for a uniaxial anisotropic medium. The dispersion equation for the extraordinary wave, i.e. the one polarized in the (x, z) plane, can be written as

$$\frac{\mu_x^2}{\epsilon_{zz}} + \frac{\mu_z^2}{\epsilon_\perp} = 1. \tag{2.14}$$

The transverse components of the dielectric tensor are always positive, whereas the ϵ_{zz} component becomes negative for frequencies below the plasmon resonance, $\omega^2 < \omega_p^2/\epsilon_b$. In this case Eq. (2.14) becomes hyperbolic and its isofrequency lines are hyperbolae. Therefore, a magnetized WSM is a natural hyperbolic material at low enough frequencies. Another natural hyperbolic material is hexagonal boron nitride, where the hyperbolic dispersion exists in two narrow spectral ranges near the phonon bands [22]. Otherwise, hyperbolic dispersion is achieved in the effective medium approximation in metal/dielectric metamaterials prepared by nanofabrication [23]. It is promising for numerous applications from superlenses and nanoimaging to photonic integrated circuits. The plasmon resonance frequency $\omega = \omega_p/\sqrt{\epsilon_b}$ in WSMs which determines the upper bound for hyperbolic dispersion is in the THz to far-infrared range for a magnetic field of 1-10 Tesla, $\epsilon_b \sim 10$ and $v_F \sim 10^8$ cm/s. It is lower than the inter-LL absorption edge for all magnetic fields, so the only loss mechanism is due to scattering on impurities which depends on the material quality.

The ordinary wave in this limit is linearly polarized along y-axis and has a standard dispersion $\mu^2 = \epsilon_\perp$.

Fig. 2.1 shows the dispersion (real part of μ) for the extraordinary waves for several different propagation angles θ. Far from inter-LL transitions, we can neglect any dispersion in the transverse part of the dielectric tensor, assuming $\epsilon_\perp = \epsilon_b \sim 10$. We also added the scattering rate as an imaginary part of frequency ($\omega + i\gamma$) in the first term of Eq. (2.5) and took γ to be 0.01 of the plasmon resonance frequency $\omega_{\rm res} = \omega_p/\epsilon_b^{1/2}$. For longitudinal propagation $\theta = 0$ the photon dispersion is trivial: $\mu = \sqrt{\epsilon_b}$. For any nonzero angle, plasmons and photons hybridize. At the hybrid plasmon-polariton resonance μ diverges in the absence of dissipation. The stop band appears between the hybrid resonance and plasmon resonance. It is defined by the condition $\mu^2 < 0$ so that Re$[\mu] = 0$ and the wave cannot propagate. At the boundaries of the stop band Re[μ] goes through the value of 1 with a large derivative, leading to a small group velocity $v_{gr} \ll c$. This means that a layer of WSM is able to compress a pulse incident from vacuum by a factor c/v_{gr}. All spectral features are tunable by varying the magnetic field or the angle θ.

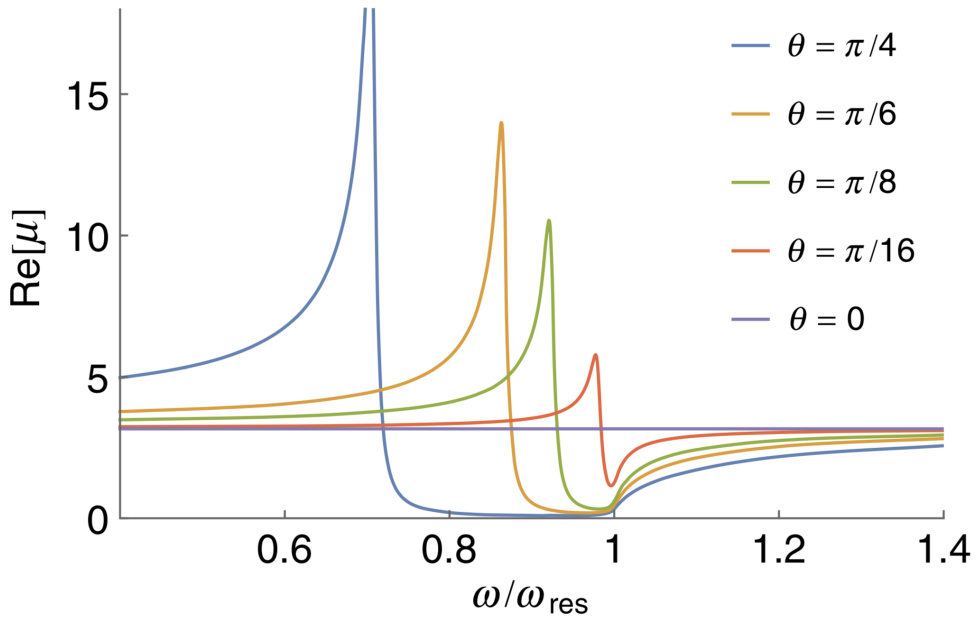

Figure 2.1: Dispersion (real part of $\mu(\omega)$) of the extraordinary waves in a magnetic field of 10 T for several different propagation angles θ.

Going back to the general case of an arbitrary Fermi level, Eqs. (2.11), and arbitrary values of g leads to a biquadratic dispersion equation for μ:

$$\frac{\mu^4}{2}\left((\epsilon_+ + \epsilon_-)\sin^2\theta + 2\epsilon_{zz}\cos^2\theta\right) - \Big(\epsilon_+\epsilon_-\sin^2\theta + \frac{1}{2}\epsilon_{zz}(\epsilon_+ + \epsilon_-)(1+\cos^2\theta)\Big)\,\mu^2 + \epsilon_+\epsilon_-\epsilon_{zz} = 0. \tag{2.15}$$

The polarization coefficients of the normal modes are

$$\frac{E_\pm}{E_z} = \frac{-\frac{1}{\sqrt{2}}\mu^2\sin\theta\cos\theta(\epsilon_\mp - \mu^2)}{\epsilon_+\epsilon_- - \frac{1}{2}\mu^2(1+\cos^2\theta)(\epsilon_+ + \epsilon_-) + \mu^4\cos^2\theta}. \tag{2.16}$$

Equations (2.15), (2.16), and (2.10) provide a complete description of the electromagnetic wave propagation in WSMs. They can be plotted numerically or solved analytically, leading to cumbersome formulas. In the low temperature limit we obtain analytic expressions for all components of the dielectric tensor, see [20]. Leaving detailed numerical studies to future publications,

here we highlight the most interesting cases. Note that a finite separation between Weyl nodes in momentum space by a vector $2\boldsymbol{b}$ creates an additional anisotropy vector and gives rise to an additional gyrotropic effect $g \propto b$ [21]. Therefore, the dispersion shown in Fig. (1) is valid only if this additional g is small. This will be the case when the Weyl semimetal is created by applying an external magnetic field to a Dirac semimetal, so that the separation of Weyl points is only due to a Zeeman-type interaction which is typically small. We also note that the expressions for the magnetopolariton dispersion for a nonzero g Eqs. (2.15) are analytic functions around $g = 0$, so the dispersion curves in Fig. (1) will change little when g is small. The most significant effect of a nonzero g is the appearance of an elliptical polarization, Eq. (2.16) instead of the linear one when $g = 0$.

2.3.4 Coupling-induced transparency

For quasi-longitudinal propagation, $\sin^2\theta \ll 1$ and plasmon-polariton hybridization occurs in the vicinity of the plasmon resonance, $|\epsilon_{zz}| \ll 1$. In this case the approximate solution of Eq. (2.15) is

$$\mu_{1,2}^2 = \frac{1}{(\epsilon_+ + \epsilon_-)\sin^2\theta + 2\epsilon_{zz}} \Big[\epsilon_+\epsilon_- \sin^2\theta + \epsilon_{zz}(\epsilon_+ + \epsilon_-) \pm\sqrt{(\epsilon_+\epsilon_- \sin^2\theta)^2 + \epsilon_{zz}^2(\epsilon_+ - \epsilon_-)^2}\Big]. \tag{2.17}$$

The polarization coefficients become

$$K_\pm = \frac{E_\pm}{E_z} = \frac{-\frac{1}{\sqrt{2}}\mu^2 \sin\theta}{\epsilon_\pm - \mu^2}. \tag{2.18}$$

In the "non-gyrotropic" limit when $E_F = 0$ and $\epsilon_+ = \epsilon_- = \epsilon_\perp$, the extraordinary wave has dispersion

$$\mu_2^2 = \frac{\epsilon_{zz}\epsilon_\perp}{\epsilon_\perp \sin^2\theta + \epsilon_{zz}};\ K_+ = K_- = -\frac{1}{\sqrt{2}}\frac{\epsilon_{zz}}{\epsilon_\perp \sin\theta}. \tag{2.19}$$

The hybrid resonance corresponds to the vanishing real part of the denominator for μ_2^2 in Eq. (2.17) or (2.19), when $|\mu_2^2| \gg 1$.

The effect of *coupling-induced transparency* emerges near the plasmon resonance where μ_2 can be of the order of 1 or smaller. When the angle θ is not too small, $|\epsilon_{zz}| \ll 1$, $\sin^2\theta \ll 1$, but $|\epsilon_\pm| \sin^2\theta \gg |\epsilon_{zz}|$, the dispersion and polarization of the "extraordinary" wave (the wave that becomes extraordinary if $E_F = 0$) are simply

$$\mu_2^2 = \frac{\epsilon_{zz}}{\sin^2\theta};\ \frac{E_{x,y}}{E_z} = -\frac{\epsilon_{zz}}{2\sin\theta}\frac{\epsilon_- \pm \epsilon_+}{\epsilon_+\epsilon_-}. \tag{2.20}$$

In this case one can have $|\mu^2| \ll \epsilon_\pm$ whereas the electric field of the wave is directed almost along the magnetic field, i.e. still quasi-longitudinal. Note that μ_2^2 in Eq. (2.20) depends only on the ϵ_{zz} component, which means that the propagation is not affected at all by the resonant inter-LL absorption losses described by the imaginary parts of $\epsilon_\pm$. The medium effectively becomes transparent for this wave! More accurately, its losses are determined only by the imaginary part of ϵ_{zz}, i.e. disorder-related scattering. Within the transparency band, strong plasmon-photon coupling forces the polarization of the wave to be oriented almost along B, and therefore it is nearly decoupled from the transitions between LLs. The narrow band of transparency within a broad line of inter-LL absorption is defined by the range of frequencies where $|\epsilon_{zz}|$ is small enough, namely $|\epsilon_{zz}| \ll |\epsilon_\pm| \sin^2\theta$. The situation is similar to the electromagnetically induced transparency (EIT) [24], only in the case of EIT the coupling between two quantum oscillators is provided by a coherent EM drive; see the comparison in [25]. The transparency will be visible if the disorder-related losses determined by $\mathrm{Im}\epsilon_{zz}$ are lower than the inter-Landau level absorption losses determined by $\mathrm{Im}\epsilon_\pm$. Introducing the electron scattering rate γ in ϵ_{zz}, one can derive the visibility condition as $\sqrt{\frac{\gamma}{\omega\sin^2\theta}} < \mathrm{Im}\epsilon_\pm$. The value of γ depends on the particular material, material quality, and temperature. For example, far-infrared spectroscopy of TaAs [11] (without the magnetic field) found the scattering time varying between 3 and 0.4 ps from low to room temperature. A value of $\mathrm{Im}\epsilon_+ \sim 3 - 5$ around $\hbar\omega \sim 100$ meV as in Fig. 2 would lead to the visibility condition

$\sin\theta > 0.01 - 0.03$.

In the same limit the "ordinary" wave has the dispersion $\mu_1^2 = \dfrac{2\epsilon_+\epsilon_-}{\epsilon_+ + \epsilon_-}$ and elliptical polarization in the plane of vectors $\boldsymbol{q}$ and $\boldsymbol{y_o}$: $\dfrac{E_x}{E_z} = \sin\theta$ and $\dfrac{E_y}{E_z} = \dfrac{i(\epsilon_+ + \epsilon_-)}{\epsilon_+ - \epsilon_-}\sin\theta$.

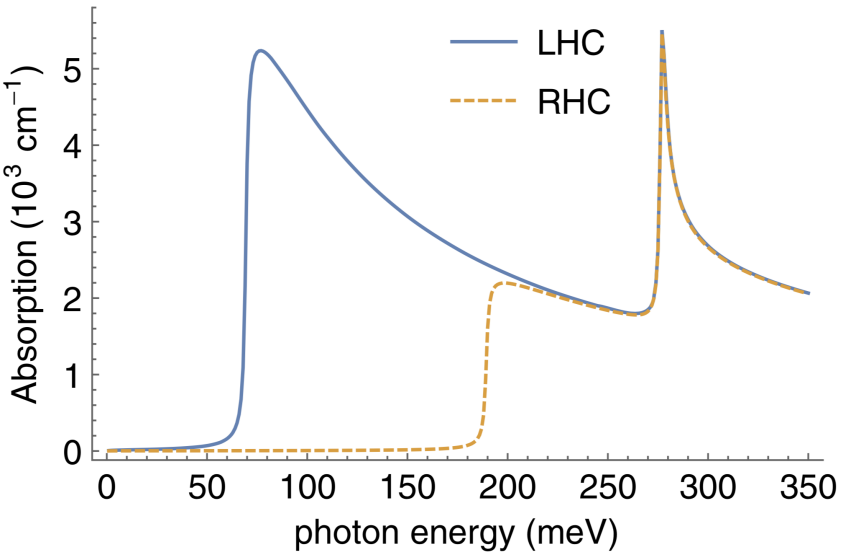

Figure 2.2: Absorption spectrum for LHC (solid line) and RHC (dashed line) polarizations in a magnetic field $B = 10$ T at zero temperature, the Fermi energy of 60 meV, and the relaxation constant $\gamma = 1$ meV.

2.4 Intersubband transitions and optical detection of the chiral anomaly

So far we considered peculiar optical properties of WSMs due to massless 1D chiral fermions at the $n = 0$ LL. Here we show that resonant inter-LL absorption from $n = 0$ to $n \neq 0$ states provides another sensitive method of studying chiral fermions near Weyl nodes and in particular, detecting the chiral anomaly. Consider the propagation of transverse modes in the Faraday geometry when the eigenmodes are left-hand or right-hand circularly polarized (LHC or RHC). The derivation of the conductivity is outlined in [20]. Fig. 2.2 gives an example of the absorption spectrum at low temperatures when the Fermi level $E_F = 60$ meV is between $n = 0$ and $n = 1$ LLs and has

the same value for both chiralities. Absorption edges of the lowest-energy transitions $0 \to 1$, then $-1 \to 0$, $-2 \to 1$, and $-1 \to 2$ are clearly visible in different polarizations (the last two transitions coincide). In particular, there is a broad range of frequencies between 50 and 200 meV when only the LHC polarization is absorbed. Therefore, a several μm thin WSM film can serve as a broadband polarizer converting from linear into circular polarization. Note that both the frequency bandwidth and the polarization coefficient are tunable by a magnetic field and/or Fermi level position. Other obvious applications include optical isolators and saturable absorbers.

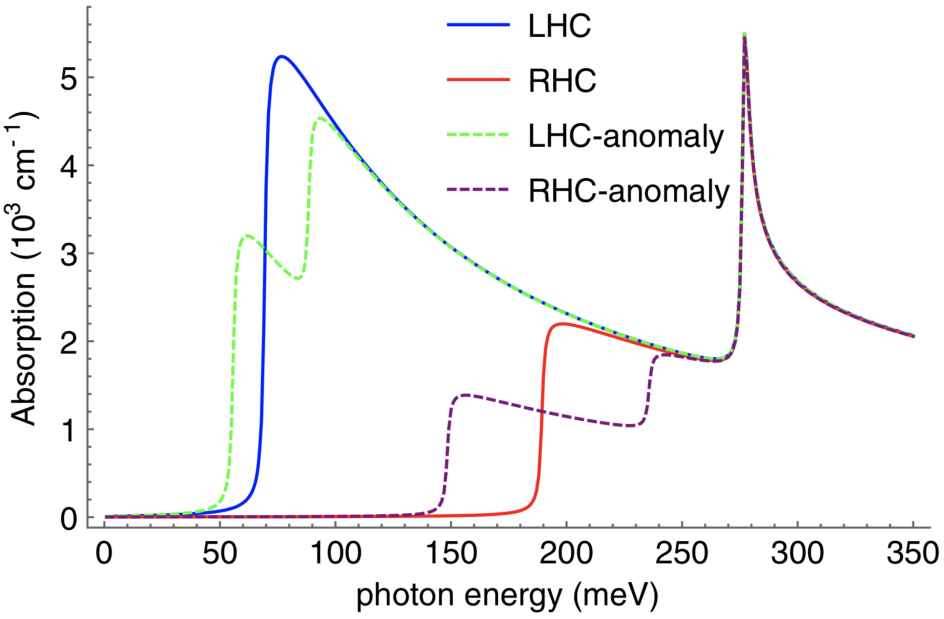

Figure 2.3: Absorption spectrum before (solid line) and after (dashed line) a constant electric field $\boldsymbol{E} \| \boldsymbol{B}$ is applied which shifts the Fermi levels by ± 30 meV in the two Weyl nodes. The magnetic field is 10 T and the relaxation constant $\gamma = 1$ meV.

Fig. 2.3 shows the evolution of this spectrum when a constant voltage is applied parallel to the magnetic field, which shifts the Fermi levels for the two chiralities by ± 30 meV. Here we assumed that before applying bias, the Fermi energy was equal to 60 meV at both Weyl points. As is clear from Fig. 3, when a voltage is applied, an additional absorption edge appears in the spectrum for

each polarization, which will be clearly distinguishable as long as the magnitude of the Fermi energy shift is larger than k_BT. Note that this behavior and the possibility of the optical detection of the chiral anomaly was predicted in Ref. [16].

In conclusion, we showed that unique topological properties of low-energy quasiparticles in WSMs give rise to a plethora of highly unusual magneto-optical effects, which provide an efficient way of studying these fascinating materials and can be utilized in future photonic devices in the terahertz through mid-infrared range. All effects are broadly tunable by varying the magnetic field, electric bias, or the propagation angle. We hope that our study will stimulate further experimental work in this rapidly developing field.

2.4 References

[1] X. Wan, A. M. Turner, A. Vishwanath, and S. Y. Savrasov, Phys. Rev. B 83, 205101 (2011).

[2] P. Hosur and X. Qi, Compt. Rend. Phys. 14, 857-870 (2013).

[3] O. Vafek and A. Vishwanath, Ann. Rev. Condens. Matter Phys. 5, 83-112 (2014).

[4] S. Y. Xu, I. Belopolski, N. Alidoust, M. Neupane, G. Bian, et al., Science 349, 613-617 (2015).

[5] B. Q. Lv, H. M. Weng, B. B. Fu, X. P. Wang, H. Miao, et al., Phys. Rev. X 5, 031013 (2015).

[6] S. Y. Xu, N. Alidoust, I. Belopolski, Z. Yuan, G. Bian, et al., Nat. Phys. 11, 748-754 (2015).

[7] J. Xiong, S. K. Kushwaha, T. Liang, J. W. Krizan, M. Hirschberger, et al., Science 350, 413-416 (2015).

[8] X. Huang, L. Zhao, Y. Long, P. Wang, D. Chen, et al., Phys. Rev. X 5, 031023 (2015).

[9] D. T. Son and B. Z. Spivak, Phys. Rev. B 88, 104412 (2013).

[10] Q. Li, D.E. Kharzeev, C. Zhang, Y. Huang, I. Pletikosic, et al., Nat. Phys. 12, 550-554 (2016).

[11] B. Xu, Y. M. Dai, L. X. Zhao, K. Wang, R. Yang, et al., Phys. Rev. B 93, 121110(R) (2016).

[12] B. Z. Spivak and A. V. Andreev, Phys. Rev. B 93, 085107 (2016).

[13] J. Zhou, H. Chang, and D. Xiao, Phys. Rev. B 91, 035114 (2015).

[14] F.M.D. Pellegrino, M. I. Katsnelson, and M. Polini, Phys. Rev. B 92, 201407(R) (2015).

[15] C. J. Tabert, J. P. Carbotte, and E. J. Nicol, Phys. Rev. B 93, 085426 (2016).

[16] P.E.C. Ashby and J. P. Carbotte, Phys. Rev. B 89, 245121 (2014).

[17] J. Ma and D. A. Pesin, Phys. Rev. B 92, 235205 (2015).

[18] E.V. Gorbar, V.A. Miransky, I.A. Shovkovy, and P.O. Sukachov, Phys. Rev. B 95, 115202 (2017).

[19] P.E.C. Ashby and J. P. Carbotte, Phys. Rev. B. 87, 245131 (2013).

[20] Appendix A.

[21] A.A. Zyuzin and A.A. Burkov, Phys. Rev. B 86, 115133 (2012).

[22] S. Dai, Q. Ma, M. K. Liu, T. Andersen, Z. Fei, et al., Nat. Nanotech. 10, 682-686 (2015).

[23] A. Poddubny, I. Iorsh, P. Belov, and Y. Kivshar, Nat. Phot. 7, 948-957 (2013).

[24] M. Fleischhauer, A. Imamoglu, and J. P. Marangos, Rev. Mod. Phys. 77, 633 (2005).

[25] M. D. Tokman, M. A. Erukhimova, Radiophysics and Quantum Electronics 57, 821-836 (2015).

3. SUPERFLUORESCENCE IN CARBON NANOTUBES

3.1 Single Wall Carbon Nanotubes and Lasing

Carbon nanotubes were first discovered in 1992 by Iijima [1, 2]. They consisted of multiple concentric tubes of rolled graphene. Later single wall carbon nanotubes (SWCNT) were produced [3]. SWCNT's properties change significantly with its structure. Its band gap could range from 0 to several eV, showing metallic or semiconducting behavior. Also as a quasi one dimensional material, SWCNT shows an enhanced density of states and stronger Coulomb interactions. With all those unique properties, people have done intensive research on their applications in field-effect transistors [4], detectors [5], and lasers [6].

Time-resolved pump-probe spectroscopy reveals multi-exponential behavior of the decay of photoluminescence [7, 8]: a fast non-radiative decay with several picoseconds characteristic decay time, and a slow radiative decay with dozens picoseconds characteristic decay time. Fig. 3.1 is the experimental result of SWCNT(6,5) from Rice University. This phenomenon makes SWCNT very inefficient emitters for conventional lasing. Here we are exploring its potential in SF which could generate ultrafast and efficient radiation pulses.

3.2 Superfluorescence

Superradiance (SR) was first predicted by Dicke in 1954 [9], as a phenomenon of coherent decay of excited atoms. In SR, or SF, an ensemble of initially incoherent quantum oscillators demonstrates a coherent behavior created by strong self-phasing. The emitted pulse has an intensity proportional to N^2 instead of N as in conventional lasing, and is developed much faster. Fig. 3.2 shows the formation process of SF. In SWCNT , if SF could be developed, it will dominate the decay process and make SWCNT an efficient emitter. To achieve SF, the growth rate of the field has to be greater than the dephasing rate of the optical polarization $1/T_2$ which is in the 10-100 fs range. SF is possible in SWCNTs because their quasi one dimensional structure leads to the

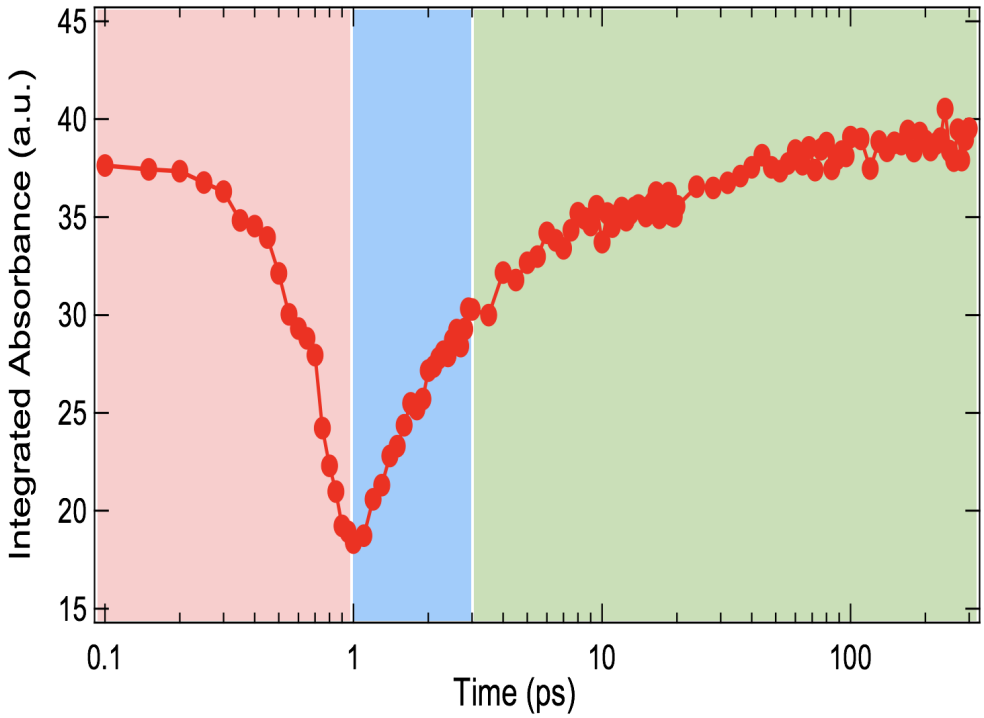

Figure 3.1: Pump-probe spectroscopy of SWCNT(6,5) from Dr. Junichiro Kono's group from Rice University.

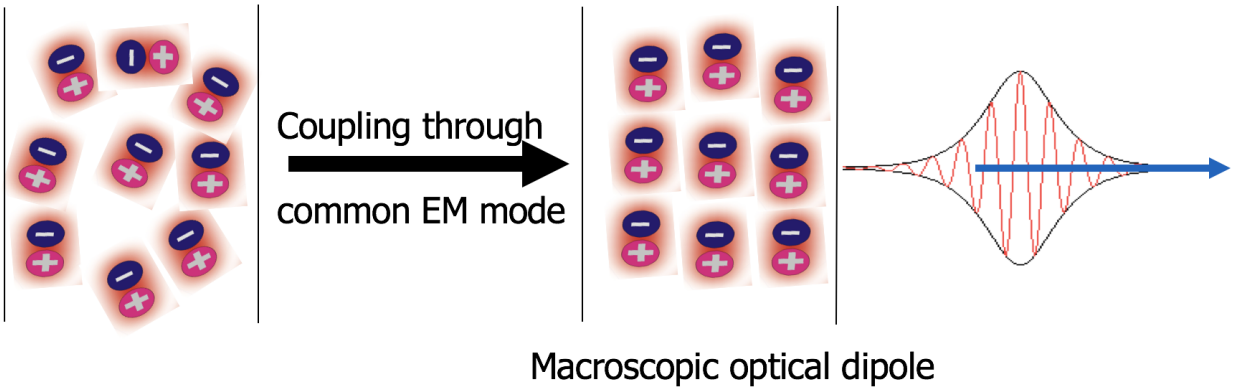

Figure 3.2: Superfluorescence formation.

enhanced Coulomb interaction and higher electron density of states. This gives stronger interaction between light and matter, in other words, larger gain or absorption. Here we explore how much gain we can reach, and how many excitons are needed to have that gain.

3.3 Methods

Analytical calculation of excited SWCNT's optical response is difficult due to the complex non-negligible many body effects. For ab initio computational simulation, a generally accepted approach is the combination of Density Functional Theory, GW approximation and Bethe-Salpeter equation [10, 11]. However, this simulation is highly time consuming for most carbon nanotubes because of their asymmetrical structure. In this project, we start with analytical calculation of SWCNT in a single electron picture with tight binding model. After that, we use semiconductor Bloch equations to calculate excited SWCNT's optical responses numerically.

3.3.1 Carbon Nanotubes in Single Electron Picture

The optical properties of graphene have been studied extensively [12, 13]. Carbon nanotubes could be viewed as rolled-up graphene, therefore we could get a single electron wavefunction of carbon nanotubes by simply adding a periodic boundary condition to graphene [14].

In graphene, a unit cell consists of two carbon atoms A and B. Within the π-band approximation, only the interaction of P_z orbitals of carbon atoms needs to be considered. The wavefunciton of a single electron under tight-binding model in graphene can be written as

$$\Psi(\boldsymbol{k},\boldsymbol{r}) = \frac{1}{\sqrt{N_{cell}}}\sum_{\boldsymbol{l}} e^{i\boldsymbol{k}\cdot\boldsymbol{r}}\left[C_A(\boldsymbol{k})P_z(\boldsymbol{r}-\boldsymbol{r}_A-\boldsymbol{l}) + C_B(\boldsymbol{k})P_z(\boldsymbol{r}-\boldsymbol{r}_B-\boldsymbol{l})\right] \tag{3.1}$$

$$= C_A(\boldsymbol{k})\tilde{P}_z^A(\boldsymbol{k},\boldsymbol{r}) + C_B(\boldsymbol{k})\tilde{P}_z^B(\boldsymbol{k},\boldsymbol{r}). \tag{3.2}$$

Here N_{cell} is the number of unit cells, $\boldsymbol{l}$ is the position of lth unit cell, $\boldsymbol{r}_A(\boldsymbol{r}_B)$ is the local position of atom A(B) in one unit cell. $C_A(\boldsymbol{k})$ and $C_B(\boldsymbol{k})$ are coefficients for this Bloch wavefunction which can be solved later.

Then we chose $\tilde{P}_z^A(\boldsymbol{k},\boldsymbol{r})$ and $\tilde{P}_z^B(\boldsymbol{k},\boldsymbol{r})$ as our basis. The Hamiltonian could be written as:

$$H_{AA} = \langle \tilde{P}_z^A(\boldsymbol{k},\boldsymbol{r})|H|\tilde{P}_z^A(\boldsymbol{k},\boldsymbol{r})\rangle = 0, \tag{3.3}$$

$$H_{BB} = 0, \tag{3.4}$$

$$H_{AB} = \langle \tilde{P}_z^A(\boldsymbol{k},\boldsymbol{r})|H|\tilde{P}_z^B(\boldsymbol{k},\boldsymbol{r})\rangle = (1 + e^{-\boldsymbol{k}\cdot\boldsymbol{a}_1} + e^{-\boldsymbol{k}\cdot\boldsymbol{a}_2})\gamma_0, \tag{3.5}$$

$$H_{AB} = (1 + e^{\boldsymbol{k}\cdot\boldsymbol{a}_1} + e^{\boldsymbol{k}\cdot\boldsymbol{a}_2})\gamma_0, \tag{3.6}$$

$$\gamma_0 = \langle P_z(\boldsymbol{r} - \boldsymbol{r}_A)|H|P_z(\boldsymbol{r} - \boldsymbol{r}_B)\rangle. \tag{3.7}$$

Here the self energy part has been set to 0, and under tight-binding model, only the interaction of adjacent atoms has been considered. The value of γ_0 is generally accepted as 2.89 eV.

Solving the matrix form of the Schrodinger equation:

$$\begin{pmatrix} H_{AA} & H_{AB} \\ H_{BA} & H_{BB} \end{pmatrix} \begin{pmatrix} C_A \\ C_B \end{pmatrix} = E \begin{pmatrix} C_A \\ C_B \end{pmatrix}, \tag{3.8}$$

the bandstructure of graphene is obtained:

$$\begin{aligned} E &= \pm\gamma_0 \sqrt{(1 + e^{\boldsymbol{k}\cdot\boldsymbol{a}_1} + e^{\boldsymbol{k}\cdot\boldsymbol{a}_2})\,(1 + e^{-\boldsymbol{k}\cdot\boldsymbol{a}_1} + e^{-\boldsymbol{k}\cdot\boldsymbol{a}_2})} \\ &= \pm\gamma_0 \sqrt{3 + 2\cos\boldsymbol{k}\cdot\boldsymbol{a}_1 + 2\cos\boldsymbol{k}\cdot\boldsymbol{a}_2 + 2\cos\boldsymbol{k}\cdot(\boldsymbol{a}_1 - \boldsymbol{a}_2)}. \end{aligned} \tag{3.9}$$

For large diameter SWCNT(n,m), the curvature barely affects the interaction between atoms. However, the existing wavefunction should satisfy periodic boundary condition. Dispersion relation would be discrete along the chiral vector $\boldsymbol{C}_h = n\boldsymbol{a}_1 + m\boldsymbol{a}_2$. $\boldsymbol{C}_h$ connects two crystallographically equivalent points on a graphene sheet after curvature.

The periodic boundary condition is

$$\Psi(\boldsymbol{k},\boldsymbol{r} + \boldsymbol{C}_h) = \Psi(\boldsymbol{k},\boldsymbol{r}), \tag{3.10}$$

$$\Psi(\boldsymbol{k},\boldsymbol{r} + \boldsymbol{C}_h) = \Psi(\boldsymbol{k},\boldsymbol{r} + n\boldsymbol{a}_1 + m\boldsymbol{a}_2) = e^{i\boldsymbol{k}\cdot(n\boldsymbol{a}_1 + m\boldsymbol{a}_2)}\Psi(\boldsymbol{k},\boldsymbol{r}). \tag{3.11}$$

So

$$\boldsymbol{k} \cdot (n\boldsymbol{a}_1 + m\boldsymbol{a}_2) = \boldsymbol{k} \cdot \boldsymbol{C}_h = 1. \tag{3.12}$$

This gives us two types of carbon nanotubes: metallic nanotubes ($n-m = 3q$) and semiconducting nanotubes ($n - m = 3q \pm 1$). Here we are more interested in the semiconducting types. Eq.3.12 suggests that $\boldsymbol{k} = \boldsymbol{K} \mp \frac{2\pi}{3|\boldsymbol{C}_h|}(3p+1)\widehat{C}_h + \boldsymbol{k}_\parallel$. Here p is an integer, $\boldsymbol{k}_\parallel$ is any vector along the axis of the tube (perpendicular to $\boldsymbol{C}_h$). Thus the band structure is:

$$E_{q,k_\parallel} = \pm\frac{\sqrt{3}a\gamma_0}{2}\sqrt{(\frac{2\pi}{|\boldsymbol{C}_h|})^2(q \pm \frac{1}{3})^2 + k_\parallel^2}. \tag{3.13}$$

And the energy gap is

$$E_{cv} = \frac{2\sqrt{3}a\gamma_0}{3|\boldsymbol{C}_h|}. \tag{3.14}$$

.

We can further calculate the transition matrix element of the dipole moment $\mathbf{d}_{c\boldsymbol{k},v\boldsymbol{k}}$:

$$\mathbf{d}_{c\boldsymbol{k},v\boldsymbol{k}} = -e\langle\Psi_c(\boldsymbol{k},\boldsymbol{r})|\boldsymbol{r}|\Psi_v(\boldsymbol{k},\boldsymbol{r})\rangle = \frac{e}{2}\mathrm{Re}[\frac{\boldsymbol{\nu}}{\alpha}].$$

Here

$$\boldsymbol{\nu}(\boldsymbol{k}) = \frac{1}{3}(\boldsymbol{a}_1 + \boldsymbol{a}_2) + e^{-\boldsymbol{k}\cdot\boldsymbol{a}_1}(-\frac{2}{3}\boldsymbol{a}_1 + \frac{1}{3}\boldsymbol{a}_2) + e^{-\boldsymbol{k}\cdot\boldsymbol{a}_2}(\frac{1}{3}\boldsymbol{a}_1 - \frac{2}{3}\boldsymbol{a}_2). \tag{3.15}$$

At the band edge, we have

$$\mathbf{d}_{cv} = \mp\frac{3ea}{8\pi}(-n+m, \sqrt{3}(n+m)). \tag{3.16}$$

3.3.2 Nanotubes in Semiconductor Bloch Equations

The semiconductor Bloch equations describe the optical response of semiconductors excited by coherent classical light sources, such as lasers. They are based on a full quantum theory, and form a closed set of integro-differential equations for the quantum dynamics of microscopic polarization

and charge carrier distribution.

Hamiltonian in the electron-hole representation coupled to light field is

$$H = \sum_{\boldsymbol{k}} (E_{e,k}\alpha^{\dagger}_{\boldsymbol{k}}\alpha_{\boldsymbol{k}} + E_{h,k}\beta^{\dagger}_{-\boldsymbol{k}}\alpha_{-\boldsymbol{k}}) \tag{3.17}$$

$$+ \frac{1}{2}\sum_{\boldsymbol{k},\boldsymbol{k'},q\neq 0} (V^{ee}\alpha^{\dagger}_{\boldsymbol{k+q}}\alpha^{\dagger}_{\boldsymbol{k'-q}}\alpha_{\boldsymbol{k}}\alpha_{\boldsymbol{k'}} + V^{hh}\beta^{\dagger}_{\boldsymbol{k+q}}\beta^{\dagger}_{\boldsymbol{k'-q}}\beta_{\boldsymbol{k}}\beta_{\boldsymbol{k'}} + V^{eh}2\alpha^{\dagger}_{\boldsymbol{k+q}}\beta^{\dagger}_{\boldsymbol{k'-q}}\beta_{\boldsymbol{k'}}\alpha_{\boldsymbol{k}}) \tag{3.18}$$

$$- \sum_{\boldsymbol{k}} \mathcal{E}(t)(d_{cv}\alpha^{\dagger}_{\boldsymbol{k}}\beta^{\dagger}_{-\boldsymbol{k}} + h.c.). \tag{3.19}$$

Here α and β are electron and hole operators, $E_{e/h}$ is the corresponding energy, V is Fourier transformed Coulomb interaction, $\mathcal{E}$ is the light field and d_{cv} is the interband dipole moment.

Calculating the equations of motion for this system from this Hamiltonian, we get semiconductor Bloch equations:

$$\frac{\partial \boldsymbol{P_k}}{\partial t} = -i(e_{e,k} + e_{h,k})P_k - i(n_{e,k} + n_{h,k-1})\omega_{R,k} + \frac{\partial P_k}{\partial t}|_{\text{scatter}}, \tag{3.20}$$

$$\frac{\partial n_{e,k}}{\partial t} = -2\text{Im}(\omega_{R,k}P^*_k) + \frac{\partial n_{e,k}}{\partial t}|_{\text{scatter}}, \tag{3.21}$$

$$\frac{\partial n_{h,k}}{\partial t} = -2\text{Im}(\omega_{R,k}P^*_k) + \frac{\partial n_{h,k}}{\partial t}|_{\text{scatter}}. \tag{3.22}$$

Here $P_k(t) =< \beta_{-k}\alpha_k >$ is pair function, $n_e =< \alpha^{\dagger}\alpha >$ is electron density, $n_h =< \beta^{\dagger}\beta >$ is hole density, $\hbar e_{i,k} = E_{i,k} + \sum_q V^{i,e}_{k,q} n_{e,q} + \sum_q V^{i,h}_{k,q}(1 - n_{h,q})$ is renormalized energy, $\omega_{R,k}$ is renormalized Rabi frequency:

$$\omega_{R,k} = \frac{1}{\hbar}(d_{cv}\mathcal{E} + \sum_k V^{e,h}_{k,q} P_{k+q}). \tag{3.23}$$

After we calculate polarization P, the following equations yield our gain or absorption:

$$P = \chi\epsilon_0\mathcal{E}, \tag{3.24}$$

$$g(\omega) = \frac{4\pi\omega}{n_b c}\chi''(\omega). \tag{3.25}$$

3.4 Results and Discussion

The numerical calculation is based on dense, purified, highly aligned SWCNT(6,5) films, with area density $1/100^{-2}$ in cross section. Fig. 3.3 is the schematic representation of using SWCNT thin films to obtain SF.

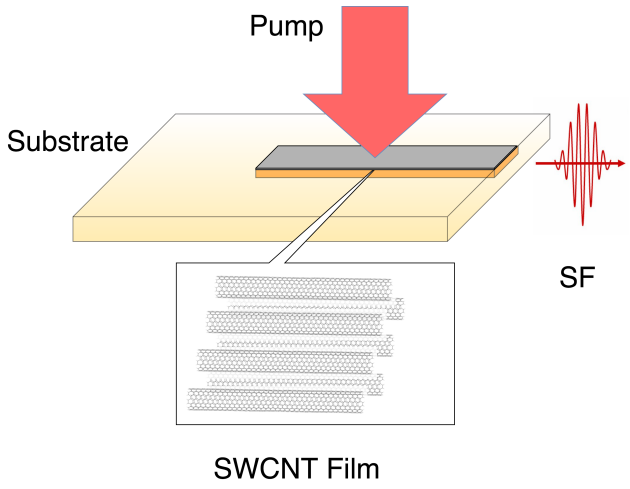

Figure 3.3: Schematic representation of obtaining SF with SWCNT thin film.

Fig. 3.4 shows the numerical calculation result of the absorption spectrum when different effects are included. For the tight-binding model in a single electron picture, SWCNT(6,5) shows an absorption peak at about 1100 meV with a tail. If electron-electron exchange is included, the absorption peak blue shifts to around 1500 meV. However, if electron-hole attraction is included, the absorption peak red shifts back to about 1180 meV, without a tail. This excitonic absorption shape agrees well with experimental results. Coulomb effects in this result are of the order of 100 meV, which is much larger than in conventional 3D semiconductors.

Fig. 3.5 shows the optical response of SWCNT(6,5) with different electron-hole densities. As the density grows, gain emerges within a specific energy region. In this calculation, the maximum

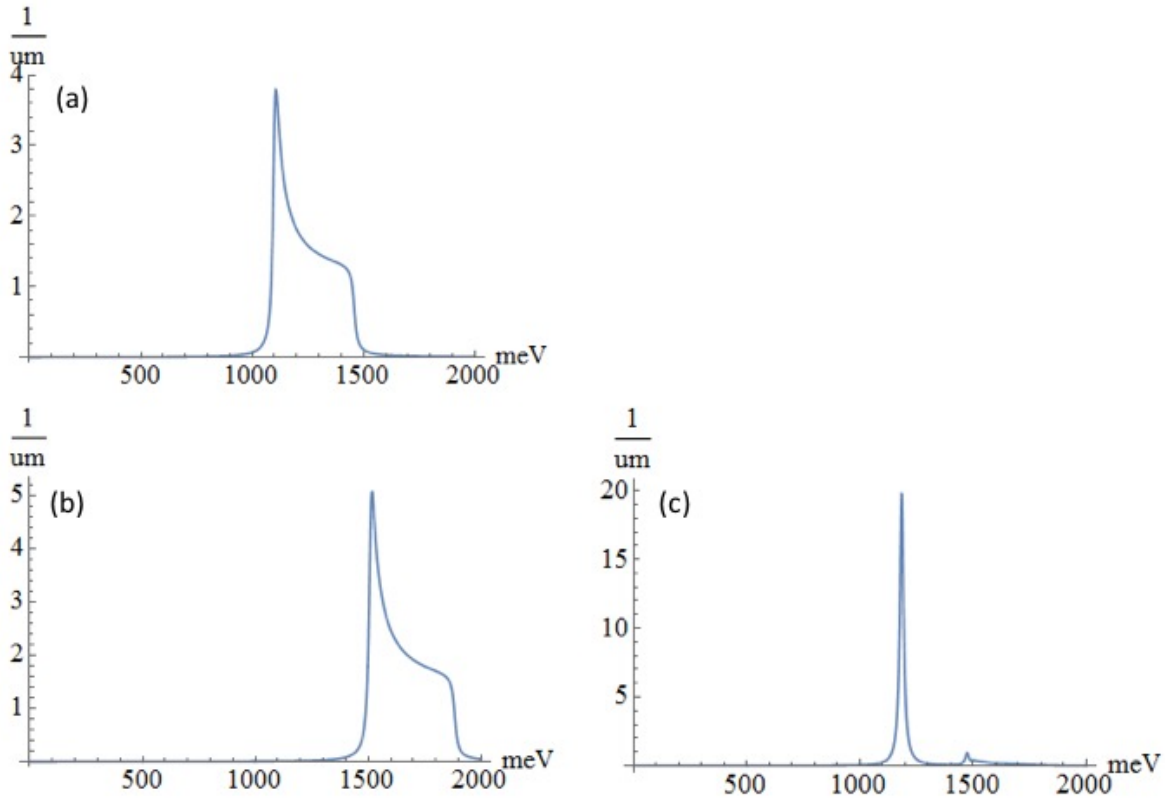

Figure 3.4: Numerical calculation of absorption with different models for SWCNT(6,5). (A) single-electron model with tight-binding approximation; (B) with screened electron-electron exchange energy; (C) with screened electron-hole attraction.

gain is obtained when electron-hole density is 0.17 N ($N = 1/40000^{-3}$). If one considers a waveguide mode with 10% overlap with a SWCNT film, the growth rate would be $10^{14}s^{-1}$, which is faster than the dephasing rate.

Our simulation result shows that for strong enough excitation, the growth rate of the EM field can be as high as 10^{14} s^{-1}, i.e. exceed the dephasing rate, which can lead to efficient generation of SF pulses. Future works could be done for the detailed calculation of the SF process, especially at the nonlinear stage.

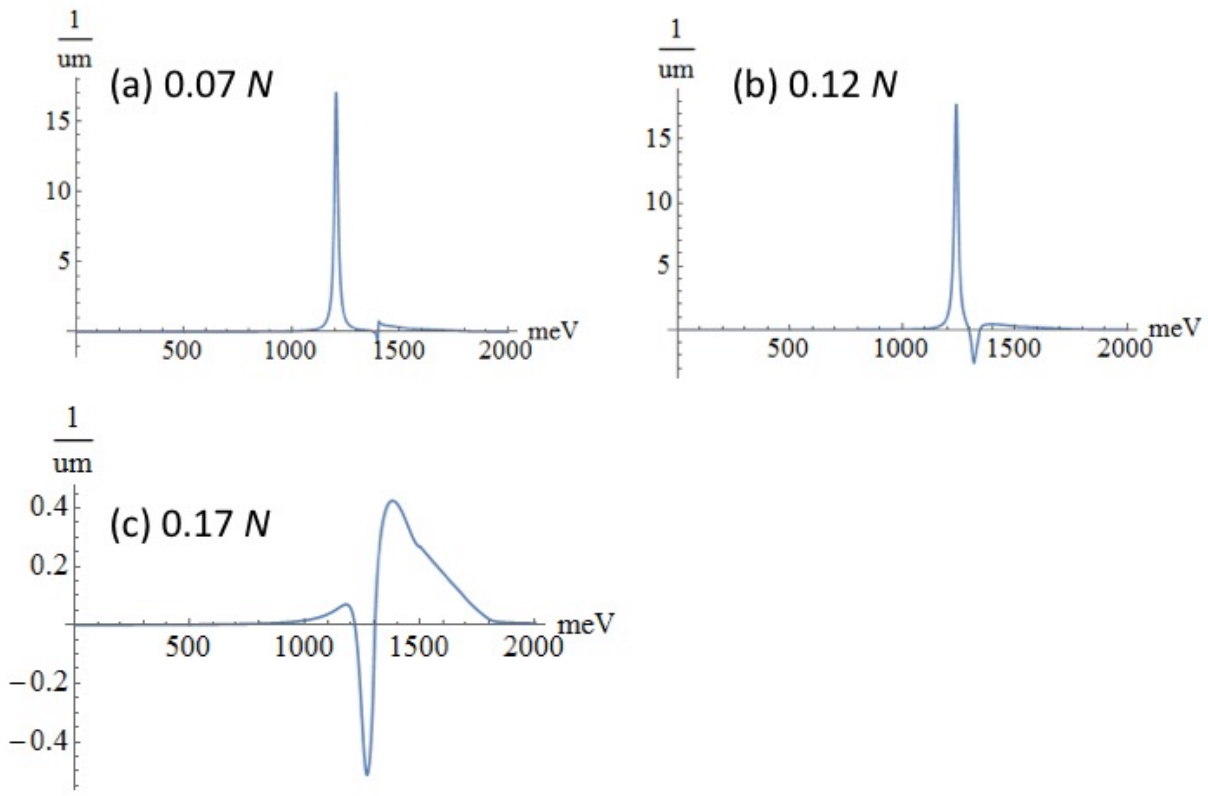

Figure 3.5: Numerical calculation of absorption with different electron-hole densities for SWCNT(6,5). (A) electron-hole density 0.07 N ($N = 1/40000^{-3}$); (B) density 0.12 N; (C) density 0.17 N.

3.4 References

[1] S. Iijima, Nature 354, 56-58 (1991).

[2] S. Iijima, T. Ichihashi, Y. Ando, Nature 356, 776-778 (1992).

[3] S. iijima, T. Ichihashi, Nature 363 603-605 (1993).

[4] R. Martel, V. Derycke, C. Lavoie, J. Appenzeller, K. K. Chan, et al., Phys. Rev. Lett. 87, 256805 (2001).

[5] M. Itkis, F. Borondics, A. Yu, R. Haddon, Science 312, 413-416 (2006).

[6] E. Gaufres, N. Izard, X. Le Roux, D. Marris-Morini, S. Kazaoui, et al., Appl. Phys. Lett. 96, 231105 (2010).

[7] G. D. Scholes, S. Tretiak, T. J. McDonald, W. K. Metzger, C. Engtrakul, et al., J. Phys. Chem. C 111, 11139-11149 (2007).

[8] Z. Zhu, J. Crochet, M. S. Arnold, M. C. Hersam, H. Ulbricht, et al., J. Phys. Chem. C 111, 3831-3835 (2007).

[9] R. H. Dicke, Phys. Rev. 93, 99-110 (1954).

[10] M. S. Hybertsen, S. G. Louie, Phys. Rev. B 34, 5390 (1986).

[11] M. Rohlfing, S. G. Louie, Phys. Rev. B 62, 4927 (2000).

[12] L. A. Falkovsky, J. Phys.: Conf. Ser. 129, 012004(2008).

[13] B. Partoens, F. M. Peeters, Phys Rev B 74, 075404 (2006).

[14] P. Avouris, Z. Chen, V. Perebeinos, Nat. Nanotechnol 2, 605-615 (2007).

4. ENHANCEMENT OF THE SPONTANEOUS EMISSION IN SUBWAVELENGTH QUASI TWO-DIMENSIONAL WAVEGUIDES AND RESONATORS*

4.1 Introduction

Enhancement of the radiative processes due to the localization of emitters in a subwavelength cavity (so-called Purcell enhancement [1]) is a fundamental cavity-quantum electrodynamics (QED) effect which finds an increasingly broad range of applications in the areas as diverse as nanophotonics, plasmonics, linear and nonlinear optical sensing, and high-speed communications, to name a few. It has been studied theoretically and experimentally so many times that it is hard to believe that any further development is needed. However, there seems to be a significant gap in the formalism for the situations typically encountered in quantum optoelectronic devices, when the electron ensemble is out of equilibrium and there is strong dissipation both in the optical dipole oscillations in a macroscopic ensemble of fermionic emitters (e.g. electrons and holes in a semiconductor quantum well or a layer of quantum dots, or a 2D semiconductor such as MoS_2, or monolayer graphene) and for the electromagnetic (EM) field in a cavity. Examples include subwavelength semiconductor lasers [2, 3, 4, 5, 6] and other devices or circuits with subwavelength confinement in one or more dimensions e.g. [7, 8, 9]. In this case using a simple Purcell-type factor $\sim Q\lambda^3/V$, where Q is a quality factor of EM modes in a cavity of volume V and λ is the emission wavelength, can drastically overestimate the cavity enhancement of the spontaneous emission. Although this fact is well known, a consistent QED theory including dissipation and fluctuations is usually replaced by a more phenomenological rate equations approach [3]. Recent theoretical analysis of subwavelength lasers [2] did include QED Heisenberg-Langevin equations for the EM cavity modes, but not for the dynamics of the active medium.

Here we use a consistent Heisenberg-Langevin approach [10, 11] which includes dissipation

and fluctuations in the fermionic ensemble and in the EM field of a subwavelength cavity on equal footing. Note that the description of dissipation and noise of a quantum field due to its interaction with an active nonequilibrium medium require a completely different approach as compared to the effects of Ohmic losses or radiation losses in an electrodynamic system. The latter effects can be analyzed within a standard fluctuation-dissipation theorem [12]. The standard description would also work for a popular model of a dissipative reservoir as an equilibrium ensemble of oscillators [13]. This approach would only allow one to describe thermal emission from a medium in thermal equilibrium. In contrast, our formalism allows us to treat radiation effects and obtain a correct expression for the current operator including fluctuations due to nonequilibrium electron systems, e.g. in the presence of pumping, beyond the applicability of the standard fluctuation-dissipation theorem. The Langevin noise operators that we introduce are not based on a model of a thermal reservoir. Instead, they are derived directly from the condition of preserving the commutation relations and generalized Einstein relations [13]. Therefore, they can be applied to any dissipation/fluctuation mechanism.

We apply the general formalism to the problem of spontaneous emission in a quasi-2D waveguide or cavity with subwavelength confinement in one direction. Remarkably, we are able to derive closed-form analytic results for all relevant quantities such as spontaneous emission power for simple but practically important geometries: strip lines and rectangular cavities. Our results provide general framework and convenient formulas for the evaluation of enhancement of radiative processes in such systems. Our results also indicate that a significant enhancement of the spontaneous emission, by a factor of order 100 or higher, is possible for QWs and other 2D emitters sandwiched between metal plates in a subwavelength cavity.

Section II describes the spatial structure of the EM field in a subwavelength quasi-2D electrodynamic structure and develops the quantization procedure. Section III introduces coupling to the fermionic system. Section IV derives and solves Heisenberg-Langevin equations for the density operator of quasiparticles and EM field operators. It derives the expression for the spontaneous emission power and its useful limiting cases.

4.2 Electromagnetic field of a subwavelength cavity

4.2.1 Spatial structure of the EM field modes

Consider a very thin layer of quantum dipole emitters (which we will call a quantum well (QW) for brevity, although it can be any fermionic system), placed inside a strip line or a cavity formed by two metallic planes at $z = \pm L_z/2$ where $L_z \ll c/\sqrt{\bar{\varepsilon}}\omega$, where $\bar{\varepsilon}$ is a typical (average) value of the dielectric constant $\varepsilon = \varepsilon(z)$ of the filling; see Fig. 1.

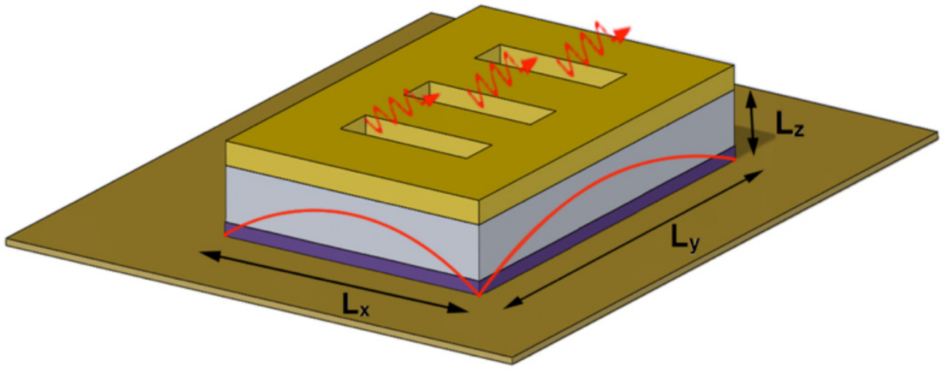

Figure 4.1: A sketch of a nanocavity with thickness L_z much smaller than wavelength. An active layer of 2D emitters is shown in dark blue. The profile of the electric field of the fundamental TE_{011} mode is sketched on the sides. The radiation can be outcoupled through the gratings or cavity edges.

A TM-polarized EM field is described by the following components of the electric field, magnetic field and electric induction:

$$(\boldsymbol{E}_{x,z}, \boldsymbol{B}_y, \boldsymbol{D}_{x,z}) = \mathrm{Re}\left[\left(\tilde{\boldsymbol{E}}_{x,z}(z), \tilde{\boldsymbol{B}}_y(z), \tilde{\boldsymbol{D}}_{x,z}(z)\right) e^{-i\omega t + iqx}\right] \tag{4.1}$$

Where we assumed that the strip line is oriented along x. From Maxwell's equations,

$$\nabla \cdot \boldsymbol{D} = 0, \quad \nabla \times \boldsymbol{B} = \frac{\dot{\boldsymbol{D}}}{c}, \quad \nabla \times \boldsymbol{E} = -\frac{\dot{\boldsymbol{B}}}{c} \tag{4.2}$$

together with the material equation,

$$\boldsymbol{D} = \varepsilon(z)\boldsymbol{E} \tag{4.3}$$

we obtain:

$$\frac{\partial \tilde{D}_z}{\partial z} = -iq\tilde{D}_x, \quad iq\tilde{B}_y = -\frac{i\omega\tilde{D}_z}{c}, \quad \frac{\partial \tilde{E}_x}{\partial z} = i\frac{\omega}{c}\tilde{B}_y(z) + i\frac{q}{\varepsilon(z)}\tilde{D}_z \tag{4.4}$$

The first equation in (4) yields

$$\tilde{D}_z = \tilde{D}_z\left(-\frac{L_z}{2}\right) - iq\int\limits_{-\frac{L_z}{2}}^{z}\tilde{D}_x dz'$$

For subwavelength thickness $L_z q \ll 1$ the previous equation gives $\tilde{D}_z \approx$ const, which corresponds to the quasi-electrostatic structure of the field in the (y, z) cross section of the strip line. From the second and third equations in Eq. (4.4) we can obtain

$$\frac{\partial \tilde{E}_x}{\partial z} = -i\frac{\omega^2\tilde{D}_z}{qc^2} + i\frac{q}{\varepsilon(z)}\tilde{D}_z \tag{4.5}$$

Next we integrate Eq. (4.5) as $\int\limits_{-\frac{L_z}{2}}^{\frac{L_z}{2}} dz \ldots$, taking into account $\tilde{D}_z \approx const$ and the boundary conditions on the metal planes: $\tilde{E}_x(+\frac{L_z}{2}) = \tilde{E}_x(-\frac{L_z}{2}) = 0$. As a result, we obtain the dispersion relation:

$$\frac{\omega^2}{q^2c^2} = \frac{1}{L_z}\int\limits_{-\frac{L_z}{2}}^{\frac{L_z}{2}}\frac{dz}{\varepsilon(z)}. \tag{4.6}$$

Since the direction of x-axis was arbitrary, we can represent the electric field vector as

$$\boldsymbol{E} = D_q\boldsymbol{F_q}(\boldsymbol{r})e^{-i\omega_q t} + \text{C.C.}, \tag{4.7}$$

where the factor $\boldsymbol{F_q}(\boldsymbol{r})$ determines the spatial structure of the field:

$$\boldsymbol{F_q}(\boldsymbol{r}) = \boldsymbol{z_o}\frac{e^{i\boldsymbol{qr}}}{\varepsilon(z)}, \tag{4.8}$$

vector $\boldsymbol{q}$ is in the (x, y) plane, D_q is a constant which in this case corresponds to a z-independent amplitude of the electric induction. According to the Brillouin concept, one can use the waves defined by Eqs. (4.6)-(4.8) to construct any waveguide and cavity modes. They have quasi-TEM polarization. In particular, if the sides $y = \pm L_y/2$ are also metal-coated, consider the lowest order (01) waveguide mode:

$$\boldsymbol{E} = D_{q_x}\boldsymbol{F}_{q_x}(\boldsymbol{r})e^{-i\omega_{q_x}t} + \text{C.C.}, \quad q_x^2 + \left(\frac{\pi}{L_y}\right)^2 = \frac{\omega^2}{c^2}\frac{L_z}{\int\limits_{-\frac{L_z}{2}}^{\frac{L_z}{2}} \varepsilon(z)^{-1}dz} \tag{4.9}$$

where the explicit form to the factor $\boldsymbol{F_{q_x}}(\boldsymbol{r}) \propto e^{-iq_x x}$ is given below. If the facets $x = \pm L_x/2$ are metal-coated as well, the waveguide becomes a resonator and the lowest order modes are TE_{01N}:

$$\boldsymbol{E} = D_N\boldsymbol{F}_N(\boldsymbol{r})e^{-i\omega_N t} + \text{C.C.}, \quad \left(\frac{N\pi}{L_x}\right)^2 + \left(\frac{\pi}{L_y}\right)^2 = \frac{\omega^2}{c^2}\frac{L_z}{\int\limits_{-\frac{L_z}{2}}^{+\frac{L_z}{2}} \varepsilon(z)^{-1}dz} \tag{4.10}$$

In Eqs. (4.9) and (4.10) the factors D_{q_x} and D_N are coordinate-independent amplitudes of the electric induction. The factors $\boldsymbol{F}_{\boldsymbol{q},q_x,N}(\boldsymbol{r})$ in Eqs. (4.7), (4.9), (4.10) can be written in the same form using the index $\nu = \boldsymbol{q}, q_x, N$ to denote a corresponding spatial structure:

$$\boldsymbol{F}_\nu(\boldsymbol{r}) = \boldsymbol{z_o}\frac{\zeta_\nu(x,y)}{\varepsilon(z)}, \;\; \zeta_{\boldsymbol{q}} = e^{i\boldsymbol{qr}}, \;\; \zeta_{q_x} = \cos\left(\frac{\pi y}{L_y}\right)e^{iq_x x}, \;\; \zeta_N = \cos\left(\frac{\pi y}{L_y}\right) \times \begin{cases} \cos\left(\dfrac{N_{odd}\pi x}{L_x}\right) \\ \sin\left(\dfrac{N_{even}\pi x}{L_x}\right) \end{cases} \tag{4.11}$$

where $\int_S \zeta_\nu \zeta_{\nu'}^* d^2r \propto \delta_{\nu\nu'}$. For a particular case of a uniform dielectric constant, Eqs. (4.6)-(4.11) are exact. Similar equations can be derived if one simply utilizes jumps of the dielectric constants

on the sides instead of metal coating. Even without any jump in the dielectric constants, an open end of a thin waveguide with vertical size much smaller than wavelength is a good reflector and therefore any radiation losses through the facets are small and are not affecting the mode spatial structure significantly.

4.2.2 Field quantization in a subwavelength waveguide/cavity

Here we consider field quantization in a volume $V = L_z S$, where $S = L_x \times L_y$. The field operator can be represented in a standard form [14, 15]:

$$\hat{\boldsymbol{E}} = \sum_{\nu} [\boldsymbol{E}(\boldsymbol{r})_{\nu} \hat{c}_{\nu} + \boldsymbol{E}^{*}(\boldsymbol{r})_{\nu} \hat{c_{\nu}}^{\dagger}] \tag{4.12}$$

where $\hat{c}_{\nu}$ and $\hat{c_{\nu}}^{\dagger}$ are boson annihilation and creation operators, $\boldsymbol{E}_{\nu}(\boldsymbol{r}) = \boldsymbol{z_{\mathrm{o}}} \dfrac{\zeta_{\nu}(x,y)}{\varepsilon(z)} D_{\nu}$, and D_{ν} is the normalization constant corresponding to the z-independent amplitude of the electric induction. The value of D_{ν} needs to be chosen in such a way that the commutation relation for boson operators $\hat{c}_{\nu}$ and $\hat{c_{\nu}}^{\dagger}$ have a standard form $[\hat{c}_{\nu}, \hat{c_{\nu}}^{\dagger}] = \delta_{\nu\nu'}$. In this case the field Hamiltonian will also be standard:

$$\hat{H}_f = \sum_{\nu} \hbar\omega_{\nu} (\hat{c_{\nu}}^{\dagger} \hat{c}_{\nu} + \frac{1}{2}) \tag{4.13}$$

To find the explicit expression for D_{ν} we apply the phenomenological procedure of field quantization in a medium [14, 16] which was justified in [17] based on a rigorous quantum electrodynamics theory. According to this approach, the normalization is determined by the requirement that the classical energy density W of the EM field $\boldsymbol{E} = \boldsymbol{E_{\nu}}(\boldsymbol{r}) e^{-i\omega_{\nu} t} + \mathrm{C.C.}$, $\boldsymbol{B} = \boldsymbol{B_{\nu}}(\boldsymbol{r}) e^{-i\omega_{\nu} t} + \mathrm{C.C}$ give the total energy of $\int_V W d^3 r = \hbar\omega_{\nu}$. For our strip line this procedure yields the following expression for the normalization constant (see Appendix A):

$$|D_{\nu}|^2 = \frac{2\pi\hbar\omega_{\nu}}{\int_S \zeta_{\nu}\zeta_{\nu}^{*} d^2 r \times \int\limits_{-\frac{L_z}{2}}^{\frac{L_z}{2}} \dfrac{1}{2\varepsilon^2(\omega_{\nu}, z)\omega_{\nu}} \left[\dfrac{\partial(\omega^2 \varepsilon(\omega, z)}{\partial\omega}\right]_{\omega=\omega_{\nu}} dz}, \tag{4.14}$$

where $\int_S \zeta_{\boldsymbol{q}}\zeta^*_{\boldsymbol{q}} d^2r = S$, $\int_S \zeta_{q_x}\zeta^*_{q_x} d^2r = S/2$ and $\int_S \zeta_N\zeta^*_N d^2r = S/4$. In the limiting case of plane waves in a homogeneous medium Eq. (4.14) corresponds to a standard normalization of the electric field [14, 17, 16]; indeed, taking into account that in a homogeneous medium $D_\nu = E_\nu\varepsilon(\omega_\nu)$, Eq. (4.14) gives $|E_\nu|^2 = \dfrac{2\pi\hbar\omega_\nu}{\dfrac{V}{2\omega_\nu}\left[\dfrac{\partial(\omega^2\varepsilon(\omega,z)}{\partial\omega}\right]_{\omega=\omega_\nu}}$, where $V = L_z S$ is the quantization volume.

4.3 Non-dissipative dynamics of a coupled system of photons and electrons

4.3.1 General formalism

We will denote a quantum state of an electron in a QW or any other 2D nanostructure by a band index m which may include also the subband, spin, and valley index as needed, and the 2D quasimomentum $\boldsymbol{k}$ corresponding to the motion in (x, y) plane. The second-quantized energy of a system of such quasiparticles is

$$\hat{H}_e = \sum_{m\boldsymbol{k}} W_{m\boldsymbol{k}} \hat{a}^\dagger_{m\boldsymbol{k}} \hat{a}_{m\boldsymbol{k}} \tag{4.15}$$

where $\hat{a}^\dagger_{m\boldsymbol{k}}, \hat{a}_{m\boldsymbol{k}}$ are creation and annihilation operators of fermions, $W_{m\boldsymbol{k}} \equiv W_{mm\boldsymbol{kk}}$ are the diagonal matrix elements of the energy operator of a quasiparticle. The eigenfunctions can be written as

$$|m, \boldsymbol{k}\rangle = \frac{e^{i\boldsymbol{kr}}}{\sqrt{S}}\psi_m(z) \tag{4.16}$$

where $\int_S e^{i(\boldsymbol{k}-\boldsymbol{k}')\boldsymbol{r}} d^2r = S\delta_{\boldsymbol{kk}'}$, $\int\limits_{-\frac{l}{2}}^{\frac{l}{2}} \psi_m(z)\psi^*_n(z)dz = \delta_{mn}$. Here we assume that a 2D nanostructure occupies a region $-l/2 \le z \le l/2$, $l \le L_z$. The total Hamiltonian of a coupled system of photons and electrons is

$$\hat{H} = \hat{H}_f + \hat{H}_e + \hat{V} \tag{4.17}$$

where the operators $\hat{H}_f$ and $\hat{H}_e$ are given by Eqs. (4.13) and (4.15), and $\hat{V}$ is the interaction Hamiltonian, which can also be written in the second-quantized form:

$$\hat{V} = \sum_{mn\boldsymbol{kk}'} \hat{V}_{nm\boldsymbol{k}'\boldsymbol{k}} \hat{\rho}_{nm\boldsymbol{kk}'} \tag{4.18}$$

where $\hat{\rho}_{nm\boldsymbol{k}\boldsymbol{k}'} = \hat{a}^{\dagger}_{n\boldsymbol{k}'}\hat{a}_{m\boldsymbol{k}}$ is the density operator. Matrix elements $\hat{V}_{nm\boldsymbol{k}'\boldsymbol{k}}$ in Eq. (4.18) are operators since they depend on the quantum field.

Taking into account the quasi-electrostatic structure of the electric field in the transverse cross-section of a strip line, we can write the interaction Hamiltonian in the electric potential approximation:

$$\hat{V} = e \int\limits_{-l/2}^{z} \hat{E}_z dz \tag{4.19}$$

Using Eq. (4.12) for the field operator, the matrix elements of the interaction Hamiltonian are

$$\hat{V}_{nm\boldsymbol{k}'\boldsymbol{k}} = -\tilde{d}_{nm} \sum_{\nu} (D_\nu \hat{c}_\nu \zeta^{(\nu)}_{\boldsymbol{k}'\boldsymbol{k}} + D^*_\nu \hat{c}^{\dagger}_\nu \zeta^{(\nu)\dagger}_{\boldsymbol{k}'\boldsymbol{k}}) \tag{4.20}$$

where $\tilde{d}_{nm}$ is the effective dipole moment of the optical transition:

$$\tilde{d}_{nm} = -e \int\limits_{-l/2}^{l/2} \left[\psi^*_n(z) \left(\int\limits_{-l/2}^{z} \frac{dz'}{\varepsilon(z')} \right) \psi_m(z) \right] dz \tag{4.21}$$

$$\zeta^{(\nu)}_{\boldsymbol{k}'\boldsymbol{k}} = \frac{1}{S} \int_S e^{-i\boldsymbol{k}'r} \zeta_\nu(x,y) e^{i\boldsymbol{k}r} d^2r, \zeta^{(\nu)\dagger}_{\boldsymbol{k}'\boldsymbol{k}} = (\zeta^{(\nu)}_{\boldsymbol{k}'\boldsymbol{k}})^* \tag{4.22}$$

For a homogeneous medium, in which $E_\nu = D_\nu/\varepsilon$, Eq. (20) will contain a standard expression $\tilde{d}_{nm} D_\nu = -e\langle n|z|m\rangle E_\nu$.

The Hamiltonian Eq. (4.17) gives rise to the Heisenberg equations for photon operators:

$$\begin{aligned} \dot{\hat{c}}_\nu &= \frac{i}{\hbar}[\hat{H}, \hat{c}_\nu] = -i\omega_\nu \hat{c}_\nu + \frac{i}{\hbar} D^*_\nu \sum_{mn\boldsymbol{k}\boldsymbol{k}'} \tilde{d}_{nm} \zeta^{(\nu)\dagger}_{\boldsymbol{k}'\boldsymbol{k}} \hat{\rho}_{mn\boldsymbol{k}\boldsymbol{k}'}, \\ \dot{\hat{c}}^{\dagger}_\nu &= \frac{i}{\hbar}[\hat{H}, \hat{c}^{\dagger}_\nu] = i\omega_\nu \hat{c}^{\dagger}_\nu - \frac{i}{\hbar} D_\nu \sum_{mn\boldsymbol{k}\boldsymbol{k}'} \tilde{d}_{nm} \zeta^{(\nu)}_{\boldsymbol{k}'\boldsymbol{k}} \hat{\rho}_{mn\boldsymbol{k}\boldsymbol{k}'} \end{aligned} \tag{4.23}$$

We write a similar equation for the density operator using a shortcut notation $|m, \boldsymbol{k}\rangle = |\mu\rangle$ for brevity. Using the fundamental commutation relation [17, 18, 19]

$$[\hat{\rho}_{\mu'\eta'}, \hat{\rho}_{\mu\eta}] = (\delta_{\mu'\eta}\hat{\rho}_{\mu\eta'} - \delta_{\mu\eta'}\hat{\rho}_{\mu'\eta}) \tag{4.24}$$

which is valid whether the creation and annihilation operators $\hat{a}_\eta^\dagger$ and $\hat{a}_\mu$ satisfy the commutation relations for bosons or fermions, we obtain:

$$\dot{\hat{\rho}}_{\mu\eta} = \frac{i}{\hbar}[\hat{H}, \hat{\rho}_{\mu\eta}] = -\frac{i}{\hbar}\sum_{\mu'}(\hat{H}_{\mu\mu'}\hat{\rho}_{\mu'\eta} - \hat{\rho}_{\mu\mu'}\hat{H}_{\mu'\eta}) \tag{4.25}$$

The resulting equation for the density operator has the same form as the von Neumann equation, although the original Heisenberg equation had an opposite sign in front of the commutator [17, 18, 19]. This is to be expected, because for time-dependent Heisenberg operators $\hat{a}_\eta^\dagger$ and $\hat{a}_\mu$ the average of dyadics $\hat{\rho}_{\mu\eta} = \hat{a}_\eta^\dagger\hat{a}_\mu$ over the initial quantum state should correspond to a usual density matrix.

4.3.2 Matrix elements of the interaction Hamiltonian

The form of the interaction Hamiltonian for the fields with different spatial structure depends on the matrix elements $\zeta_{\boldsymbol{k}'\boldsymbol{k}}^{(\nu)}$ defined in Eq. (4.22). In particular, for plane waves we obtain $\zeta_{\boldsymbol{k}'\boldsymbol{k}}^{(\boldsymbol{q})} = \delta_{\boldsymbol{k}';\boldsymbol{k}+\boldsymbol{q}}$. For a waveguide or a cavity the corresponding expressions for $\zeta_{\boldsymbol{k}'\boldsymbol{k}}^{(q_x)}$ and $\zeta_{\boldsymbol{k}'\boldsymbol{k}}^{(N)}$ are quite cumbersome and are given in Appendix B.

If we take into account that the de Broglie wavelength of electrons is typically much smaller than the spatial scale of the EM field, i.e. $k \gg |\boldsymbol{q}|, q_x, \frac{\pi N}{L_x}, \frac{\pi N}{L_y}$, the expressions for matrix elements are simplified. Indeed, in this case we can assume that the optical transitions are direct in momentum space and take $\zeta_{\boldsymbol{k}'\boldsymbol{k}}^{(\nu)} \approx \alpha_\nu\delta_{\boldsymbol{k}'\boldsymbol{k}}$. The factor in front of the delta-function is one for plane waves; for a waveguide or a cavity one should choose $\alpha_\nu = \sqrt{\sum_{\boldsymbol{k}'}\zeta_{\boldsymbol{k}'\boldsymbol{k}}^{(\nu)}\zeta_{\boldsymbol{k}\boldsymbol{k}'}^{(\nu)\dagger}}$. With this choice, a resonance line which is âĂIJsmearedâĂİ in the quasimomentum space can be reduced to the delta-function $\alpha_\nu\delta_{\boldsymbol{k}'\boldsymbol{k}}$ while conserving the sum of intensities of all transitions within the line. The Parseval theorem then gives $\sum_{\boldsymbol{k}'}\zeta_{\boldsymbol{k}'\boldsymbol{k}}^{(\nu)}\zeta_{\boldsymbol{k}\boldsymbol{k}'}^{(\nu)\dagger} = S^{-1}\int_S \zeta_\nu\zeta_\nu^* d^2r$ (see Appendix B). As a result the matrix element can be written in the same form for plane waves, in a waveguide, and in a cavity:

$$\hat{V}_{nm\boldsymbol{k}\boldsymbol{k}'} \approx -\tilde{d}_{nm}\sum_\nu(\tilde{D}_\nu\hat{c}_\nu + \tilde{D}_\nu^*\hat{c}_\nu^\dagger)\delta_{\boldsymbol{k}'\boldsymbol{k}} \tag{4.26}$$

where

$$|\tilde{D}_\nu|^2 = \frac{2\pi\hbar\omega_\nu}{SG(L_z,\omega_\nu)} \tag{4.27}$$

$$G(L_z,\omega_\nu) = \int\limits_{-\frac{L_z}{2}}^{\frac{L_z}{2}} \frac{1}{2\varepsilon^2(\omega_\nu,z)\omega_\nu}\left[\frac{\partial(\omega^2\varepsilon(\omega,z)}{\partial\omega}\right]_{\omega=\omega_\nu} dz \tag{4.28}$$

Note that in a uniform nondispersive medium $\tilde{d}_{mn} = d_{mn}/\varepsilon$ and $G = L_z/\varepsilon$.

4.3.3 The probability of the spontaneous emission

Consider a spontaneous radiative transition $m \to n$ for a quasiparticle in an open electrodynamic system, e.g. in the space between two conducting planes or in a waveguide. The transition probability is usually calculated using Fermi's golden rule [20]:

$$A_{m\to n} = \frac{2\pi}{\hbar^2}\int d\Pi_f |V_{fi}|^2 \delta\left(\frac{W_i}{\hbar} - \frac{W_f}{\hbar} - \omega_\nu\right) \tag{4.29}$$

where the integration $\int d\Pi_f$ is taken over all final states of a system labeled by f. The matrix element V_{fi} in this case is equal to $\langle 1_\nu|\hat{V}_{nm\boldsymbol{k}'\boldsymbol{k}}|0_\nu\rangle$, where $|n_\nu\rangle$ is a Fock state of photons. Using Eqs. (4.20) and (4.26)-(4.28) we obtain

$$V_{fi} = -\tilde{d}_{nm} D^*_\nu \zeta^{(\nu)\dagger}_{\boldsymbol{k}'\boldsymbol{k}} \approx -\tilde{d}_{nm}\tilde{D}^*_\nu \delta_{\boldsymbol{k}'\boldsymbol{k}} \tag{4.30}$$

Taking into account the photon density of states, one can get for the radiation emitted into space between two conducting planes

$$d\Pi_f = \frac{S|\boldsymbol{q}|d\theta d\omega_q}{(2\pi)^2|\partial\omega_q/\partial\boldsymbol{q}|}$$

where θ determines the direction of vector $\boldsymbol{q}$ in the (x,y) plane. For the radiation emitted into a waveguide,

$$d\Pi_f = \frac{L_x d\omega_{q_x}}{2\pi|\partial\omega_{q_x}/\partial q_x|}$$

The resulting expressions for the spontaneous emission probabilities are

$$A^{(\boldsymbol{q})}_{m\to n} = \frac{2\pi|\tilde{d}_{mn}|^2\omega_{mn}|\boldsymbol{q}|}{\hbar G(L_z,\omega_{mn})|\partial\omega_q/\partial\boldsymbol{q}|_{\omega_q=\omega_{mn}}} \tag{4.31}$$

$$A^{(q_x)}_{m\to n} = \frac{2\pi|\tilde{d}_{mn}|^2\omega_{mn}}{\hbar L_y G(L_z,\omega_{mn})|\partial\omega_{q_x}/\partial q_x|_{\omega_{qx}=\omega_{mn}}} \tag{4.32}$$

where ω_{mn} is the transition frequency.

In order to use Fermi's golden rule in a cavity, one has to formally introduce the density of states assuming that the modal spectrum is spread near the resonance frequency ω_{mn} by the linewidth $\Delta\omega$:

$$d\Pi_f = \frac{(\Delta\omega/2\pi)}{(\omega_{mn}-\omega_N)^2+(\Delta\omega/2)^2}d\omega \tag{4.33}$$

which results in

$$A^{(N)}_{m\to n}(\Delta\omega) = \frac{2\pi|\tilde{d}_{mn}|^2\left(\dfrac{4\omega_{mn}}{\Delta\omega}\right)}{\hbar L_x L_y G(L_z,\omega_{mn})} \tag{4.34}$$

Eq. (4.34) is also valid for a waveguide at a critical frequency, i.e. for $|\partial\omega_{q_x}/\partial q_x| = 0$, because such a system is effectively a cavity. In a homogeneous medium, expressions (4.31), (4.32) and (4.34) can be simplified. In this case Eqs. (4.21) and (4.28) lead to

$$\frac{|\tilde{d}_{mn}|^2}{G(L_z,\omega_{mn})} = \frac{|d_{mn}|^2}{\dfrac{L_z}{2\omega_\nu}\left[\dfrac{\partial(\omega^2\varepsilon)}{\partial\omega}\right]_{\omega=\omega_{mn}}}$$

Finally we compare the spontaneous emission probability in a cavity with that in free space. The latter is equal to $A^{(0)} = \dfrac{4\omega^3|d_{mn}|^2\sqrt{\varepsilon}}{3\hbar c^3}$. Their ratio is

$$\frac{A^{(N)}_{m\to n}}{A^{(0)}} \approx \frac{3\pi}{2}\frac{(c/\omega\sqrt{\varepsilon})^3}{L_x L_y L_z}\left(\frac{4\omega_{21}}{\Delta\omega}\right) \tag{4.35}$$

Note that in Eq. (4.35) the minimal lateral sizes of an electrodynamic system we consider are $L_{x,y} = \pi c/\omega\sqrt{\varepsilon}$, whereas the value of L_z can be much smaller.

Up to a numerical factor which depends on geometry, Eq. (4.35) is a widely used expression for the Purcell enhancement of the spontaneous emission. However, Eqs. (4.31), (4.32), and (4.34) do not include the effects of nonradiative relaxation in an ensemble of fermions. Moreover, the above approach does not allow one to determine the line broadening in a cavity in a consistent way. To include all dissipation processes consistently, we use the Heisenberg-Langevin formalism.

4.4 Dissipative dynamics in an ensemble of photons and electrons

4.4.1 Heisenberg-Langevin equations for the quasiparticle density operator

Dissipative effects in an open quantum system can be taken into account by adding the relaxation operator $\hat{R}_{\mu\eta}$ and corresponding Langevin noise operator $\hat{F}_{\mu\eta}$ to the right-hand side of Eq. (4.25)[15, 10, 11, 21, 18, 19]. One cannot add dissipation phenomenologically, without including Langevin sources, because this would violate the fundamental commutation relation Eq. (4.24) [10, 11, 18, 19]. For the simplest model of "transverse" relaxation, when

$$\hat{R}_{\mu\neq\eta} = -\gamma_{\mu\eta}\hat{\rho}_{\mu\eta}. \tag{4.36}$$

Refs. [10, 11] derived the following expressions for the commutator and correlator of the Langevin noise (for a particular case of a two-level system):

$$\begin{aligned}[\hat{F}_{\mu\eta}(t'), \hat{F}^{\dagger}_{\mu\eta}(t)] &= (-\gamma_{\mu\eta}(\hat{\rho}_{\eta\eta} - \hat{\rho}_{\mu\mu}) + \hat{R}_{\eta\eta} - \hat{R}_{\mu\mu})\delta(t'-t) \\ \langle \hat{F}^{\dagger}_{\mu\eta}(t), \hat{F}_{\mu\eta}(t')\rangle &= (2\gamma_{\mu\eta}\langle\hat{\rho}_{\mu\mu}\rangle + \langle\hat{R}_{\mu\mu}\rangle)\delta(t'-t)\end{aligned} \tag{4.37}$$

where $\hat{F}^{\dagger}_{\mu\eta} = \hat{F}_{\eta\mu}$ and the symbol $\langle \dots \rangle$ means in this case the averaging over both the initial quantum state and the statistics of a dissipative reservoir. The dissipation operator in its simplest form of Eq. (4.36) implies the absence of any inertia in a dissipative subsystem; that is why the noise operator turns out to be delta-correlated in time. Note that for degenerate fermion distributions Eqs. (4.37) are valid if the evolution equation for the density operator includes exchange effects which take care of Pauli blocking.

The nonzero value of the relaxation operator for populations, $\hat{R}_{\mu\mu} \neq 0$ in Eq. (4.37) cor-

responds to the nonequilibrium distribution. A steady-state distribution can be nonequilibrium because of an external pumping. An incoherent pumping generally redistributes populations over many subbands; therefore within the model taking into account a limited number of subbands such a pumping is convenient to introduce as a source $\hat{J}_{\mu\eta}$ in the evolution equation for the density operator. This way we can assume that there is a âĂIJgeneralizedâĂİ relaxation operator $\hat{\tilde{R}}_{\mu\eta} = \hat{R}_{\mu\eta} + \hat{J}_{\mu\eta}$ on the right-hand side of Eq. (4.25), and the steady-state (but not necessarily equilibrium) distribution corresponds to the condition $\langle \hat{\tilde{R}}_{\mu\mu} \rangle = 0$ for all μ. Of course, the modification of the relaxation operator causes the noise operator to change. However, within the simplest model of Eq. (4.36) this does not affect the general form of Eqs. (4.37). One just needs to keep in mind that the relaxation constants $\gamma_{\mu\eta}$ and operators $\hat{R}_{\mu\mu}$ in Eq. (4.36), (4.37) contain the contribution from incoherent pumping.

The equation for the density operator can be further simplified if we (i) include only two subbands, i.e. $m, n = 1, 2$; (ii) assume that optical transitions in the interaction Hamiltonian are direct; see Eq. (4.26). In this case the equation for the off-diagonal density operator elements includes only the elements $\hat{\rho}_{21\boldsymbol{kk}}$ and $\hat{\rho}_{12\boldsymbol{kk}} = \hat{\rho}^{\dagger}_{21\boldsymbol{kk}}$ Finally, (iii) we assume populations to satisfy $\hat{R}_{11\boldsymbol{kk}} = \hat{R}_{22\boldsymbol{kk}} = 0$. This gives

$$\dot{\hat{\rho}}_{21\boldsymbol{kk}} + i\omega_{21}(\boldsymbol{k})\hat{\rho}_{21\boldsymbol{kk}} + \gamma_{21\boldsymbol{kk}}\hat{\rho}_{21\boldsymbol{kk}} = \frac{i\tilde{d}_{21}}{\hbar}\left(\sum_{\nu}\tilde{D}_{\nu}\hat{c}_{\nu}\right)\cdot(\hat{\rho}_{11\boldsymbol{kk}} - \hat{\rho}_{22\boldsymbol{kk}}) + \hat{F}_{21\boldsymbol{kk}}, \qquad (4.38)$$

where $\omega_{21}(\boldsymbol{k}) = \dfrac{W_{2\boldsymbol{k}} - W_{1\boldsymbol{k}}}{\hbar}$.

As usual, the properties pf the Langevin source $\hat{F}_{21\boldsymbol{kk}}(t)$ in Eq. (4.38) are convenient to express through the properties of its spectral components: $\hat{F}_{21\boldsymbol{kk}}(t) = \int\limits_{\infty} \hat{F}_{\omega;21\boldsymbol{kk}} e^{i\omega t} d\omega$, $\hat{F}_{-\omega;12\boldsymbol{kk}} = \hat{F}^{\dagger}_{\omega;21\boldsymbol{kk}}$. Taking into account that $\hat{R}_{11\boldsymbol{kk}} = \hat{R}_{22\boldsymbol{kk}} = 0$, we can get from Eq. (4.37) (see also [10, 19])

$$\langle \hat{F}^{\dagger}_{\omega;21\boldsymbol{kk}} \hat{F}_{\omega';21\boldsymbol{kk}} \rangle = \frac{\gamma_{21\boldsymbol{kk}}}{\pi} n_{2\boldsymbol{k}} \delta(\omega - \omega'), \quad \langle \hat{F}_{\omega;21\boldsymbol{kk}} \hat{F}^{\dagger}_{\omega';21\boldsymbol{kk}} \rangle = \frac{\gamma_{21\boldsymbol{kk}}}{\pi} n_{1\boldsymbol{k}} \delta(\omega - \omega'), \qquad (4.39)$$

where $n_{1\boldsymbol{k}} = \langle \hat{\rho}_{11\boldsymbol{kk}} \rangle$ and $n_{2\boldsymbol{k}} = \langle \hat{\rho}_{22\boldsymbol{kk}} \rangle$ are constant populations supported by pumping.

4.4.2 Heisenberg-Langevin equations for field operators

Similarly to relaxation in the medium, relaxation of the EM field gives rise to the noise sources in the equations for field operators [15]. When field absorption by fermions is included, the noise term for the EM field appears due to Langevin noise terms in the density operator equations [10, 11, 19, 22]. Including any additional field absorption unrelated to absorption in the medium should be accompanied by adding Langevin noise terms directly to field equations. We take into account this additional absorption for the νth mode of the field by including phenomenological dissipative operators $-\Gamma\hat{c}_\nu$ and $-\Gamma\hat{c}_\nu^\dagger$ to the right-hand side of the field equations (4.23). To preserve the commutation relation $[\hat{c}_\nu, \hat{c}_\nu^\dagger]$ we need to add the Langevin noise operator $\hat{L}(t)$, satisfying the commutation relation $[\hat{L}(t'), \hat{L}^\dagger(t)] = 2\Gamma\delta(t-t')$ (see Appendix C). Its correlator is equal to $\langle\hat{L}^\dagger(t')\hat{L}(t)\rangle = \Xi \cdot 2\Gamma\delta(t-t')$, where the parameter Ξ is determined by a state of a dissipative resevoir. When the latter is in equilibrium, we obtain [15] $\Xi = (e^{\hbar\omega_\nu/T} - 1)^{-1}$.

Next we take into account that the dissipation of a given νth mode of the EM field could also be due to absorption in metal walls and bulk material unrelated to the active medium. In this case we add the dissipative operators to the right-hand side of Eq. (4.23), $-(\Gamma_r + \Gamma_\sigma)\hat{c}_\nu$ and $-(\Gamma_r + \Gamma_\sigma)\hat{c}_\nu^\dagger$, together with corresponding Langevin noise terms, $\hat{L}_r^{(\nu)}$ and $\hat{L}_\sigma^{(\nu)}$. Here the factor Γ_r describes radiative and diffraction losses out from the cavity and Γ_σ describes Ohmic losses. Taking into account Eq. (4.26) for the interaction Hamiltonian, we obtain

$$\dot{\hat{c}}_\nu + (i\omega_\nu + \Gamma_r + \Gamma_\sigma)\cdot\hat{c}_\nu = \frac{i\tilde{d}_{12}\tilde{D}_\nu^*}{\hbar}\sum_{\nu}\hat{\rho}_{21\boldsymbol{kk}} + \hat{L}_r^{(\nu)} + \hat{L}_\sigma^{(\nu)}. \tag{4.40}$$

Here the Langevin sources can again be defined through the properties of their spectral compo-

nents:

$$\hat{L}^{(\nu)}_{r,\sigma} = \int_{\infty} \hat{L}^{(\nu)}_{r,\sigma;\omega} e^{-i\omega t} d\omega, \quad \hat{L}^{(\nu)}_{r,\sigma;-\omega} = \hat{L}^{(\nu)\dagger}_{r,\sigma;\omega};$$
$$\langle \hat{L}^{(\nu')\dagger}_{r,\sigma';\omega'} \hat{L}^{(\nu)}_{r,\sigma;\omega} \rangle = n_{T_{r,\sigma}}(\omega_\nu) \frac{\Gamma_{r,\sigma}\delta_{\nu\nu'}}{\pi} \delta(\omega - \omega'),$$
$$\langle \hat{L}^{(\nu)}_{r,\sigma;\omega} \hat{L}^{(\nu'\dagger)}_{r,\sigma';\omega'} \rangle = [n_{T_{r,\sigma}}(\omega_\nu) + 1] \frac{\Gamma_{r,\sigma}\delta_{\nu\nu'}}{\pi} \delta(\omega - \omega'), \tag{4.41}$$

where $n_{T_{r,\sigma}}(\omega_\nu) = \dfrac{1}{e^{\hbar\omega_\nu/T_{r,\sigma}} - 1}$ and $T_{r,\sigma}$ are the temperature of the ambient space which controls radiative losses and the bulk material inside the cavity. The presence $\delta_{\nu\nu'}$ in Eq. (4.41) corresponds to the Langevin sources that are δ-correlated not only in space but also in time [10, 19].

4.4.3 Spontaneous emission from an ensemble of nonequilibrium fermions in a single-mode cavity

If we assume the populations to be given, the Heisenberg equations for the off-diagonal elements of the density operator can be averaged over the original state of quasiparticles. After averaging, the off-diagonal elements will depend on the field operators, noise operators, and populations $n_{m\boldsymbol{k}}$. The operators of populations $\hat{\rho}_{mm\boldsymbol{kk}}$ in Eq. (4.38) will be replaced by c-numbers: $\hat{\rho}_{mm\boldsymbol{kk}} \implies n_{m\boldsymbol{k}}$; see [17, 19].

The structure of Eqs. (4.38) and (4.40) suggests the substitution $\hat{c}_\nu = \hat{c}_{0\nu}(t)e^{-i\omega_\nu t}, \hat{c}^\dagger_\nu = \hat{c}^\dagger_{0\nu}(t)e^{+i\omega_\nu t}$. Here $\hat{c}_{0\nu}(t)$ and $\hat{c}^\dagger_{0\nu}(t)$ are "slow" amplitudes in the following sense: $\langle \dot{\hat{c}}_{0\nu} \rangle \ll \omega_\nu \langle \hat{c}_{0\nu} \rangle$; see [17]. Neglecting any inhomogeneous broadening of the resonance line, a steady-state solution of Eq. (4.38) for a single-mode cavity is

$$\hat{\rho}_{21\boldsymbol{kk}} \approx \frac{i\tilde{d}_{21}\tilde{D}_\nu}{\hbar} \frac{\hat{c}_{0\nu}e^{-i\omega_\nu t}(n_{1\boldsymbol{k}} - n_{2\boldsymbol{k}})}{i(\omega_{21} - \omega_\nu) + \gamma_{21\boldsymbol{kk}}} + \int_{\infty} \frac{\hat{F}_{\omega;21\boldsymbol{kk}}e^{-i\omega t}d\omega}{i(\omega_{21} - \omega) + \gamma_{21\boldsymbol{kk}}}. \tag{4.42}$$

Substituting Eq. (4.42) into Eq. (4.40) we obtain

$$\dot{\hat{c}}_{0\nu} + (\Gamma_r + \Gamma_\sigma + i\delta\omega + \gamma)\hat{c}_{0\nu} = \frac{i\tilde{d}_{21}\tilde{D}^*_\nu}{\hbar}\sum_{\boldsymbol{k}}\int_\infty \frac{\hat{F}_{\omega;21\boldsymbol{kk}}e^{-i(\omega-\omega_\nu)t}d\omega}{i(\omega_{21}-\omega)+\gamma_{21\boldsymbol{kk}}} + \int_\infty \hat{L}^{(\nu)}_{r\omega'}e^{-i(\omega'-\omega_\nu)t}d\omega' + \int_\infty \hat{L}^{(\nu)}_{\sigma\omega''}e^{-i(\omega''-\omega_\nu)t}d\omega'' \tag{4.43}$$

where

$$\delta\omega = \Omega^2 \mathrm{Re}\sum_k \frac{n_{1\boldsymbol{k}}-n_{2\boldsymbol{k}}}{(\omega_{21}-\omega_\nu)-i\gamma_{21\boldsymbol{kk}}}, \quad \gamma = \Omega^2 \mathrm{Im}\sum_k \frac{n_{1\boldsymbol{k}}-n_{2\boldsymbol{k}}}{(\omega_{21}-\omega_\nu)-i\gamma_{21\boldsymbol{kk}}}, \tag{4.44}$$

$$\Omega^2 = \frac{|\tilde{d_{21}}|^2|\tilde{D}_\nu|^2}{\hbar^2} = \frac{|\tilde{d_{21}}|^2 2\pi\omega_\nu}{\hbar L_x L_y G(L_z,\omega_\nu)}. \tag{4.45}$$

The frequency shift $\delta\omega$ of the "cold" cavity mode is due to the optical transitions between electron states in a QW. We can redefine the cavity mode frequency assuming that the effect of electrons has been included in ω_ν from the very beginning (a "hot" cavity mode). The decay rate γ describes absorption by electrons; the population inversion corresponds to $\gamma < 0$. If $(\gamma+\Gamma_r+\Gamma_\sigma) < 0$ the instability develops and the field grows with time; we don't consider this case here.

The steady-state solution of Eq. (4.43) has the form

$$\hat{c}_{0\nu} = \frac{i\tilde{d}_{12}\tilde{D}^*_\nu}{\hbar}\sum_{\boldsymbol{k}}\int_\infty \frac{\hat{F}_{\omega;21\boldsymbol{kk}}e^{-i(\omega-\omega_\nu)t}d\omega}{[i(\omega_\nu-\omega)+\Gamma_r+\Gamma_\sigma+\gamma]\times[i(\omega_{21}-\omega)+\gamma_{21\boldsymbol{kk}}]} + \int_\infty \frac{\hat{L}^{(\nu)}_{r\omega'}e^{-i(\omega'-\omega_\nu)t}d\omega'}{[i(\omega_\nu-\omega')+\Gamma+\Gamma_\sigma+\gamma]} + \int_\infty \frac{\hat{L}^{(\nu)}_{\sigma\omega''}e^{-i(\omega''-\omega_\nu)t}d\omega''}{[i(\omega_\nu-\omega'')+\Gamma+\Gamma_\sigma+\gamma]}. \tag{4.46}$$

Next, we use the Hermitian conjugate of Eq. (4.46) to find the value of $\langle\hat{c}^\dagger_{0\nu}\hat{c}_{0\nu}\rangle$, assuming that the statistics of noise operators $\hat{F}_{21\boldsymbol{kk}}(t)$, $\hat{L}^{(\nu)}_r(t)$ and $\hat{L}^{(\nu)}_\sigma(t)$ are independent from each other. Using

Eqs. (4.39) and (4.41) we obtain

$$\langle \hat{c}^{\dagger}_{0\nu}\hat{c}_{0\nu}\rangle = \Omega^2 \sum_{\boldsymbol{k}} \int_{\infty} \frac{d\omega}{\pi} \frac{\gamma_{21\boldsymbol{kk}} n_{2\boldsymbol{k}}}{[(\omega_\nu-\omega)^2+(\Gamma_r+\Gamma_\sigma+\gamma)^2]\times[(\omega_{21}-\omega)^2+\gamma^2_{21\boldsymbol{kk}}]} + \frac{\Gamma_r}{\Gamma_r+\Gamma_\sigma+\gamma} n_{T_r}(\omega_\nu) + \frac{\Gamma_\sigma}{\Gamma_r+\Gamma_\sigma+\gamma} n_{T_\sigma}(\omega_\nu). \quad (4.47)$$

For simplicity, we neglect the last two terms in Eq. (4.47) which describe the contribution of the EM background of a surrounding medium and thermal radiation of the material inside a cavity. The power emitted by electrons into the outside space is $P = 2\Gamma_r \times \hbar\omega_\nu \times \langle \hat{c}^{\dagger}_{0\nu}\hat{c}_{0\nu}\rangle$:

$$P = \hbar\omega_\nu \Omega^2 \sum_{\boldsymbol{k}} \int_{\infty} \frac{d\omega}{\pi} \frac{2\Gamma_r \gamma_{21\boldsymbol{kk}} n_{2\boldsymbol{k}}}{[(\omega_\nu-\omega)^2+(\Gamma_r+\Gamma_\sigma+\gamma)^2]\times[(\omega_{21}-\omega)^2+\gamma^2_{21\boldsymbol{kk}}]}. \quad (4.48)$$

Equation (4.48) for the spontaneous emission power is the main result of this section. It has two obvious limiting cases:

(i) The transition line is much narrower than the cavity resonance: $\Gamma_r + \Gamma_\sigma + \gamma \gg \gamma_{21\boldsymbol{kk}}$. In this case we can get from Eq. (4.48)

$$P = \hbar\omega_\nu [A^{(N)}_{2\to1}(\Delta\omega)_{\Delta\omega=\Delta\omega^{(1)}_{eff}}] \cdot \frac{\Gamma_r}{\Gamma_r+\Gamma_\sigma+\gamma} \cdot \frac{\Gamma_r+\Gamma_\sigma+\gamma}{(\omega_\nu-\omega_{21})^2+(\Gamma_r+\Gamma_\sigma+\gamma)^2} \cdot \sum_{\boldsymbol{k}} n_{2\boldsymbol{k}}, \quad (4.49)$$

where $A^{(N)}_{2\to1}(\Delta\omega)$ is the probability of the spontaneous emission in a cavity given by Eq. (4.34) and $\Delta\omega^{(1)}_{eff} = 2(\Gamma_r + \Gamma_\sigma + \gamma)$. The second factor in Eq. (4.49) determines the fraction of the radiation which escaped outside. The third factor is due to a position of the narrow transition line within a broader cavity mode line. The last factor is a number of radiating particles: $\sum_k n_{2\boldsymbol{k}} \Rightarrow \frac{S}{(2\pi)^2}\int n_{2\boldsymbol{k}} d^2k$.

(ii) The transition line is much wider than the cavity resonance: $\Gamma_r + \Gamma_\sigma + \gamma \ll \gamma_{21\boldsymbol{kk}}$. In this case

$$P = \hbar\omega_\nu [A^{(N)}_{2\to1}(\Delta\omega)_{\Delta\omega=\Delta\omega^{(2)}_{eff}}] \cdot \frac{\Gamma_r}{\Gamma_r+\Gamma_\sigma+\gamma} \cdot \sum_{\boldsymbol{k}} \frac{\langle\gamma_{21}\rangle\,\gamma_{21\boldsymbol{kk}} n_{2\boldsymbol{k}}}{(\omega_\nu-\omega_{21})^2+\gamma^2_{21\boldsymbol{kk}}}. \quad (4.50)$$

Instead of the cavity linewidth $2(\Gamma_r + \Gamma_\sigma + \gamma)$ Eq. (4.50) contains the homogeneous linewidth

$\Delta\omega_{eff}^{(2)} = \langle\gamma_{21}\rangle$ where the right-hand side is an average value of $\gamma_{21\boldsymbol{kk}}$. Now the third factor is due to a position of the narrow cavity mode line within a broader transition line. Therefore, the effective quality factor is determined by greater of the two values, $\Gamma_r + \Gamma_\sigma + \gamma$ or $\langle\gamma_{21}\rangle$. The spontaneous emission efficiency is proportional to the factor $\dfrac{\Gamma_r}{\Gamma_r + \Gamma_\sigma + \gamma}$, where γ is the decay rate of the field due to absorption by electrons. Since γ depends on the electron density, the spontaneous emission efficiency per particle also depends on their density.

One can further simplify Eq. (4.48) if relaxation constants $\gamma_{21\boldsymbol{kk}}$ do not depend on $\boldsymbol{k}$, i.e. $\gamma_{21\boldsymbol{kk}} \equiv \gamma_{21}$:

$$P = \hbar\omega_\nu \Omega^2 \int\limits_{\infty} \frac{d\omega}{\pi} \frac{2\Gamma_r\gamma_{21}}{[(\omega_\nu - \omega)^2 + (\Gamma_r + \Gamma_\sigma + \gamma)^2] \times [(\omega_{21} - \omega)^2 + \gamma_{21}^2]} \sum_{\boldsymbol{k}} n_{2\boldsymbol{k}}. \tag{4.51}$$

Here γ is defined by Eq. (4.44); for $\gamma_{21\boldsymbol{kk}} \equiv \gamma_{21}$ it becomes

$$\gamma = \Omega^2 \frac{\gamma_{21}}{(\omega_{21} - \omega_\nu)^2 + \gamma_{21}^2} \sum_k \left(n_{1\boldsymbol{k}} - n_{2\boldsymbol{k}}\right), \tag{4.52}$$

where Ω^2 is given by Eq. (4.45). Using Eq. (4.34), one can rewrite Eq. (4.51) as

$$P = \hbar\omega_\nu A_{2\to1}^{(N)} \sum_{\boldsymbol{k}} n_{2\boldsymbol{k}}, \tag{4.53}$$

where

$$A_{2\to1}^{(N)} = \frac{2\pi|\tilde{d}_{21}|^2 \left(\dfrac{4\omega_{21}}{\Delta\omega_{eff}}\right)}{\hbar L_x L_y G(L_z, \omega_\nu)} \tag{4.54}$$

and

$$\frac{1}{\Delta\omega_{eff}} = \int\limits_{\infty} \frac{d\omega}{4\pi} \frac{2\Gamma_r\gamma_{21}}{[(\omega_\nu - \omega)^2 + (\Gamma_r + \Gamma_\sigma + \gamma)^2] \times [(\omega_{21} - \omega)^2 + \gamma_{21}^2]}. \tag{4.55}$$

For a cavity filled with a uniform and dispersionless medium with dielectric constant ε one can

further simplify Eq. (4.53) as

$$P = \left[\hbar\omega_\nu A^{(0)} \sum_{\boldsymbol{k}} n_{2\boldsymbol{k}}\right] \left[\frac{6}{\pi^2} \frac{(\lambda/2\sqrt{\varepsilon})^3}{L_x L_y L_z}\right] Q_{eff}, \tag{4.56}$$

Where $A^{(0)} = \dfrac{4\omega^3 |d_{21}|^2 \sqrt{\varepsilon}}{3\hbar c^3}$ is the spontaneous emission rate into free space filled with dielectric medium ε and $Q_{eff} = \dfrac{\omega_{21}}{\Delta\omega_{eff}}$ is the effective quality factor. The term in the first brackets on the rhs of Eq. (4.56) is the power of spontaneous emission into free space; the term in the second brackets is the geometric enhancement due to a subwavelength cavity.

The integral in Eq. (4.55) is a product of two Lorentzians which can be easily evaluated analytically but is a bit cumbersome. Assuming for simplicity exact resonance between the transition frequency and the cavity resonance, $\omega_\nu = \omega_{21}$, we obtain

$$Q_{eff} = \frac{\omega_{21}\Gamma_r}{2(\Gamma_r + \Gamma_\sigma + \gamma)(\gamma_{21} + \Gamma_r + \Gamma_\sigma + \gamma)} \to \frac{\omega_{21}}{2(\gamma_{21} + \Gamma_r)}, \tag{4.57}$$

where the last expression is in the limit $\Gamma_r \gg \Gamma_\sigma + \gamma$.

For a fixed transition linewidth γ_{21} we normalize Q_{eff} by the Q-factor of the radiative transition $\dfrac{\omega_{21}}{2\gamma_{21}}$ and plot the normalized Q-factor $Q_{norm} = \dfrac{2\gamma_{21}}{\Delta\omega_{eff}}$ as a function of the cavity linewidth Γ_r for different values of the total normalized intracavity absorption rate $(\Gamma_\sigma + \gamma)/\gamma_{21}$; see Fig. 4.2. As shown in Fig. 4.2, the total magnitude of the intracavity absorption rate should be kept below the total linewidth γ_{21} of the emission line. Figure 4.2 also shows that it makes no sense to increase the Q-factor of the cavity mode $\dfrac{\omega_\nu}{2\Gamma_r}$ beyond the value of Γ_r corresponding to the peak value of the effective Q-factor Q_{eff}. For smaller values of Γ_r the intracavity quantum efficiency will stay roughly the same, limited by the dissipation rate γ_{21} of the optical polarization, whereas the radiation power outcoupled from the cavity reduces $\propto \Gamma_r$. The effective Q-factor quickly drops down with detuning of the cavity mode from the emission line; see Fig. 4.3.

For mid-infrared intersubband transitions in multiple QW nanocavities at $\hbar\omega_{21} \sim 100 - 200$

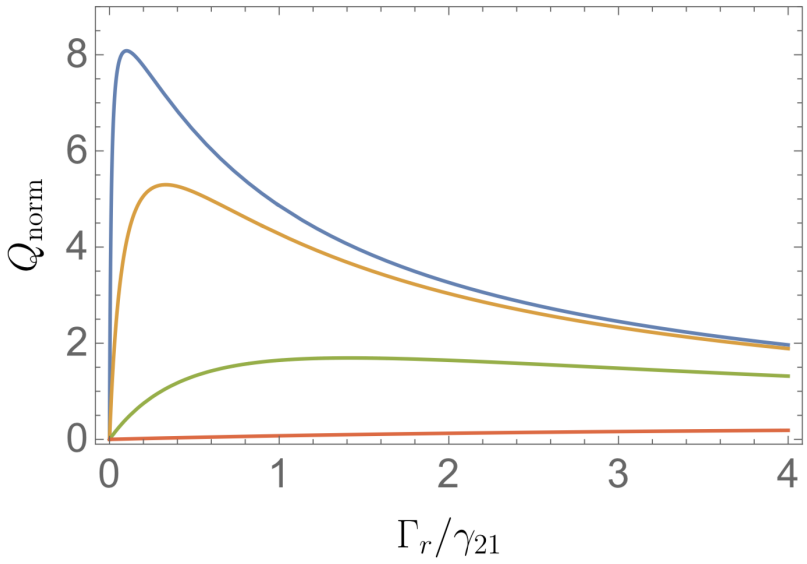

Figure 4.2: The normalized effective Q-factor as a function of the normailzed cavity linewidth Γ_r/γ_{21} at exact resonance $\omega_{21} = \omega_\nu$. Four curves correspond to four different values of the total intracavity absorption rate $(\Gamma_\sigma + \gamma)/\gamma_{21}$: 0.01, 0.1, 1, and 10, from top to bottom curve.

meV and full linewidth $2\gamma_{21} = 10$ meV [23] the maximum $Q_{eff} \sim 50 - 100$ and the geometric enhancement in Eq. (4.56) can add another factor of $10 - 100$. For THz intersubband transitions Q_{eff} is similar whereas the geometric enhancement is a factor of 10 higher. For a near-infrared interband transition in semiconductor QWs the frequency is $\sim 5 - 10$ times higher, but the linewidth is $2 - 3$ times higher as well, so Q_{eff} can be about 100-300. This example also suggests that an optimal radiative loss from a cavity (or a cavity mode linewidth) for semiconductor 2D emitters should be of the order of 5-10 meV. 2D semiconductors such as MoS_2 have excitonic emission lines that are quite broad, up to 50-100 meV. They are ideally suited for integration with plasmonic nanocavities which have a relatively low Q-factor but a very small effective mode volume. As an example, Ref. [26] reports a 2000-fold enhancement in the photoluminescence intensity from MoS_2 monolayer in a plasmonic nanocavity formed by a gold substrate and a patch silver nanoantenna. Since the emission line of MoS_2 was so broad (about 30 nm at 660 nm wavelength), according to Eqs. (4.56), (4.57) the authors made an optimal choice of using a plasmonic nanocavity with strong radiative outcoupling and comparably broad nanocavity modes, but with an ultrasmall

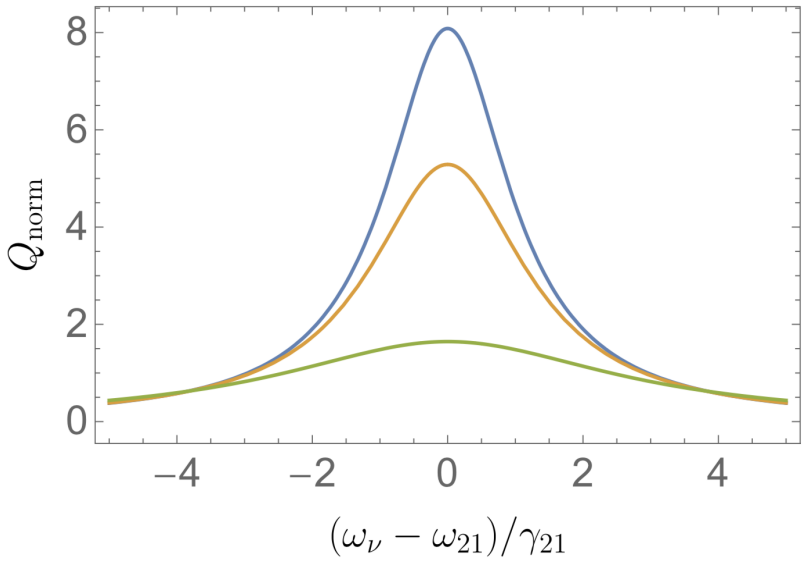

Figure 4.3: The normalized effective Q-factor as a function of frequency detuning at $\Gamma_r = \gamma_{21}$. Three curves correspond to three different values of the total intracavity absorption rate $(\Gamma_\sigma + \gamma)/\gamma_{21}$: 0.01, 0.1, and 1, from top to bottom curve. They are plotted for the value of the normailzed cavity linewidth Γ_r/γ_{21} = 0.1, 0.3, and 1, respectively, which correspond to the maximum Q_{eff} in Fig. 4.2.

effective mode volume of $\sim 10^{-3}(\lambda/\sqrt{\epsilon})^3$.

All results in this section are applicable to a waveguide at the cutoff frequency.

In conclusion, using consistent Heisenberg-Langevin approach we derived general analytic formulas describing the spontaneous emission of 2D emitters placed in plane-parallel subwavelength cavities or waveguides. We found that a significant enhancement of the outcoupled spontaneous emission and quantum efficiency of semiconductor quantum devices can be achieved for realistic device parameters. The present formalism can be extended to the nonlinear optical processes in 2D subwavelength cavities [27].

4.4 References

[1] E. M. Purcell, H. C. Torrey, R. V. Pound, Phys. Rev. 69, 37 (1946).

[2] Q. Gu, B. Slutsky, F. Vallini, J. S. T. Smalley, M. P. Nezhad, et al., Opt. Express 21,15603-15617 (2013).

[3] C.-Y. A. Ni, S. L. Chuang, Opt. Express 20, 16450-16470 (2012).

[4] K. Ding, C. Z. Ning, Light: Science & Applications (2012) 1, e20; doi:10.1038/lsa.2012.20.

[5] C. Walther, G. Scalari, M. Amanti, M. Beck, J. Faist, Science 327, 1495-1497 (2010).

[6] S. Gwo, C.-K. Shih, Rep. Prog. Phys. 79, 086501 (2016).

[7] S. V. Gaponenko, Introduction to Nanophotonics (Cambridge Univ. Press, 2010).

[8] G. M. Akselrod, C. Argyropoulos, T. B. Hoang, C. Ciraci, C. Fang, et al., Nature Phot. 8, 835-840 (2014).

[9] J. Lee, M. Tymchenko, C. Argyropoulos, P. Y. Chen, F. Lu, et al., Nature 511, 65-69 (2014).

[10] M. Erukhimova, M. Tokman, Optics Lett. 40, 2739-2742 (2015).

[11] M. Erukhimova, M.Tokman, Phys. Rev. A 95, 013807 (2017).

[12] L.D. Landau, E. M. Lifshitz, Statistical Physics, Part 1 (Butterworth-Heinemann, Oxford, 1980).

[13] C. Cohen-Tannoudji, J. Dupont-Roc, G. Grynberg, Atom-Photon Interactions: Basic Processes and Applications (Wiley, New York, 1992).

[14] V. M. Fain, Ya. I. Khanin, Quantum Electronics, Vol. 1 (The MIT Press, Cambridge, MA, 1969).

[15] M. O. Scully, M. S. Zubairy, Quantum Optics (Cambridge Univ. Press, Cambridge, 1997).

[16] V. L. Ginzburg, Theoretical Physics, Astrophysics (Pergamon, Oxford, 1979).

[17] M. D. Tokman, M. A. Erukhimova, V. V. Vdovin, Annals of Physics 360, 571-595 (2015).

[18] M. Tokman, M. Erukhimova, Journal of Lumin. 137, 148-156 (2013).

[19] M.Tokman, X. Yao, A. Belyanin, Phys. Rev. Lett. 110, 077404 (2013).

[20] L. D. Landau, E. M. Lifshitz, Quantum Mechanics (Pergamon, Oxford, 1977).

[21] L. Davidovich, Rev. Mod. Phys. 68, 127 (1996).

[22] M. Tokman, Y. Wang, A. Belyanin, Phys. Rev. B 92, 075409 (2015).

[23] J. Lee, N. Nookala, J. S. GomezâĂŘDiaz, M. Tymchenko, F. Demmerle, et al., Adv. Optical Mater. 2016, DOI: 10.1002/adom.201500723.

[24] L.D. Landau, E. M. Lifshitz, Electrodynamics of Continuous Media (Pergamon Oxford, 1984).

[25] M. Tokman, Y. Wang, I. Oladyshkin, A. R. Kutayiah, A. Belyanin, Phys. Rev. B 93, 235422 (2016).

[26] G. M. Akselrod, T. Ming, C. Argypoulos, T. B. Hoang, Y. Lin, et al., Nano Lett. 15, 3578-3584 (2015).

[27] M. Tokman, Z. Long, S. AlMutairi, Y. Wang, V. Vdovin, et al., APL Photonics 4, 034403(2019).

5. PURCELL ENHANCEMENT OF THE PARAMETRIC DOWN-CONVERSION IN TWO-DIMENSIONAL NONLINEAR MATERIALS*

5.1 Introduction

Enhancement of the radiative processes due to the localization of emitters in a subwavelength cavity (so-called Purcell enhancement [1]) is a fundamental cavity quantum electrodynamics (QED) effect of great importance for numerous applications. The bulk of the research has been focused on exploring the enhancement of spontaneous emission in various compact radiation sources from single quantum emitters to LEDs and nanolasers. The nonlinear optics has received relatively less attention; however, recent advancements in strong light localization using subwavelength cavities, photonic crystals, metamaterials, and metasurfaces enabled the nonlinear optics in ultrasmall volumes and at relatively low power levels; see e.g. [2, 3, 4, 5, 6, 7, 8, 9, 10] and references therein. The rise of 2D materials with atomic monolayer thickness and excellent nonlinear optical properties, such as graphene [11, 12, 13, 14] and transition metal dichalcogenide monolayers [15, 16] has enabled quasi-2D cavities and waveguides only a few nm thick [17, 18]. These advances create new exciting opportunities for ultracompact nonlinear optical devices, but also raise important issues of the correct description of quantum fields in systems with strong dissipation both in a macroscopic ensemble of fermionic emitters (e.g. a 2D semiconductor or monolayer graphene, or a 2D electron gas in a quantum well) and for the electromagnetic (EM) field in a cavity.

One important application for Purcell-enhanced nonlinear optics is compact systems for generation of squeezed and entangled photon states as a result of parametric down-conversion. Such systems are inevitably lossy. The general approach to introducing dissipation and corresponding fluctuations has been known for a long time and is based on the Heisenberg-Langevin formalism; e.g. [19, 20, 21, 22, 23]. Its generalization to systems far from equilibrium, with arbitrary dissipation mechanisms and arbitrary photon density of states is nontrivial; see e.g. [24, 25]. Recent work

[10] considered the process of spontaneous parametric down-conversion in hyperbolic metamaterials, in which the EM field dissipation and fluctuations are due to an equilibrium thermal reservoir. In the present paper we consider both spontaneous and stimulated parametric down-conversion in a generic quasi-2D subwavelength cavity, taking into account dissipation and fluctuations both due to absorption in the intracavity material and due to in/outcoupling of the intracavity EM field with the outside world.

We generalize the properties of Langevin noise sources known for a single mode of a quantized field (e.g. [19, 20, 26]) to an ensemble of coupled field oscillators. We derive the properties of the Langevin sources needed to conserve their commutation relations and show that they are not affected by a more complicated dynamics of coupled Heisenberg field operators; moreover, this statement does not depend on any specific microscopic model of a dissipative reservoir. We are able to derive closed-form analytic results for the spontaneous parametric signal, the parametric gain, and the threshold for parametric amplification. These expressions include the contributions from all relevant dissipation and fluctuation effects such as absorption and radiation losses, interaction with thermal and zero-point fluctuations, parametric amplification of thermal noise and seed photons at the signal frequency, etc.; see e.g. Eqs. (5.32), (5.35) below.

Our approach has obvious limitations of a Heisenberg-Langevin formalism, namely it assumes that the coupling of a dynamic subsystem to a dissipative reservoir is sufficiently weak. If this is not the case and the coupling to other EM modes, photons, etc. is strong, one would have to include it as part of an "exact" Hamiltonian dynamics, in which case there would be no need in adding the corresponding Langevin sources and the commutation relations would be satisfied automatically. We also do not investigate the nonlinear stage of parametric oscillations accompanied by the pump depletion, nonlinear evolution of phasematching conditions, nonlinear modification of refraction and diffraction losses, and other nonlinear effects that are essentially classical and depend on a particular experimental setup.

Section II describes the spatial structure of the EM field in a subwavelength quasi-2D electrodynamic structure, develops the quantization procedure in a dissipationless system, and dis-

cusses three-wave mode matching conditions. Section III introduces the Heisenberg-Langevin approach for the parametric down-conversion in a dissipative cavity. It derives convenient analytic expressions for the spontaneous parametric signal, the parametric amplification threshold in plane-parallel cavities, and the signal evolution at the linear stage. We discuss several numerical examples for the parametric down-conversion in quasi-2D systems studied by other groups. Section IV compares parametric amplification threshold in a subwavelength cavity with the one in a standard Fabry-Perot cavity containing a 2D nonlinear layer. In this case the performance tradeoff is between the cavity losses and the modal overlap with a nonlinear layer. Larger cavities tend to have a higher Q-factor but lower coupling to a nonlinear 2D layer. Our results show that it is possible to achieve a significant reduction of the parametric amplification threshold due to Purcell enhancement in quasi-2D subwavelength cavities.

5.2 Parametric down-conversion in a conservative system

Consider three cavity modes with frequencies related by the energy conservation in the parametric down-conversion process:

$$\omega_p = \omega_s + \omega_i. \tag{5.1}$$

Here the pumping at frequency ω_p will be considered a classical coherent field,

$$\boldsymbol{E}_p = \boldsymbol{E}_p(\boldsymbol{r})e^{-i\omega_p t} + C.C. \tag{5.2}$$

The field at signal and idler frequencies, ω_s and ω_i , will be the quantum field described by the operator

$$\hat{\boldsymbol{E}} = \sum_{\nu=s,i} [\boldsymbol{E}_\nu(\boldsymbol{r})\hat{c}_\nu + \boldsymbol{E}^*_\nu(\boldsymbol{r})\hat{c}^\dagger_\nu], \tag{5.3}$$

where $\hat{c}_\nu$ and $\hat{c_\nu}^\dagger$ are boson annihilation and creation operators. The functions $\boldsymbol{E}_{p,s,i}(\boldsymbol{r})$ in Eqs. (5.2) and (5.3) are determined by the spatial structure of the cavity modes. The normalization of functions $\boldsymbol{E}_\nu(\boldsymbol{r})$ needs to be chosen in such a way that the commutation relation for boson operators $\hat{c}_\nu$

and $\hat{c_\nu}^\dagger$ have a standard form $[\hat{c}_\nu, \hat{c_\nu}^\dagger] = \delta_{\nu\nu'}$. Following [27, 28, 29], one can obtain

$$\int_V E^*_{\nu j}(\boldsymbol{r}) \frac{1}{2\omega_\nu} \left[\frac{\partial \left(\omega^2 \varepsilon_{jk}(\omega, \boldsymbol{r})\right)}{\partial \omega} \right]_{\omega=\omega_\nu} E_{\nu k}(\boldsymbol{r})\, d^3 r = 2\pi\hbar\omega_\nu, \tag{5.4}$$

where ω_ν is the eigenfrequency of a cavity mode, $E_{\nu j}(\boldsymbol{r})$ is a Cartesian component of the vector field $\boldsymbol{E}_\nu(\boldsymbol{r})$, $\varepsilon_{jk}(\omega, \boldsymbol{r})$ is the dielectric tensor, and V is a cavity volume (a quantization volume).

Equation (5.4) is valid when the dissipation is weak enough. Specifically, the following three conditions have to be satisfied for a dissipation rate Γ of a given cavity mode. The first condition is obvious: $\Gamma \ll \omega$ has to be true for the frequencies of all modes involved in the parametric process. The second condition implies that the change of the Hermitian dielectric function $\varepsilon_{jk}(\omega)$ has to be small over the frequency interval of the order of Γ: $|(\partial\varepsilon_{jk}(\omega)/\partial\omega)\Gamma| \ll |\varepsilon_{jk}(\omega)|$. The third condition states that the change in the derivative of $\varepsilon_{jk}(\omega)$ which enters the expression for the EM energy density in Eq. (5.4) must also be small: $|(\partial^2\varepsilon_{jk}(\omega)/\partial\omega^2)\Gamma| \ll |(\partial\varepsilon_{jk}(\omega)/\partial\omega)|$.

Consider a 3D cavity filled with an isotropic dielectric medium, as sketched in Fig. 1. The cavity thickness in z-direction is much smaller than wavelength: $L_z \ll c/\sqrt{\bar{\varepsilon}}\omega$, where $\bar{\varepsilon}$ is a typical (average) value of the dielectric constant of the filling. As was shown in [26], if the dielectric filling consists of plane-parallel layers, i.e. $\varepsilon = \varepsilon(z)$, the structure of the cavity eigenmodes is quasi-electrostatic along the z-axis, i.e. $E_z\varepsilon(z) \approx$ const, $E_{x,y} \ll E_z$. In this case the field of a cavity mode can be written as

$$\boldsymbol{E}_{p,s,i}(\boldsymbol{r}) \approx \boldsymbol{z}_0 D_{p,s,i} \frac{\zeta_{p,s,i}(x,y)}{\varepsilon(\omega_{p,s,i}, z)}, \tag{5.5}$$

where the constants $D_{p,s,i}$ are coordinate-independent amplitudes of the electric induction. To find the functions $\zeta_{p,s,i}(x,y)$ we solve the wave equation

$$\nabla \cdot (\nabla \cdot \boldsymbol{E}_{p,s,i}) - \nabla^2 \boldsymbol{E}_{p,s,i} - \frac{\omega^2_{p,s,i}}{c^2} \varepsilon(\omega_{p,s,i}, z) \boldsymbol{E}_{p,s,i} = 0.$$

Consider a z-component of this equation,

$$\frac{\partial}{\partial z}\left(\frac{\partial E_{(p,s,i)x}}{\partial x}+\frac{\partial E_{(p,s,i)y}}{\partial y}\right)=\left[\frac{\partial^2}{\partial x^2}+\frac{\partial^2}{\partial y^2}+\frac{\omega_{p,s,i}^2}{c^2}\varepsilon(\omega_{p,s,i},z)\right]E_{(p,s,i)z}. \tag{5.6}$$

Following the procedure described in [26], we integrate Eq. (5.6) over $\int_{-L_z/2}^{L_z/2}dz$ taking into account the boundary conditions on the metal planes of the cavity, $E_{x,y}(\pm L_z/2)=0$. Then we substitute Eq. (5.5) into the result of integration, which gives

$$\left[\frac{\partial^2}{\partial x^2}+\frac{\partial^2}{\partial y^2}+\frac{\omega_{p,s,i}^2}{c^2\frac{1}{L_z}\int_{-L_z/2}^{L_z/2}\frac{1}{\varepsilon(\omega_{p,s,i},z)}dz}\right]\zeta_{p,s,i}=0. \tag{5.7}$$

The solution to Eq. (5.7) with zero boundary conditions at the edges of the cavity determines eigenfrequencies and the structure of the eigenmodes for a quasi-2D cavity with an arbitrary shape in the (x,y)-plane.

Similar equations can be derived if one simply utilizes jumps of the dielectric constants on the sides instead of metal coating. Even without any jump in the dielectric constants, an open end of a thin waveguide with vertical size much smaller than wavelength is a good reflector and therefore any radiation losses through the facets are small and are not affecting the mode spatial structure significantly.

The expression for the constants $D_{p,s,i}$ for quantized fields can be obtained from the general equation Eq. (5.4) (see also [26]),

$$|D_\nu|^2=\frac{2\pi\hbar\omega_\nu}{\int_S|\zeta_\nu(x,y)|^2d^2r\frac{1}{2\omega_\nu}\int_{-L_z/2}^{L_z/2}\left[\frac{\partial(\omega^2\varepsilon(\omega,z))}{\partial\omega}\right]_{\omega=\omega_\nu}dz}, \tag{5.8}$$

where $\nu=p,s,i$. For a simple case of a rectangular-shaped cavity, when $S=L_x\times L_y$, where L_x and L_y are the cavity dimensions along x and y directions, it is easy to obtain useful analytic expressions for the modal spatial structure and frequencies. For eigenmodes with one half-wavelength

along the y-axis and N half-wavelengths along the x-axis, we obtain the modal profile

$$\zeta_\nu = \cos\left(\frac{\pi y}{L_y}\right) \times \begin{cases} \cos\left(\dfrac{N_{odd}^{(\nu)}\pi x}{L_x}\right) \\ \sin\left(\dfrac{N_{even}^{(\nu)}\pi x}{L_x}\right) \end{cases}, \tag{5.9}$$

$$\int_S |\zeta_\nu(x,y)|^2 d^2r = \frac{S}{4}. \tag{5.10}$$

The eigenfrequencies are given by

$$\left(\frac{N_\nu \pi}{L_x}\right)^2 + \left(\frac{\pi}{L_y}\right)^2 = \frac{\omega_\nu^2}{c^2} \frac{L_z}{\int\limits_{-\frac{L_z}{2}}^{+\frac{L_z}{2}} \frac{1}{\varepsilon(\omega_\nu, z)} dz}. \tag{5.11}$$

For a particular case of a uniform dielectric constant, Eqs. (5.9) and (5.11) are exact, i.e. they do not require an assumption of a quasielectrostatic field structure.

We assume that a 2D electron system with the second-order nonlinear susceptibility is positioned in the cavity. The material can be a quantum well (QW), a 2D semiconductor, and even graphene, which has a strong second-order nonlinearity beyond electric-dipole approximation, despite being centrosymmetric [14]. The second-order nonlinearity gives rise to the nonlinear polarization at signal and idler frequencies. The excitation equations for the cavity modes derived from the operator-valued Maxwell's equations [27] take the form

$$\dot{\hat{c}}_\nu + i\omega_\nu \hat{c}_\nu = -\frac{i}{\hbar\omega_\nu^2} \int\limits_V \ddot{\hat{\boldsymbol{P}}}_{NL}(\boldsymbol{r}, t) \boldsymbol{E}_\nu^*(\boldsymbol{r}) d^3r. \tag{5.12}$$

The nonlinear polarization $\hat{\boldsymbol{P}}_{NL}(\boldsymbol{r}, t)$ should be determined for a given electron system; in general, it has a nonuniform distribution over the cavity cross-section. However, it is obvious from Eq. (5.12) that only the integral over the nonlinear polarization matters. Therefore it is convenient to consider a nonlinear layer with uniform dielectric constant $\varepsilon_{QW}(\omega_{p,s,i}) = \varepsilon_{p,s,i}$ and uniform

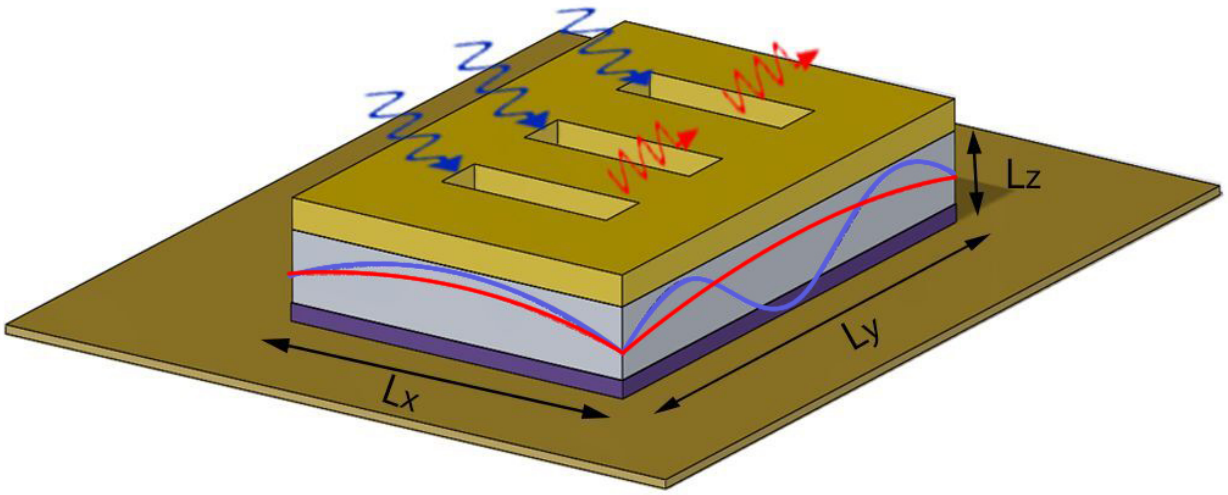

Figure 5.1: A sketch of a nanocavity with thickness L_z much smaller than wavelength. The profiles of the electric fields of the TE_{013} pump mode (blue) and TE_{011} signal and idler modes (red) are sketched on the sides. Dark blue layer indicates a 2D nonlinear material; light blue layer is a cavity filling. Top and bottom gold layers are metal plates. The radiation can be in/outcoupled through the gratings or cavity edges.

second-order nonlinear susceptibilities $\chi^{(2)}(\omega_s = \omega_p - \omega_i) = \chi_s^{(2)}$, $\chi^{(2)}(\omega_i = \omega_p - \omega_s) = \chi_i^{(2)}$, $\chi^{(2)}(\omega_p = \omega_s + \omega_i) = \chi_p^{(2)}$. For a general case of a nonuniform layer the above quantities can be considered as parameters obtained as a result of integration in Eq. (5.12).

For a uniform layer the nonlinear polarization can be expressed as

$$\hat{\boldsymbol{P}}_{NL} = \boldsymbol{z}_0 \zeta_p(x,y)[\zeta_i(x,y)\chi_s^{(2)} E_p E_i^* e^{-i\omega_p t}\hat{c}_i^\dagger + \zeta_s(x,y)\chi_i^{(2)} E_p E_s^* e^{-i\omega_p t} c_s^\dagger] + H.C.; \qquad (5.13)$$

where $c_s^\dagger \propto e^{i\omega_s t}$, $c_i^\dagger \propto e^{i\omega_i t}$,

$$|E_{s,i}|^2 = \frac{8\pi\hbar\omega_{s,i}}{L_x L_y L_z \dfrac{1}{2\omega_{s,i}} \left[\dfrac{\partial(\omega^2\epsilon)}{\partial\omega}\right]_{\omega=\omega_{s,i}}}, \tag{5.14}$$

and $E_p = \text{const}$. In Eq. (5.14) we assumed a rectangular cavity shape for simplicity.

If the nonlinearity is non-dissipative, the nonlinear susceptibilities satisfy the symmetry properties which ensure than Manley-Rowe relationships are satisfied in a conservative system [30, 31].

$$\chi_s^{(2)} = \chi_i^{(2)} = \chi_p^{(2)*} = \chi^{(2)}. \tag{5.15}$$

Using the rotating wave approximation, Eqs. (5.12) and (5.13) give the following parametrically coupled equations for a given classical pumping:

$$\dot{\hat{c}}_s + i\omega_s \hat{c}_s + \varsigma e^{-i\omega_p t}\hat{c}_i^\dagger = 0, \quad \dot{\hat{c}}_i^\dagger - i\omega_i \hat{c}_i^\dagger + \varsigma^* e^{+i\omega_p t}\hat{c}_s = 0 \tag{5.16}$$

where

$$\varsigma = -\frac{i}{\hbar}\chi^{(2)} l E_p E_i^* E_s^* \times J, \tag{5.17}$$

$$J = \int\limits_{L_x \times L_y} \zeta_p(x,y)\zeta_i(x,y)\zeta_s(x,y)d^2r \tag{5.18}$$

is a modal overlap factor and l is the thickness of the nonlinear layer in z direction.

Equations (5.16) are Heisenberg equations for the effective Hamiltonian

$$\hat{H} = \hbar\omega_s\left(\hat{c}_s^\dagger\hat{c}_s + \frac{1}{2}\right) + \hbar\omega_i\left(\hat{c}_i^\dagger\hat{c}_i + \frac{1}{2}\right) - i\hbar\varsigma e^{-i\omega_p t}\hat{c}_s^\dagger\hat{c}_i^\dagger + i\hbar\varsigma^* e^{i\omega_p t}\hat{c}_s\hat{c}_i. \tag{5.19}$$

For a parametric down-conversion of a pump photon into two identical photons, when

$$\omega_p = 2\omega_s \tag{5.20}$$

we arrive at the Hamiltonian

$$\hat{H} = \hbar\omega_s \left(\hat{c}_s^\dagger \hat{c}_s + \frac{1}{2} \right) - i\hbar \frac{\varsigma}{2} e^{-i\omega_p t} \hat{c}_s^\dagger \hat{c}_s^\dagger + i\hbar \frac{\varsigma^*}{2} e^{i\omega_p t} \hat{c}_s \hat{c}_s. \tag{5.21}$$

The condition $J \neq 0$ is similar to the three-wave phase matching condition for the wave vectors of modes participating in the parametric down-conversion. The phase matching needs to be satisfied together with frequency matching in Eq. (5.1), which could be highly nontrivial in a 3D geometry and in a dispersive medium. An important advantage of a subwavelength cavity is that these conditions are straightforward to satisfy by adjusting the cavity geometry. Indeed, consider the decay of the pump into two lowest-order TE_{011} modes satisfying Eq. (5.20); in this case $\zeta_s(x,y) = \cos\left(\frac{\pi y}{L_y}\right)\cos\left(\frac{\pi x}{L_x}\right)$. For a pumping mode of TE_{01N} type with N even, $J = 0$; however for N odd we get $J \neq 0$. For example, for a TE_{013} pumping mode (see Fig. 1), when $\zeta_p(x,y) = \cos\left(\frac{\pi y}{L_y}\right)\cos\left(\frac{3\pi x}{L_x}\right)$, we obtain: $J = \frac{L_x L_y}{\pi^2} \times \frac{16}{45}$. In this case from Eq. (5.20) and mode frequencies given by Eq. (5.11) one can get a condition for cavity sizes:

$$\frac{L_x}{L_y} = \sqrt{\frac{9 - 4\frac{\varepsilon(2\omega_s)}{\varepsilon(\omega_s)}}{4\frac{\varepsilon(2\omega_s)}{\varepsilon(\omega_s)} - 1}}$$

5.3 Equations for parametric down-conversion in a dissipative system: Heisenberg-Langevin approach

Here we take into account absorption and radiative losses within the Heisenberg-Langevin formalism. We remind the reader that this approach assumes that the coupling of a dynamic subsystem to a dissipative reservoir is sufficiently weak. If this is not the case and the coupling is strong, the process of energy loss by a given EM mode should be described within a closed Hamiltonian system (e.g. as a coupling to other EM modes, phonons etc.). In this case one does not need any Langevin sources, because in a Hamiltonian system proper commutation relations are satisfied automatically. Whenever the energy exchange of a dynamical subsystem with a reservoir is relatively

weak and can be considered within a phenomenological approach, the "dissipation + the Langevin noise" model should be valid for any mechanism of dissipation.

For example, we assume here that the spatial mode structure corresponds to the one in an ideal cavity, whereas diffraction losses of the field out of a cavity can be described by an effective loss rate. This assumption obviously works as long as losses do not affect the mode structure significantly. If the latter is not true, one would have to solve a rigorous diffraction problem which couples the field modes in the cavity and outside. For such a rigorous problem all commutation relations would be satisfied automatically.

Introducing operators of slowly varying field amplitudes, namely $\hat{c}_{s,i} = \hat{c}_{0s,i}(t)e^{-i\omega_{s,i}t}$, $\hat{c}^{\dagger}_{s,i} = \hat{c}^{\dagger}_{0s,i}(t)e^{+i\omega_{s,i}t}$, we obtain from Eqs. (5.16) the following equations:

$$\left.\begin{aligned} \dot{\hat{c}}_{0s} + \Gamma_s \hat{c}_{0s} + \varsigma \hat{c}^{\dagger}_{0i} = \hat{L}_s \\ \dot{\hat{c}}_{0i} + \Gamma_i \hat{c}_{0i} + \varsigma \hat{c}^{\dagger}_{0s} = \hat{L}_i \end{aligned}\right\}, \tag{5.22}$$

where $\Gamma_{s,i} = \Gamma_{r(s,i)} + \Gamma_{\sigma(s,i)}$, the coefficients $\Gamma_{r(s,i)}$ and $\Gamma_{\sigma(s,i)}$ denote, respectively, radiative losses due to the outcoupling of radiation from the cavity and absorption losses due to intracavity absorption. $\hat{L}_{s,i}$ are the Langevin noise operators. We show in Appendix A that to preserve commutation relations $[\hat{c}_{0i}, \hat{c}^{\dagger}_{0i}] = [\hat{c}_{0s}, \hat{c}^{\dagger}_{0s}] = 1$ at $\Gamma_{s,i} \neq 0$ the noise operators in the right-hand side of Eqs. (5.22) should satisfy the same commutation relations as in the case of one quantum oscillator [19, 20, 26] and they should also commute with each other:

$$\left[\hat{L}_s(t'), \hat{L}^{\dagger}_s(t)\right] = 2\Gamma_s \delta(t-t'), \quad \left[\hat{L}_i(t'), \hat{L}^{\dagger}_i(t)\right] = 2\Gamma_i \delta(t-t'), \quad \left[\hat{L}_s(t'), \hat{L}^{\dagger}_i(t)\right] = 0. \tag{5.23}$$

The fact that commutation relations are the same for one quantum oscillator and for two (or more) interacting oscillators is expected, since the processes within the Hamiltonian dynamics do not affect the commutators; this can be easily checked, for example for the system described by the Hamiltonian Eq. (5.19). Noise correlators can be defined by generalizing the simplest expression

in [19] to the case of two absorbers with different temperatures:

$$\left.\begin{aligned}\langle \hat{L}_s^\dagger(t)\hat{L}_s(t')\rangle &= 2\left[\Gamma_{\sigma s} n_{T_\sigma}(\omega_s) + \Gamma_{rs} n_{T_r}(\omega_s)\right]\delta(t-t') \\ \langle \hat{L}_i^\dagger(t)\hat{L}_i(t')\rangle &= 2\left[\Gamma_{\sigma i} n_{T_\sigma}(\omega_i) + \Gamma_{ri} n_{T_r}(\omega_i)\right]\delta(t-t')\end{aligned}\right\} \tag{5.24}$$

where $n_{T_{r,\sigma}}$ is the average number of thermal photons at temperature $T_{r,\sigma}$; T_r and T_σ denote the temperature outside and inside the cavity, respectively. Expressions (5.24) imply that dissipative and radiative noises are not correlated.

The solution to Eqs. (5.22) can be represented as [21, 23]

$$\begin{pmatrix}\hat{c}_{0s}\\ \hat{c}_{0s}^\dagger\end{pmatrix} = \begin{pmatrix}1\\ K_1\end{pmatrix} e^{-\lambda_1 t}\left(\hat{c}_1 + \int_0^t e^{\lambda_1 t'}\hat{L}_1(t')dt'\right) + \begin{pmatrix}1\\ K_2\end{pmatrix} e^{-\lambda_2 t}\left(\hat{c}_2 + \int_0^t e^{\lambda_2 t'}\hat{L}_2(t')dt'\right), \tag{5.25}$$

where $\lambda_{1,2}$ and $\begin{pmatrix}1\\ K_{1,2}\end{pmatrix}$ are eigenvalues and eigenvectors of the 2×2 matrix:

$$\begin{pmatrix}\Gamma_s & \varsigma\\ \varsigma^* & \Gamma_i\end{pmatrix} \times \begin{pmatrix}1\\ K_{1,2}\end{pmatrix} = \lambda_{1,2}\begin{pmatrix}1\\ K_{1,2}\end{pmatrix}, \tag{5.26}$$

$$\left.\begin{aligned}\hat{c}_1 &= \frac{K_2\hat{c}_s(0) - \hat{c}_i^\dagger(0)}{K_2 - K_1}, & \hat{c}_2 &= -\frac{K_1\hat{c}_s(0) - \hat{c}_i^\dagger(0)}{K_2 - K_1}\\ \hat{L}_1 &= \frac{K_2\hat{L}_s - \hat{L}_i^\dagger}{K_2 - K_1}, & \hat{L}_2 &= -\frac{K_1\hat{L}_s - \hat{L}_i^\dagger}{K_2 - K_1}\end{aligned}\right\}, \tag{5.27}$$

$\hat{c}_s(0)$ and $\hat{c}_i^\dagger(0)$ are initial conditions.

From the solution (5.25)-(5.26) one can derive a standard-looking condition for the parametric instability(see e.g. [32]):

$$|\varsigma|^2 > \Gamma_s\Gamma_i. \tag{5.28}$$

Consider the inequality (5.28) in more detail, neglecting for clarity the frequency dispersion of the

dielectric filling of a cavity. Taking into account Eq. (5.14), one can derive from Eq. (5.17) that

$$|\varsigma| = |\chi^{(2)} E_p| \sqrt{\omega_s \omega_i} \frac{8\pi l}{L_z \varepsilon} \frac{J}{L_x L_y}, \tag{5.29}$$

where the dimensionless factor $J/(L_x L_y)$ depends only on the spatial structure of the modes with frequencies $\omega_{p,s,i}$. From Eqs. (5.28), (5.29) the instability condition takes the form

$$\frac{256\pi^2}{\varepsilon^2 L_z^2} (\chi^{(2)} l)^2 |E_p|^2 \left(\frac{\omega_s}{\Delta\omega_s}\right) \left(\frac{\omega_i}{\Delta\omega_i}\right) \left(\frac{J}{L_x L_y}\right)^2 > 1, \tag{5.30}$$

where $\Delta\omega_{s,i} = 2\Gamma_{s,i}$ are the linewidths for the signal and idler modes.

To avoid cumbersome expressions, consider the decay of a pump photon into identical quanta as in Eq. (5.20). In this case the instability condition is $|\varsigma| > \Gamma_s$. It is convenient to choose the phase of the pump mode so that the value of is real and positive. Then Eqs. (5.25)-(5.27) yield

$$\hat{c}_{0s} = e^{-\Gamma_s t} \left[\hat{c}_s(0)\text{cosh}(\varsigma t) - \hat{c}_s^\dagger(0)\text{sinh}(\varsigma t)\right] + \int_0^t e^{(-\varsigma+\Gamma_s)(t'-t)} \frac{\hat{L}_s(t') - \hat{L}_s^\dagger(t')}{2} dt' + \\ + \int_0^t e^{(\varsigma+\Gamma_s)(t'-t)} \frac{\hat{L}_s(t') + \hat{L}_s^\dagger(t')}{2} dt'. \tag{5.31}$$

Taking into account the properties of Langevin operators in Eq. (5.22) and taking $\left\langle \hat{c}_s^\dagger(0)\hat{c}_s^\dagger(0)\right\rangle = \langle \hat{c}_s(0)\hat{c}_s(0)\rangle = 0$ as an initial state, one can derive from Eq. (5.31) the average photon numbers for signal modes $n_s = \left\langle \hat{c}_s^\dagger \hat{c}_s \right\rangle = \left\langle \hat{c}_{0s}^\dagger \hat{c}_{0s} \right\rangle$:

$$n_s = e^{-2\Gamma_s t} \left\{ n_s(0) \left[\text{cosh}^2(\varsigma t) + \text{sinh}^2(\varsigma t)\right] + \text{sinh}^2(\varsigma t) \right\} \\ + \left[\Gamma_{\sigma s} n_{T_\sigma}(\omega_s) + \Gamma_{rs} n_{T_r}(\omega_s)\right] \times \left(\frac{1 - e^{2(\varsigma-\Gamma_s)t}}{2(-\varsigma+\Gamma_s)} + \frac{1 - e^{2(-\varsigma-\Gamma_s)t}}{2(\varsigma+\Gamma_s)} \right) \\ + \Gamma_s \left(\frac{1 - e^{2(\varsigma-\Gamma_s)t}}{4(-\varsigma+\Gamma_s)} + \frac{1 - e^{2(-\varsigma-\Gamma_s)t}}{4(\varsigma+\Gamma_s)} - \frac{1 - e^{-2\Gamma_s t}}{2\Gamma_s} \right), \tag{5.32}$$

where $\Gamma_s = \Gamma_{\sigma s} + \Gamma_{rs}$. When the parametric amplification starts from the level of vacuum fluctu-

ations, one should put $n_s(0) = 0$ in Eq. (5.32).

In the limit of zero pumping intensity, Eq. (5.32) gives an expression which describes how the initial perturbation of a photon number approaches equilibrium:

$$n_s = e^{-2\Gamma_s t} n_s(0) + \frac{\Gamma_{\sigma s} n_{T_\sigma}(\omega_s) + \Gamma_{rs} n_{T_r}(\omega_s)}{\Gamma_s} \times \left(1 - e^{-2\Gamma_s t}\right). \tag{5.33}$$

Above the instability threshold, when $\varsigma \gg \Gamma_s$, it is enough to keep only exponentially growing terms in Eq. (5.32). We can also assume that an average number of thermal photons in an ambient space $n_{T_r}(\omega_s)$ is negligible. This gives an expression for the parametric signal power $P_s \approx 2\varsigma\hbar\omega_s n_s$:

$$P_s \approx \varsigma\hbar\omega_s e^{2\varsigma t}\left[n_s(0) + \frac{\Gamma_{\sigma s}}{\varsigma} n_{T_\sigma}(\omega_s) + \frac{1}{2}\right]. \tag{5.34}$$

Obviously this expression is valid only at the initial linear stage. The subsequent evolution is governed by the nonlinear pump depletion and nonlinear modification of phasematching conditions and losses. An order-of magnitude estimate of the maximum steady-state power can be obtained from Manley-Rowe relations as shown below for a specific example.

The fractions of the power emitted outside and absorbed inside a cavity are $P_{rs} \approx \Gamma_{rs} P_s/\varsigma$ and $P_{\sigma s} \approx \Gamma_{\sigma s} P_s/\varsigma$ respectively; most of the power is accumulated in a cavity. From Eq. (5.34) one can see that the amplification of intrinsic thermal noise of a QW layer with temperature T_σ can be ignored if $\dfrac{\Gamma_{\sigma s}}{\varsigma} \cdot \dfrac{2}{\exp(\hbar\omega_s/T_\sigma) - 1} \ll 1$.

When the parametric growth rate is lower than losses, $\varsigma < \Gamma_s$, the general solution Eq. (5.32) describes the regime of spontaneous parametric down-conversion. In the stationary limit, when $(\Gamma_s - \varsigma)t \to \infty$, the radiated signal power $P_{rs} \approx 2\Gamma_{rs}\hbar\omega_s n_s$ becomes

$$P_{rs} = \hbar\omega_s \frac{2\Gamma_{rs}\Gamma_s}{\Gamma_s^2 - \varsigma^2}\left[\Gamma_{\sigma s} n_{T_\sigma}(\omega_s) + \Gamma_{rs} n_{T_r}(\omega_s)\right] + \hbar\omega_s \frac{\Gamma_{rs}\varsigma^2}{\Gamma_s^2 - \varsigma^2}. \tag{5.35}$$

The first term in the right-hand side of Eq. (5.35) is due to the thermal emission modified by the parametric decay of the pump photons. The second term originates from the parametric decay of

the pump photons under the action of vacuum fluctuations of the intracavity field; this is a purely quantum effect. Thermal effects can be neglected if

$$\frac{\Gamma_s \Gamma_{(\sigma,r)s}}{\varsigma^2} \frac{2}{\exp\left(\hbar\omega_s/(k_B T_{\sigma,r})\right) - 1} \ll 1.$$

The results in Eqs. (5.32)-(5.35) provide the dependence of the parametric signal from all relevant dissipation and fluctuation effects. In addition to dissipation and thermal fluctuations due to absorption in the cavity walls and a semiconductor heterostructure, they take into account outcoupling of a signal into the ambient space and coupling to thermal photons from the environment. Eq. (5.35) determines the spontaneous parametric signal emitted from a cavity against the background of noise created by both thermal radiation from a cavity and reemission of thermal photons coupled into a cavity from the outside. The background noise depends from the cavity temperature and the environment temperature. In addition to the spontaneous decay process we take into account the modification of background noise by pumping.

For a numerical example, consider a nanocavity filled with multiple quantum wells, excited with a mid-infrared pump, as reported in [8]. Using Eq. (5.30) for their values of intersubband nonlinearity $|\chi^{(2)}| \sim 3 \times 10^{-7}$ m/V, $\omega_{s,i}/\Delta\omega_{s,i} \sim 20$ and $J/L_x L_y \sim 0.3$ we obtain the intracavity pump field at the instability threshold to be $E_p \simeq 8$ kV/cm, which is achievable and is lower than the saturation field for the intersubband nonlinearity. Above the threshold, the signal and idler fields start growing inside the cavity until they get limited by the Manley-Rowe relations [33], i.e. the intracavity signal field reaches $|E_s| \simeq |E_p|/\sqrt{2}$. Therefore, the maximum output signal power that can be obtained per one nanocavity described in [8] is about 8×10^{-7} W for the photon leakage rate $\Gamma_{rs} = 10^{12}$ s^{-1}.

Far below the instability threshold, when $\varsigma \ll \Gamma_s$, the spontaneous rate of parametric down-conversion scales as $(\Gamma_{rs}/\Gamma_s^2)\varsigma^2$. For the parameters from the above numerical example, when $\varsigma = \Gamma_s/2$ the emission rate of signal photons is around 3×10^{11} s^{-1} and the power is 6 nW.

A very high second-order nonlinear surface conductivity for graphene was reported in [14],

corresponding to the effective bulk susceptibility $|\chi^{(2)}| \sim 10^{-3}$ m/V per monolayer in the THz range. This large susceptibility if partially offset by a small factor l/L_z in Eq. (5.29) where l is a thickness of the graphene layer. However, for hBN-encapsulated graphene utilized to fabricate low-disorder graphene samples [34] the total cavity thickness L_z can be as small as several nm, so the factor l/L_z can be as large as 0.1. Even factoring in enhanced cavity losses, this can yield a lower parametric instability threshold as compared to semiconductor quantum well samples.

5.4 Comparing parametric instability in a subwavelength cavity and in a Fabry-Perot cavity

Compare the parametric instability in a subwavelength cavity with similar instability of modes in a Fabry-Perot (FP) cavity with all three dimensions larger than wavelength, which we will call a quasi-optical cavity. Consider a planar quasi-2D cavity of the surface area $L_x L_y$, in which the waves are propagating along the nonlinear layer of thickness l much smaller than the cavity thickness L_{FP} transverse to the nonlinear layer, so the cavity volume is $L_{FP} L_x L_y$. The dielectric constant of a cavity filling is ε. In this case the parametric down-conversion is still described by Eqs. (5.22), (5.17), and (5.18), in which the relaxation constants $\Gamma_{s,i}$ and the overlap integral are determined by the FP cavity Q-factor and the corresponding spatial structure of the modes. For the normalization constants of the quantum fields entering Eq. (5.17) we use standard expressions for a two-mirror FP cavity:

$$|E_{s,i}|^2 = \frac{4\pi\hbar\omega_{s,i}}{L_x L_y L_{FP}\varepsilon}. \tag{5.36}$$

The resulting parametric instability threshold is

$$\frac{64\pi^2}{\varepsilon^2 L_{FP}^2}\left(\chi^{(2)} l\right)^2 |E_p|^2 \left(\frac{\omega_s}{\Delta\omega_s}\right)\left(\frac{\omega_i}{\Delta\omega_i}\right)\left(\frac{J}{L_x L_y}\right)^2 > 1, \tag{5.37}$$

where $\Delta\omega_{s,i} \approx 2\Gamma_{s,i}$.

As we already pointed out, in a cavity with all three dimensions larger than the wavelength the

phase matching condition for a three-wave mixing may be more difficult to satisfy. Even if we assume that phase matching is somehow arranged and the geometric factor J/L_xL_y is of the same order as in a subwavelength cavity, the latter is expected to have a lower parametric threshold. Indeed the ratio of the threshold pump intensity $|E_p|^2$ in a subwavelength cavity to that in a quasi-optical cavity scales as $\sim \left(\frac{L_z}{L_{FP}}\right)^2 \left(\frac{\Delta\omega_{eff}}{\Delta\omega_{FP}}\right)^2$, where $\Delta\omega_{eff}$ and $\Delta\omega_{FP} \approx \Delta\omega_{s,i}$ are typical linewidths of the subwavelength cavity and FP cavity modes, respectively. This ratio can be much smaller than 1, which indicates that a much lower pumping is needed to reach the parametric instability threshold in a subwavelength cavity, even if the FP cavity has a higher Q-factor as compared to the subwavelength cavity, $\Delta\omega_{FP} < \Delta\omega_{eff}$.

A plane-parallel quasi-2D subwavelength cavity geometry considered in this paper is the most natural choice for integration with 2D nonlinear materials. However, other geometries are also possible, for example plasmonic or grating structures supporting surface modes. To get an order of magnitude estimate of the parametric threshold, one can use our results in Eqs. (5.30), (5.37) after replacing L_z or L_{FP} with a mode size transversely to the nonlinear layer.

A promising example of such a plasmonic nanocavity was reported in [35]. It consists of a monolayer MoS_2, which is a 2D semiconductor, sandwiched between a gold substrate and a patch silver nanoantenna. Such a cavity has high radiative and absorption losses but a very small transverse mode size of less than 10 nm and an ultrasmall effective mode volume of $\sim 10^{-3}(\lambda/\sqrt{\epsilon})^3$. The authors of [35] used their cavities to obtain a 2000-fold enhancement in the photoluminescence intensity from MoS_2 monolayer. However, a cavity of similar design can also be used for parametric down-conversion from visible to the near-IR range. A high second-order nonlinearity, about an order of magnitude higher than in BBO or lithium niobate, has been reported for MoS_2 monolayer [36]. An even higher nonlinearity has been observed in the vicinity of exciton resonances [37]. Assuming conservatively that the effective second-order susceptibility for MoS_2 is $|\chi^{(2)}| \sim 10^{-10}$ m/V, monolayer thickness 0.6 nm, transverse mode size 5 nm, $\omega_{s,i}/\Delta\omega_{s,i} \sim 20$ and $J/L_xL_y \sim 0.3$ we obtain from Eq. (5.30) the intracavity pump field at the parametric amplification threshold to be $E_p \simeq 30$ MV/cm, which is much higher than the estimate above for a nonlinear

cavity based on mid-infrared resonant intersubband nonlinearity of quantum wells, but is below the saturation threshold for MoS_2 and easily achievable with pulsed lasers.

Ultracompact subwavelength electrodynamic structures utilizing 2D materials are promising for applications in integrated photonic circuits, whenever one needs a compact planar architecture. At the same time, due to strong dissipation they are unlikely to outperform conventional nonlinear devices made of bulk transparent nonlinear materials when it comes to the nonlinear conversion efficiency and power. For example, in [38] the authors realized low-threshold mode-matched parametric generation in whispering gallery mode resonators made entirely of bulk lithium niobate. In this case the bulk nonlinear material occupies all modal volume. The lower nonlinearity and the loss of Purcell enhancement are compensated by lower dissipation and increased interaction volume.

In conclusion, we applied a consistent Heisenberg-Langevin formalism to the process of nonlinear parametric down-conversion of cavity modes in planar subwavelength cavities containing 2D nonlinear materials. We derived general analytic formulas for the spontaneous parametric signal and threshold of stimulated parametric down-conversion of a pump cavity mode into the signal and idler modes. We found that a significant reduction in the parametric instability threshold can be achieved for realistic materials and cavity parameters due to Purcell enhancement.

5.4 References

[1] E. M. Purcell, H. C. Torrey, R. V. Pound, Phys. Rev. 69, 37 (1946).

[2] H.-B. Lin, A. J. Campillo, Phys. Rev. Lett. 73, 2440 (1994).

[3] P. Bermel, A. Rodriguez, J. D. Joannopoulos, M. Soljacic, Phys. Rev. Lett. 99, 053601 (2007).

[4] P. Genevet, J.-P. Tetienne, E. Gatzogiannis, R. Blanchard, M. A. Kats, et al., Nano Lett. 10, 4880-4883 (2010).

[5] M. Kauranen, A. V. Zayats, Nature Phot. 6, 737-748 (2012).

[6] M. Lapine, I. V. Shadrivov, Y. S. Kivshar, Rev. Mod. Phys. 86, 1093 (2014).

[7] J. Lee, M. Tymchenko, C. Argyropoulos, P.-Y. Chen, F. Lu, et al., Nature 511, 65-67 (2014).

[8] J. Lee, N. Nookala, J. S. Gomez?Diaz, M. Tymchenko, F. Demmerle, et al., Adv. Opt. Mater. 4, 664-670 (2016).

[9] D. Smirnova, Y. S. Kivshar, Optica 3, 1241-1255 (2016).

[10] A. R. Davoyan, H. A. Atwater, Optica 5, 608-611 (2018).

[11] E. Hendry, P.J. Hale, J. Moger, A.K. Savchenko, S. A. Mikhailov, Phys. Rev. Lett. 105, 097401 (2010).

[12] X. Yao, A. Belyanin, Phys. Rev. Lett. 108, 255503 (2012).

[13] X. Yao, M.D. Tokman, A. Belyanin, Phys. Rev. Lett. 112, 055501 (2014).

[14] Y. Wang, M. Tokman, A. Belyanin, Phys. Rev. B 94, 195442 (2016).

[15] L.M. Malard, T.V. Alencar, A.P.M. Barboza, K.F. Mak, A.M. de Paula, Phys. Rev. B 87, 201401 (2013).

[16] H. Liu, Y. Li, Y. S. You, S. Ghimire, T. F. Heinz, D. A. Reis, Nat. Phys. 13, 262-265 (2016).

[17] P. Alonso-Gonzalez, A. Y. Nikitin, Y. Gao, A. Woessner, M. B. Lundeberg, et al., Nat. nanotechnol. 12, 31-35 (2017).

[18] Yu Ye, Z. Wong, X. Lu, X. Ni, H. Zhu, et al., Nat. Phot. 9, 733 (2015).

[19] M. O. Scully, M. S. Zubairy, Quantum Optics (Cambridge Univ. Press, Cambridge, 1997).

[20] C. Gardiner, P. Zoller, Quantum Noise (Springer-Verlag, Berlin, Heidelberg, 2004).

[21] M. Erukhimova, M.Tokman. Phys. Rev. A 95, 013807 (2017).

[22] L. Davidovich, Rev. Mod. Phys. 68, 127 (1996).

[23] M.Tokman, X. Yao, A. Belyanin, Phys. Rev. Lett. 110, 077404 (2013).

[24] M. Erukhimova, M. Tokman, Optics Lett. 40, 2739-3742 (2015).

[25] M. Tokman, M. Erukhimova, Journal of Lumin. 137, 148-156 (2013).

[26] M. Tokman, Z. Long, S. AlMutairi, Y. Wang, M. Belkin, et al., Phys. Rev. A 97, 043801 (2018).

[27] V. M. Fain, Ya. I. Khanin, Quantum Electronics, Vol. 1 (The MIT Press, Cambridge, MA, 1969).

[28] M. D. Tokman, M. A. Erukhimova, V. V. Vdovin, Annals of Physics 360, 571-595 (2015).

[29] M. Tokman, Y. Wang, I. Oladyshkin, A. R. Kutayiah, A. Belyanin, Phys. Rev. B 93, 235422 (2016).

[30] Yu. A. Illinskii, L. V. Keldysh, Electromagnetic Response of Material Media (Springer, New York, 1994).

[31] M. D. Tokman, M. A Erukhimova, Phys. Rev. E 84, 056610 (2011).

[32] Y. R. Shen, The Principles of Nonlinear Optics (Wiley, Hoboken, NJ, 2003).

[33] L. D. Landau, E. M. Lifshitz, Electrodynamics of Continuous Media (Pergamon Oxford, 1984).

[34] T. Low, A. Chaves, J. D. Caldwell, A. Kumar, N. X. Fang, et al., Nat. Mater. 16, 182-194 (2017).

[35] G. M. Akselrod, T. Ming, C. Argypoulos, T. B. Hoang, Y. Lin, et al., Nano Lett. 15, 3578-3584 (2015).

[36] Y. Li, Y. Rao, K. F. Mak, Y. You, S. Wang, et al., Nano Lett. 13, 3329-3333 (2013).

[37] M. L. Trolle, Y.-C. Tsao, K. Pedersen, T. G. Pedersen, Phys. Rev. B 92, 161409(R) (2015).

[38] J. U. Furst, D.V. Strekalov, D. Elser, A. Aiello, U. L. Andersen, et al., Phys. Rev. Lett. 105, 263904 (2010).

6. SUMMARY

In this dissertation, we showed the unique optical properties of a specific topological material - Weyl semimetals, quasi one-dimensional materials - carbon nanotubes, and Purcell enhancement of quasi two-dimensional materials.

For Weyl semimetals, we derived its dielectric tensor from general Hamiltonian for Weyl fermions in a strong magnetic field, and then the propagation of electromagnetic waves based on this dielectric tensor. Results showed unusual magneto-optical effects for Weyl semimetals: hyperbolic dispersion, photonic stop bands, coupling-induced transparency, and broadband polarization conversion. All effects are tunable by varying the magnetic field strength, electric bias or propagation angle. These effects lead to potential applications of Weyl semimetals in photonic devices.

For carbon nanotubes, we derived their optical response under different excitation scale with tight binding model and Semiconductor Bloch equation. Results showed that the optical gain could exceed the threshold for superfluorescence, and thus make SWCNTs a fast and effective emitter.

For the Purcell effect in subwavelength quasi two-dimensional materials, we used Heisenberg-Langevin approach to study the radiative processes. This approach included dissipation and fluctuation in both fermionic ensemble and electromagnetic field. Our results provided a general framework for spontaneous emission and parametric down-conversion. We derived the analytical expression for the spontaneous emission power, the spontaneous parametric conversion power, and threshold for parametric instability. Our results provided a very detailed understanding of Purcell effect in realistic situation, and could be used as guidance for subwavelength cavity design.

In conclusion, nanostructures and topological materials have many unusual optical properties. We hope our study could help future research in photonic engineering devices based on those fascinating novel materials.

APPENDIX A

CONDUCTIVITY OF WEYL SEMIMETALS IN A STRONG MAGNETIC FIELD

A.1 Electron states in a magnetic field

When a uniform magnetic field is applied to a WSM, the Weyl cones split into Landau subbands.

The Hamiltonian of a Weyl electron in a magnetic field is

$$\mathcal{H} = \chi v_F \boldsymbol{\sigma} \left(\boldsymbol{p} + \frac{e}{c} \boldsymbol{A} \right) \tag{A.1}$$

Here $\chi = \pm 1$ is chirality index. If we choose the vector potential $\boldsymbol{A} = (0, Bx, 0)$, then the Hamiltonian is

$$\mathcal{H} = \chi v_F \begin{pmatrix} \hbar k_z & \pi_x - i\pi_y \\ \pi_x + i\pi_y & -\hbar k_z \end{pmatrix} = \chi \hbar v_F \begin{pmatrix} k_z & \frac{\sqrt{2}}{l_B} a \\ \frac{\sqrt{2}}{l_B} a^\dagger & -k_z \end{pmatrix} \tag{A.2}$$

Here $\boldsymbol{\pi} = \boldsymbol{p} + \frac{e}{c}\boldsymbol{A}$, $l_B = \sqrt{\hbar c/eB}$, and we introduced creation and annihilation operators,

$$a = \frac{l_B}{\sqrt{2}\hbar}(\pi_x - i\pi_y),\ a^\dagger = \frac{l_B}{\sqrt{2}\hbar}(\pi_x + i\pi_y),$$

which satisfy

$$a^\dagger \psi_{n0} = \sqrt{|n|}\psi_{n1},\ a\psi_{n1} = \sqrt{|n|}\psi_{n0}$$

when the eigenstates are sought in the form

$$\Psi_n(k_y, r) = \begin{pmatrix} u_n \psi_{n0} \\ v_n \psi_{n1} \end{pmatrix}.$$

Then we can obtain from $\mathcal{H}\Psi_n = W_n^{(\chi)}\Psi_n$:

$$\chi\hbar v_F \begin{pmatrix} k_z & \frac{\sqrt{2}}{l_B}a \\ \frac{\sqrt{2}}{l_B}a^\dagger & -k_z \end{pmatrix} \begin{pmatrix} u_n\psi_{n0} \\ v_n\psi_{n1} \end{pmatrix} = \chi\hbar v_F \begin{pmatrix} (k_z u_n + \frac{\sqrt{2|n|}}{l_B}v_n)\psi_{n0} \\ (-k_z v_n + \frac{\sqrt{2|n|}}{l_B}u_n)\psi_{n1} \end{pmatrix} = W_n^{(\chi)}\Psi_n.$$

The eigenenergies are

$$W_0^{(\chi)} = -\chi\hbar v_F k_z \tag{A.3}$$

$$W_n = \text{sgn}(n)\hbar v_F\sqrt{\frac{2|n|}{l_b^2} + k_z^2} \text{ for } n \neq 0 \tag{A.4}$$

$$u_n = \sqrt{\frac{1}{2}(1 + \frac{\hbar v_F k_z}{W_n})} \tag{A.5}$$

$$v_n = \sqrt{\frac{1}{2}(1 - \frac{\hbar v_F k_z}{W_n})} \tag{A.6}$$

and the full expression for eigenstates is

$$\Psi_n(k,r) = \frac{C_n}{\sqrt{L_y L_z}}\text{exp}(-i(k_y y + k_z z)) \begin{pmatrix} \text{sgn}(n) i^{|n|-1}\phi_{|n|-1}u_n \\ i^{|n|}\phi_{|n|}v_n \end{pmatrix}. \tag{A.7}$$

Here

$$C_n = \begin{cases} 1 & n = 0 \\ \frac{1}{\sqrt{2}} & n \neq 0 \end{cases} \tag{A.8}$$

$$\phi_{|n|} = \frac{\text{H}_n(\frac{x - l_B^2 k_y}{l_B})}{\sqrt{2^{|n|}|n|!\sqrt{\pi}l_B}}\text{exp}\left(-\frac{1}{2}\left(\frac{x - l_B^2 k_y}{l_B}\right)^2\right). \tag{A.9}$$

A.2 Selection rules for transitions between Landau levels

The selection rules for 3D chiral fermions in a magnetic field are very similar to that for 2D electrons in graphene. For a monochromatic optical field at frequency ω propagating along z direction and described by the vector potential $\boldsymbol{A} = -i(c/\omega)\boldsymbol{E}$ in the xy plane, the interaction

Hamiltonian is

$$\mathcal{H}_{\text{int}} = \chi v_F \boldsymbol{\sigma} \frac{e}{c} \boldsymbol{A}. \tag{A.10}$$

The probability of an optical transition between state m and n is determined by the matrix element $< m|\mathcal{H}_{\text{int}}|n >$

$$< m|\mathcal{H}_{\text{int}}|n >= -\frac{i\chi v_F e}{\omega} < m|\sigma_x \boldsymbol{x_o} + \sigma_y \boldsymbol{y_o}|n > \boldsymbol{E} \tag{A.11}$$

$$\sigma_x \boldsymbol{x_o} + \sigma_y \boldsymbol{y_o} = \begin{pmatrix} 0 & \boldsymbol{x_o} - i\boldsymbol{y_o} \\ \boldsymbol{x_o} + i\boldsymbol{y_o} & 0 \end{pmatrix} = \sqrt{2} \begin{pmatrix} 0 & \boldsymbol{e}_{RHC} \\ \boldsymbol{e}_{LHC} & 0 \end{pmatrix}$$

Writing $\boldsymbol{E} = E_L \boldsymbol{e}_{LHC} + E_R \boldsymbol{e}_{RHC}$ and substituting the wave functions from Eq. (A.9) into Eq. (A.11), we obtain

$$\begin{aligned} < m|\mathcal{H}_{\text{int}}|n > = & -\frac{i\chi v_F e}{\omega c} C_m C_n v_m u_n i^{-|m|+|n|-1} < \phi_{|m|}|\phi_{|n|-1} > \sqrt{2} E_R \\ & - \frac{i\chi v_F e}{\omega c} C_n C_m v_n u_m i^{-|m|+|n|+1} < \phi_{|m|-1}|\phi_{|n|} > \sqrt{2} E_L \end{aligned} \tag{A.12}$$

The resulting selection rules are:

$$|m| = |n| - 1 \text{ for } \boldsymbol{e}_{RHC} \text{ polarization} \tag{A.13}$$

$$|n| = |m| - 1 \text{ for } \boldsymbol{e}_{LHC} \text{ polarization} \tag{A.14}$$

A.3 Transverse optical conductivity due to transitions between Landau levels

The current density generated in response to a monochromatic field is

$$\begin{aligned} \boldsymbol{j} = & \frac{i(ev_F)^2 \hbar}{4\pi^2 l_b^2} \int \mathrm{d}k_z \sum_{mn} [(\sigma_R)_{nm} \boldsymbol{e}_{RHC} + (\sigma_L)_{nm} \boldsymbol{e}_{LHC}][(\sigma_R)_{mn} E_L + (\sigma_L)_{mn} E_R] \\ & \times \frac{f_n(k_z) - f_m(k_z)}{[\hbar\omega - (W_m(k_z) - W_n(k_z) + i\gamma)](W_m(k_z) - W_n(k_z))} \end{aligned} \tag{A.15}$$

The corresponding conductivities for LHC and RHC polarizations are given by

$$\tilde{\sigma}_{RR} = \frac{i(ev_F)^2\hbar}{4\pi^2 l_b^2}\int \mathrm{d}k_z \sum_{mn}[(\sigma_R)_{nm}(\sigma_L)_{mn}]\times \frac{f_n(k_z)-f_m(k_z)}{[\hbar\omega-(W_m(k_z)-W_n(k_z))+i\gamma](W_m(k_z)-W_n(k_z))}$$

$$\tilde{\sigma}_{LL} = \frac{i(ev_F)^2\hbar}{4\pi^2 l_b^2}\int \mathrm{d}k_z \sum_{mn}[(\sigma_L)_{nm}(\sigma_R)_{mn}]\times \frac{f_n(k_z)-f_m(k_z)}{[\hbar\omega-(W_m(k_z)-W_n(k_z))+i\gamma](W_m(k_z)-W_n(k_z))}$$

Here $f_{n,m}(k_z)$ are occupation numbers of electron states;

$$\begin{aligned}(\sigma_R)_{nm} &=< n|\begin{pmatrix} 0 & 1 \\ 0 & 0 \end{pmatrix}|m> \\ &= \sqrt{2}C_nC_mv_nu_m\delta(|n|-|m|-1) \\ (\sigma_L)_{nm} &=< n|\begin{pmatrix} 0 & 0 \\ 1 & 0 \end{pmatrix}|m> \\ &= \sqrt{2}C_nC_mv_mu_n\delta(|n|-|m|+1)\end{aligned}$$

The resulting expressions for $\tilde{\sigma}_{RR}$ and $\tilde{\sigma}_{LL}$ are

$$(\tilde{\sigma}_{RR})_{n\to m} = \frac{i(ev_F)^2\hbar}{2\pi^2 l_b^2}\int \mathrm{d}k_z (C_nC_mv_nu_m)^2 \frac{f_n-f_m}{\Delta W(\hbar\omega-\Delta W+i\gamma)}\delta(|n|-|m|-1) \quad \text{(A.16)}$$

$$(\tilde{\sigma}_{LL})_{n\to m} = \frac{i(ev_F)^2\hbar}{2\pi^2 l_b^2}\int \mathrm{d}k_z (C_nC_mv_mu_n)^2 \frac{f_n-f_m}{\Delta W(\hbar\omega-\Delta W+i\gamma)}\delta(|n|-|m|+1), \quad \text{(A.17)}$$

where $\Delta W = W_m(k_z) - W_n(k_z)$; the quantities C, v, u and W_n are defined earlier.

As an example, we provide below an explicit form of the conductivity components for lowest-

energy transitions $0 \to 1$, $-1 \to 0$, $-1 \to 2$ and $1 \to 2$ for an arbitrary chirality $\chi = \pm 1$:

$$
\begin{aligned}
(\tilde{\sigma}_{LL})_{0\to1} &= \frac{i(ev_F)^2\hbar}{2\pi^2 l_b^2}\int \mathrm{d}k_z (C_1C_0v_0u_1)^2 \frac{f_n - f_m}{\Delta W(\hbar\omega - \Delta W + i\gamma)} \\
&= \frac{i(ev_F)^2\hbar}{2\pi^2 l_b^2}\int \mathrm{d}k_z \frac{1}{4}(1 + \chi k_z(\frac{2}{l_b^2} + k_z^2)^{-0.5}) \\
&\times \frac{f_n - f_m}{\hbar v_F(\sqrt{\frac{2}{l_b^2} + k_z^2} + \chi k_z)(\hbar\omega - \hbar v_F(\sqrt{\frac{2}{l_b^2} + k_z^2} + \chi k_z) + i\gamma)} \\
(\tilde{\sigma}_{RR})_{-1\to0} &= \frac{i(ev_F)^2\hbar}{2\pi^2 l_b^2}\int \mathrm{d}k_z (C_{-1}C_0v_{-1}u_0)^2 \frac{f_n - f_m}{\Delta W(\hbar\omega - \Delta W + i\gamma)} \\
&= \frac{i(ev_F)^2\hbar}{2\pi^2 l_b^2}\int \mathrm{d}k_z \frac{1}{4}(1 - \chi k_z(\frac{2}{l_b^2} + k_z^2)^{-0.5}) \\
&\times \frac{f_n - f_m}{\hbar v_F(\sqrt{\frac{2}{l_b^2} + k_z^2} - \chi k_z)(\hbar\omega - \hbar v_F(\sqrt{\frac{2}{l_b^2} + k_z^2} - \chi k_z) + i\gamma)} \\
(\tilde{\sigma}_{LL})_{-1\to2} &= \frac{i(ev_F)^2\hbar}{2\pi^2 l_b^2}\int \mathrm{d}k_z (C_{-1}C_2v_{-1}u_2)^2 \frac{f_n - f_m}{\Delta W(\hbar\omega - \Delta W + i\gamma)} \\
&= \frac{i(ev_F)^2\hbar}{2\pi^2 l_b^2}\int \mathrm{d}k_z \frac{1}{16}(1 + \chi k_z(\frac{2}{l_b^2} + k_z^2)^{-0.5})(1 + \chi k_z(\frac{4}{l_b^2} + k_z^2)^{-0.5}) \\
&\times \frac{f_n - f_m}{\hbar v_F(\sqrt{\frac{4}{l_b^2} + k_z^2} + \sqrt{\frac{2}{l_b^2} + k_z^2})(\hbar\omega - \hbar v_F(\sqrt{\frac{4}{l_b^2} + k_z^2} + \sqrt{\frac{2}{l_b^2} + k_z^2}) + i\gamma)} \\
(\tilde{\sigma}_{LL})_{1\to2} &= \frac{i(ev_F)^2\hbar}{2\pi^2 l_b^2}\int \mathrm{d}k_z (C_1C_2v_1u_2)^2 \frac{f_n - f_m}{\Delta W(\hbar\omega - \Delta W + i\gamma)} \\
&= \frac{i(ev_F)^2\hbar}{2\pi^2 l_b^2}\int \mathrm{d}k_z \frac{1}{16}(1 - \chi k_z(\frac{2}{l_b^2} + k_z^2)^{-0.5})(1 + \chi k_z(\frac{4}{l_b^2} + k_z^2)^{-0.5}) \\
&\times \frac{f_n - f_m}{\hbar v_F(\sqrt{\frac{4}{l_b^2} + k_z^2} - \sqrt{\frac{2}{l_b^2} + k_z^2})(\hbar\omega - \hbar v_F(\sqrt{\frac{4}{l_b^2} + k_z^2} - \sqrt{\frac{2}{l_b^2} + k_z^2}) + i\gamma)}
\end{aligned}
$$

Note that the occupation number f_0 of the $n = 0$ state depends on chirality even when Fermi energies are the same for both chiralities, since the energy $W_0 = -\chi\hbar v_F k_z$ depends on chirality.

A.4 Longitudinal conductivity and plasmon dispersion for an arbitrary Fermi level

Here we consider plasmons propagating along the magnetic field of a WSM with the Fermi level crossing an arbitrary number N of Landau levels. The Hamiltonian is

$$\mathcal{H}^{(\chi)} = \chi v_F \boldsymbol{\sigma}\left(\boldsymbol{p} + \frac{e}{c}\boldsymbol{A}(\boldsymbol{r})\right) - e\phi(\boldsymbol{r}, t), \tag{A.18}$$

where $\boldsymbol{A}(\boldsymbol{r})$ defines a constant magnetic field $\boldsymbol{B}\|\boldsymbol{z_o}$ whereas the electric field $\boldsymbol{E}\|\boldsymbol{z_o}$ of the plasmon is described by the scalar potential $\phi = \mathrm{Re}\Phi e^{iqz-i\omega t}$.

The kinetic equation for the electron distribution $f_{k_z}^{(n,\chi)}$ in the nth Landau subband is

$$\frac{\partial}{\partial t} f_{k_z}^{(n,\chi)} + \frac{\partial W_{n,\chi}}{\hbar \partial k_z} \frac{\partial}{\partial z} f_{k_z}^{(n,\chi)} - eE \frac{\partial}{\hbar \partial k_z} f_{k_z}^{(n,\chi)} = 0. \tag{A.19}$$

Here we ignored relaxation. It can be added within the rate approximation as an imaginary part of frequency in the final expression for the conductivity. Note that for $n = 0$

$$\frac{\partial W_{n=0,\chi}}{\hbar \partial k_z} = \chi v_F.$$

For $n \neq 0$ the presence of R- and L-fermions with opposite chiralities $\chi = \pm 1$ leads only to the degeneracy factor $g = 2$, as long as their Fermi energies are the same.

Since we need the linear response, we linearize the distribution function in Eq. (A.19) as $f_{k_z}^{(n,\chi)} = F_{k_z}^{(n,\chi)} + \mathrm{Re}\tilde{f}_{k_z}^{(n,\chi)} e^{iqz-i\omega t}$, which yields

$$\tilde{f}_{k_z}^{(0,\chi)} = \frac{ieE}{(\omega - \chi q v_F)} \frac{\partial}{\hbar \partial k_z} F_{k_z}^{(0,\chi)};\ \tilde{f}_{k_z}^{(n\neq 0,\chi)} = \frac{ieE}{(\omega - q\frac{\partial W_n}{\hbar \partial k_z})} \frac{\partial}{\hbar \partial k_z} F_{k_z}^{(n\neq 0,\chi)}. \tag{A.20}$$

The complex amplitude of the current density is

$$j_z = \mathrm{Re}\tilde{j}_z e^{iqz-i\omega t},\ \tilde{j}_z = \tilde{j}_0 + \sum_{n\neq 0} \tilde{j}_n; \tag{A.21}$$

$$\tilde{j}_0 = -\frac{e^2 B v_F}{4\pi^2 \hbar^2 c} \int_{-\infty}^{\infty} \left(\tilde{f}_{k_z}^{(0,\chi=1)} - \tilde{f}_{k_z}^{(0,\chi=-1)} \right) dk_z, \tag{A.22}$$

$$\tilde{j}_{n\neq 0} = -2\frac{e^2 B}{4\pi^2 \hbar^2 c} \int_{-\infty}^{\infty} \frac{\partial W_n}{\hbar \partial k_z} \tilde{f}_{k_z}^{(n)}\, dk_z. \tag{A.23}$$

From Eq. (A.22) and the first of Eq. (A.20) we obtain

$$\tilde{j}_0 = -\frac{ie^3 B v_F}{4\pi^2 \hbar^2 c} \left(\frac{1}{\omega - q v_F} \int_{-\infty}^{\infty} \frac{\partial}{\partial k_z} F_{k_z}^{(0,\chi=1)}\, dk_z - \frac{1}{\omega + q v_F} \int_{-\infty}^{\infty} \frac{\partial}{\partial k_z} F_{k_z}^{(0,\chi=-1)}\, dk_z \right). \tag{A.24}$$

Now we can derive the conductivity and the longitudinal component of the dielectric tensor by equating

$$\tilde{j}_0 + \sum_{n\neq 0} \tilde{j}_n = -\frac{i\omega(\epsilon_{zz} - \epsilon_b)}{4\pi} E. \tag{A.25}$$

Note that $F^{(0,\chi=1)}_{k_z\to-\infty} \Rightarrow 1$, $F^{(0,\chi=1)}_{k_z\to\infty} \Rightarrow 0$, whereas $F^{(0,\chi=-1)}_{k_z\to-\infty} \Rightarrow 0$ and $F^{(0,\chi=-1)}_{k_z\to\infty} \Rightarrow 1$. Therefore, Eq. (A.24) yields

$$\tilde{j}_0 = \frac{ie^3 B v_F E}{2\pi^2\hbar^2 c} \frac{\omega}{\omega^2 - q^2 v_F^2}. \tag{A.26}$$

The same result can be obtained from the quantum-mechanical density-matrix approach. We can similarly evaluate the integrals in Eq. (A.23) assuming the Fermi distribution with zero temperature. The result is

$$\epsilon_{zz} = \epsilon_b - \omega_p^2 \left[\frac{1}{\omega^2 - q^2 v_F^2} + 2\sum_{n=1}^{N} \frac{\frac{1}{v_F}\left|\frac{\partial W_n}{\hbar\partial k_z}\right|_{W_n=E_F}}{\omega^2 - q^2\left(\frac{\partial W_n}{\hbar\partial k_z}\right)^2_{W_n=E_F}} \right]. \tag{A.27}$$

The dispersion relation $\epsilon_{zz} = 0$ for a plasmon propagating along the magnetic field can be solved using Eq. (A.27), leading to a cumbersome expression. In the limit of small q one can put $q = 0$ in Eq. (A.20) and replace

$$\tilde{f}^{(n\neq 0)}_{k_z} \approx \frac{ieE}{\omega} \frac{\partial}{\hbar\partial k_z} F^{(n\neq 0)}_{k_z}.$$

This gives much simpler expressions:

$$\epsilon_{zz} = \epsilon_b - \frac{\omega_p^2}{\omega^2} \left[1 + \frac{2}{v_F} \sum_{n=1}^{N} \int_{-\infty}^{\infty} \left(\frac{\partial^2 W_n}{\hbar\partial k_z^2} \right) F^{(n)}_{k_z}\, dk_z \right], \tag{A.28}$$

$$\omega^2 = \frac{\omega_p^2}{\epsilon_b} \left[1 + \frac{2}{v_F} \sum_{n=1}^{N} \int_{-\infty}^{\infty} \left(\frac{\partial^2 W_n}{\hbar\partial k_z^2} \right) F^{(n)}_{k_z}\, dk_z \right]. \tag{A.29}$$

These expressions are not limited to low temperatures and are valid for any unperturbed electron distribution $F^{(n)}_{k_z}$.

APPENDIX B

HEISENBERG-LANGEVEN FORMALISM WITHIN A SUBWAVELENGTH CAVITY

B.1 EM field quantization in a subwavelength cavity filled with a layered dispersive medium

We start from the expression for the energy of a classical EM field in a nonmagnetic medium:

$$W = \frac{B^2}{8\pi} + \frac{1}{4\pi}\int_C^t \boldsymbol{E}\dot{\boldsymbol{D}}dt. \tag{B.1}$$

According to Eq. (4.12) in our case the electric field and electric induction vectors are equal to

$$\boldsymbol{E} = \boldsymbol{z_o} D_\nu \frac{\zeta_\nu(x,y)}{\varepsilon(\omega_\nu, z)} e^{-i\omega_\nu t} + \text{C.C.}, \quad \boldsymbol{D} = \boldsymbol{z_o} D_\nu \zeta_\nu(x,y) e^{-i\omega_\nu t} + \text{C.C.} \tag{B.2}$$

For a non-uniform medium with frequency dispersion the spatial distribution of the field depends explicitly on the frequency ω_ν; this fact requires certain modification of the approach to calculate the field energy W. Assume an adiabatically slow "turning on" of the electric induction at the moment of time $t = C$, i.e. $D_\nu \implies D_\nu(t), D_\nu(C) = 0, \dot{D}_\nu \ll \omega_\nu D_\nu$. In this case one can write

$$\left.\begin{aligned} \dot{\boldsymbol{D}} &= \boldsymbol{z_o}\zeta_\nu(x,y)e^{-i\omega_\nu t}(-i\omega_\nu D_\nu + \dot{D}_\nu) + \text{C.C.} \\ \boldsymbol{E} &\approx \boldsymbol{z_o}\zeta_\nu(x,y)e^{-i\omega_\nu t}\left(\frac{D_\nu}{\varepsilon(z,\omega_\nu)} + i\dot{D}_\nu \frac{\partial}{\partial\omega}\left(\frac{1}{\varepsilon(z,\omega)}\right)_{\omega=\omega_\nu}\right) + \text{C.C.} \end{aligned}\right\}. \tag{B.3}$$

In addition, we take into account that for monochromatic fields $\boldsymbol{E} = \boldsymbol{E}_\nu(\boldsymbol{r})e^{-i\omega_\nu t} + \text{C.C.}$, $\boldsymbol{B} = \boldsymbol{B}_\nu(\boldsymbol{r})e^{-i\omega_\nu t} + \text{C.C.}$ and $\boldsymbol{D} = \boldsymbol{D}_\nu(\boldsymbol{r})e^{-i\omega_\nu t} + \text{C.C.}$ in a cavity or under periodic boundary conditions the flux of the complex vector $\boldsymbol{E}_\nu \times \boldsymbol{B}^*_\nu$ through a surface enclosing volume is equal to zero. This allows one to prove that

$$\int\limits_V \boldsymbol{B}_\nu \boldsymbol{B}_\nu^* d^3r = \int\limits_V \boldsymbol{D}_\nu \boldsymbol{E}_\nu^* d^3r, \tag{B.4}$$

Using Eqs. (B.1) - (B.4) one can get

$$\int\limits_V W d^3r = \frac{|D_\nu|^2}{4\pi} \int\limits_S \zeta_\nu \zeta_\nu^* d^2r \times \int\limits_{-\frac{L_z}{2}}^{+\frac{L_z}{2}} \left[\frac{2}{\varepsilon(z,\omega_\nu)} - \omega_\nu \frac{\partial}{\partial \omega} \left(\frac{1}{\varepsilon(z,\omega)} \right)_{\omega=\omega_\nu} \right] dz.$$

After we impose the requirement $\int_V W d^3r = \hbar\omega_\nu$ and take into account the relation

$$\frac{2}{\varepsilon} - \omega \frac{\partial}{\partial \omega} \left(\frac{1}{\varepsilon} \right) = \frac{1}{\varepsilon^2 \omega} \frac{\partial(\omega^2 \varepsilon)}{\partial \omega}$$

we arrive at the normalization condition Eq. (4.14).

B.2 Matrix elements of the interaction Hamiltonian for fermions coupled to an EM field in a cavity or a waveguide

The explicit form of the matrix elements in Eq. (4.22) is

(i) in the waveguide:

$$\zeta_{\boldsymbol{k'k}}^{(q_x)} = \delta_{k'_x, k_x + q_x} Y_{k'_y, k_y}, \tag{B.5}$$

where

$$Y_{k'_y, k_y} = \frac{\sin\left[\left(k_y + \frac{\pi}{L_y} - k'_y \right) \frac{L_y}{2} \right]}{\left(k_y + \frac{\pi}{L_y} - k'_y \right) L_y} + \frac{\sin\left[\left(k'_y + \frac{\pi}{L_y} - k_y \right) \frac{L_y}{2} \right]}{\left(k'_y + \frac{\pi}{L_y} - k_y \right) L_y};$$

(ii) in the cavity:

$$\zeta_{\boldsymbol{k'k}}^{(N)} = Y_{k'_y, k_y} X_{k'_x, k_x}, \tag{B.6}$$

where

$$X^{(odd)}_{k'_x,k_x} = \frac{\sin\left[\left(k_x + \frac{N_{odd}\pi}{L_x} - k'_x\right)\frac{L_x}{2}\right]}{\left(k_x + \frac{N_{odd}\pi}{L_x} - k'_x\right)L_x} + \frac{\sin\left[\left(k'_x + \frac{N_{odd}\pi}{L_x} - k_x\right)\frac{L_x}{2}\right]}{\left(k'_x + \frac{N_{odd}\pi}{L_x} - k_x\right)L_x},$$

$$X^{(even)}_{k'_x,k_x} = i\frac{\sin\left[\left(k'_x + \frac{N_{even}\pi}{L_x} - k_x\right)\frac{L_x}{2}\right]}{\left(k'_x + \frac{N_{even}\pi}{L_x} - k_x\right)L_x} - i\frac{\sin\left[\left(k_x + \frac{N_{even}\pi}{L_x} - k'_x\right)\frac{L_x}{2}\right]}{\left(k_x + \frac{N_{even}\pi}{L_x} - k'_x\right)L_x}.$$

These expressions are presented in the form which shows explicitly the factors of the type $\dfrac{\sin(Ax)}{x}$.

When calculating the radiated power by an ensemble of fermions we need to know the squares of matrix elements summed over electron $\boldsymbol{k}$-states, in particular $\sum_{k'_y} Y_{k'_y,k_y}Y_{k_y,k'_y}$ and $\sum_{k'_x} X_{k'_x,k_x}X_{k_x,k'_x}$. Taking into account that

$$\int\limits_{-\infty}^{+\infty} \frac{\sin^2 x}{x^2}dx = \pi, \quad \int\limits_{-\infty}^{+\infty} \frac{\cos^2 x}{\left(\frac{\pi}{2}\right)^2 - x^2}dx = 0,$$

we obtain

$$\sum_{k'_y} Y_{k'_y,k_y}Y_{k_y,k'_y} \implies \frac{L_y}{2\pi}\int\limits_{\infty} Y_{k'_y,k_y}Y_{k_y,k'_y}dk'_y = \frac{1}{2}, \ \sum_{k'_x} X_{k'_x,k_x}X_{k_x,k'_x} \implies \frac{L_x}{2\pi}\int\limits_{\infty} X_{k'_x,k_x}X_{k_x,k'_x}dk'_x = \frac{1}{2}. \tag{B.7}$$

Since $\int_S \zeta_{q_x}\zeta^*_{q_x}d^2r = S/2$ and $\int_S \zeta_N\zeta^*_N d^2r = S/4$, Eq. (B.7) give the equation $\sum_{\boldsymbol{k}'} \zeta^{(\nu)}_{\boldsymbol{k}'\boldsymbol{k}}\zeta^{(\nu)\dagger}_{\boldsymbol{k}\boldsymbol{k}'} = S^{-1}\int_S \zeta_\nu\zeta^*_\nu d^2r$, which is used in Chapter 4.

B.3 Commutation relations for Langevin sources

Consider first a single quantum oscillator described by the Hamiltonian $\hat{H} = \hbar\omega(\hat{c}^\dagger\hat{c} + 1/2)$. After substituting $\hat{c} = \hat{c}_0 e^{-i\omega t}$ and $\hat{c}^\dagger = \hat{c}^\dagger_0 e^{-i\omega t}$ the Heisenberg equations of motion take the form $\dot{\hat{c}}_0 = 0$, $\dot{\hat{c}}^\dagger_0 = 0$. The simplest model of interaction with a dissipative reservoir modifies these equations as follows: $\dot{\hat{c}}_0 + \Gamma\hat{c}_0 = 0$, $\dot{\hat{c}}^\dagger_0 + \Gamma\hat{c}^\dagger_0 = 0$. However, this modification leads to violation of boson commutation relation $[\hat{c}_0, \hat{c}^\dagger_0] = 1$. To resolve this issue and preserve the commutator one has to add the Langevin sources to the right-hand side of Heisenberg equations:

$$\dot{\hat{c}}_0 + \Gamma \hat{c}_0 = \hat{L}, \quad \dot{\hat{c}}_0^\dagger + \Gamma \hat{c}_0^\dagger = \hat{L}^\dagger. \tag{B.8}$$

Langevin noise operators in Eq. (B.8) describe fluctuations in a dissipative system. Note that $\langle \hat{L} \rangle = 0$; the notation $\langle \cdots \rangle$ means averaging over the statistics of the dissipative reservoir and over the initial quantum state $|\Psi\rangle$ within the Heisenberg picture.

The commutation relations for a noise operator can be obtained directly from the given form of the relaxation operator if we require that standard commutation relations $[\hat{c}_0, \hat{c}_0^\dagger] = 1, [\hat{c}_0, \hat{c}_0] = 0$, be satisfied at any moment of time. Indeed, let's substitute the solution of the operator-valued equations (B.8)

$$\hat{c}_0 = \hat{c}_0(0)e^{-\Gamma t} + \int_0^t e^{\Gamma(t'-t)} \hat{L}(t')dt', \quad \hat{c}_0^\dagger = \hat{c}_0^\dagger(0)e^{-\Gamma t} + \int_0^t e^{\Gamma(t'-t)} \hat{L}^\dagger(t')dt' \tag{B.9}$$

into the commutators. It is easy to see that the standard commutation relations will be satisfied if, first of all, the field operators at an initial moment of time, $\hat{c}_0(0)$ and $\hat{c}_0^\dagger(0)$, commute with Langevin operators $\hat{L}(t)$ and $\hat{L}^\dagger(t)$ in any combination. Second, the following condition has to be satisfied:

$$[\hat{L}, \hat{c}_0^\dagger] = [\hat{c}_0, \hat{L}^\dagger] = \Gamma. \tag{B.10}$$

Substituting Eq. (B.9) into Eq. (B.10) and using the identity $\int_0^t X(t')\delta(t-t')dt' = X(t)/2$ we arrive at

$$[\hat{L}(t'), \hat{L}^\dagger(t)] = 2\Gamma\delta(t-t'). \tag{B.11}$$

Now consider an ensemble of coupled oscillators Eq. (5.22). One can find directly from the solution Eq. (5.25) that the following conditions have to be satisfied in order to preserve standard commutation relations $[\hat{c}_{0s}, \hat{c}_{0s}^\dagger] = [\hat{c}_{0i}, \hat{c}_{0i}^\dagger] = 1, [\hat{c}_{0s}, \hat{c}_{0i}] = 0$ etc.:

$$\left.\begin{aligned}
[\hat{L}_s, \hat{c}_{0s}^{\dagger}] = [\hat{c}_{0s}, \hat{L}_s^{\dagger}] = \Gamma_s \\
[\hat{L}_i, \hat{c}_{0i}^{\dagger}] = [\hat{c}_{0i}, \hat{L}_i^{\dagger}] = \Gamma_i \\
[\hat{L}_s, \hat{c}_{0i}^{\dagger}] = [\hat{c}_{0s}, \hat{L}_i^{\dagger}] = [\hat{L}_s, \hat{c}_{0i}] = [\hat{c}_{0s}, \hat{L}_i] = 0
\end{aligned}\right\}. \tag{B.12}$$

It is easy to find out that Eqs. (B.12) will be satisfied if the field operators at $t = 0$ commute with Langevin noise operators in any combination, and the noise operators $\hat{L}_s$ and $\hat{L}_i$ commute with each other. In addition, substituting Eq. (5.25) - (5.27) into Eq. (B.12) one can show that in order to satisfy Eq. (B.12) the following relations must hold:

$$\frac{\int_0^t \left(K_2 e^{\lambda_1(t'-t)} - K_1 e^{\lambda_2(t'-t)}\right) \left[\hat{L}_s(t'), \hat{L}_s^{\dagger}(t)\right] dt'}{K_2 - K_1} = \Gamma_s, \tag{B.13}$$

$$\frac{\int_0^t \left(K_2 e^{\lambda_2(t'-t)} - K_1 e^{\lambda_1(t'-t)}\right) \left[\hat{L}_i(t'), \hat{L}_i^{\dagger}(t)\right] dt'}{K_2 - K_1} = \Gamma_i. \tag{B.14}$$

From Eqs. (B.13) and (B.14) one can obtain the requirement Eq. (5.23) which preserves correct commutators of the field operators. Therefore, the commutation properties of correct noise operators for coupled oscillators have to be exactly the same as for uncoupled isolated oscillators.

Here we presented a general proof which does not rely on any specific microscopic model of a dissipative subsystem coupled to the field oscillators. The proof for a particular case of two identical coupled oscillators interacting with a standard dissipative reservoir of equilibrium harmonic oscillators has been recently obtained.